TARGETING POLO-LIKE KINASE 1 IN GLIOMA-PROPAGATING CELLS

FOONG SHU FEN, CHARLENE

(*B.Sc, NUS*)

A THESIS SUBMITTED

FOR THE DEGREE OF MASTER OF SCIENCE

DEPARTMENT OF PHYSIOLOGY

NATIONAL UNIVERSITY OF SINGAPORE

2012

DECLARATION

I hereby declare that this thesis is my original work and it has been written by me in its entirety. I have duly acknowledged all the sources of information which have been used in the thesis.

This thesis has also not been submitted for any degree in any university previously.

Foong Shu Fen Charlene
20 July 2012

Acknowledgements

Research is a process more than scientific discoveries and validation of hypothesis. It is an arduous and grueling adventure, yet alluring as we venture into the unknown. This journey of mine is definitely an eye-opening experience, with its fair share of ups and downs. Getting this thesis done is surely a great challenge that would not be possible with just me alone. I would like to express my most sincere gratitude and appreciation to the following people:

First and foremost, to my supervisor Dr Carol Tang, for accepting me in this lab, a cove of hidden young talents. For the opportunities to do this M.Sc, drive projects and bringing out the best in me. Her mentorship and undying patience for me is more than one can ask for.

Also to my other supervisors, Prof Soong Tuck Wah and Dr Ang Beng Ti, for their mentorship, continual encouragement and support.

To my family and friends, for their understanding, love and concern for me.

To my wonderful lab mates, Yuk Kien, Joan, Tan Boon, Geraldene, Kendra, Lynnette and Esther, for their dependable assistance, for being my peer-mentors, and most importantly, their companionship in making this journey a fun-filled and memorable one. Special thanks to Edwin Sandanaraj for his expert knowledge and help with bioinformatics analyses.

Last but not least, to all the other wonderful souls I have encountered at NNI, for brightening up my everyday life, bringing fun, joy and laughter into this journey.

May all of us be happy and healthy always!

TABLE OF CONTENTS

SUMMARY

Glioblastoma multiforme (GBM) is the common and malignant form of adult primary brain tumor, often with poor prognosis. Survival of patients remains dismal despite surgical intervention and adjuvant therapies (chemo- and radiation therapies). There is thus an unmet need to design new therapies that significantly improve patient outcomes. Furthermore, treatment strategies have been complicated by intrinsic intratumoral heterogeneity driven by clonal evolution with distinct genomic aberrations. Using lineage tracing mouse models, neural stem cells have been identified as the cells-of-origin, thus supporting the cellular hierarchy model of GBM development. While patient-derived GBM-propagating cells (GPCs) cannot identify the cell-of-origin, we and others have demonstrated that: (i) GPCs possess extensive self-renewing and serial tumor-propagating activity; (ii) They exhibit karyotypic aberrations typically found in the primary tumor; and (iii) They reform tumor xenografts that recapitulate the patient's original histopathology and molecular fingerprint. These findings suggest that patient-derived GPCs are important and clinically relevant.

To decipher the regulatory cues of GPCs, we executed a small molecule screen in high throughput manner, using candidate compounds that targeted various central oncogenic pathways important in GBM growth. Subsequently, upon selection of potential compounds, we refined our approach using neurosphere assays to detect long-term, self-renewal of slow-growing GPCs. These assays are distinct from traditional short-term, viability-based methods used in typical drug screens which often mask the effects of the minority GPCs. It is important to determine that the small molecules target both bulk cells constituting the tumor and GPCs for an effective cure. Using a combination of pharmacological and genetic approaches, we showed that *PLK1* inhibition led to significant reduction in self-renewing spheres (GPC frequency), sphere size (proliferation), and effected G2/M cell cycle arrest with concomitant apoptosis. Additionally, GPCs were induced to differentiation upon BI2536 treatment, suggesting a possible method for inducing tumor involution as a potential treatment strategy. Importantly, when mice bearing subcutaneous tumor xenografts were intravenously treated with BI2536, a well-documented PLK1 inhibitory small molecule currently in clinical trials, tumor volume was significantly reduced compared to vehicle-treated mice. These data

provide strong support that PLK1 regulates GPC survival and consequently tumor growth, and is a viable therapeutic target.

In recognizing the experimental design limitations of patient-derived GPCs, we tapped into bioinformatics analyses utilizing large, independent patient glioma databases: REMBRANDT and Gravendeel. We found that high *PLK1*-coexpressed genes stratified patients for poor survival, independent of current clinical indicators such as age and tumor grade. Interestingly, the high *PLK1*-coexpressed module is enriched in core stem cell programs. Collectively, our findings emphasize the molecular heterogeneity of GBM, and the limitations of diagnosis depending solely on morphology-based histological methods to diagnose and subsequently treat patients. We show that GPCs are clinically relevant and targeting PLK1 serves as a viable therapeutic target.

LIST OF TABLES

LIST OF FIGURES

CHAPTER 1- INTRODUCTION

Brain tumors comprise all tumors arising from within the cranium or central nervous system[1]. These neoplasms can arise from any aberrant cellular proliferation within the brain itself, or even abnormality in lymphatic tissue, blood vessels, meninges or even glands within the skull. While there are over 120 types of brain tumors, the most common and malignant subtypes are represented by gliomas of glial cell origin. Despite advanced surgical intervention and chemotherapeutic treatment with radiation, gliomas such as glioblastoma multiforme (GBM, grade IV) present the worst prognosis, often with a mean survival period of 15 months post-diagnosis. Consequently, there is a need to develop better therapeutic strategies to target the highly aggressive and infiltrative nature of the disease. The recurrent nature of GBM has in recent years been shown to arise from stem-like neural precursor cells[2-4]. These cells display extensive self-renewal capacity and are able to differentiate into all 3 neural lineages (astrocytes, neurons, oligodendrocytes), thus reforming the tumor mass. In addition, they also possess protective mechanisms that endow the cells with chemoresistant and radioresistant traits[5-7]. While neural stem cells and oligodendrocyte progenitor cells have been shown to initiate and sustain tumors using transgenic mouse models[8-10], their cell-of-origin in patient-derived glioma-propagating cells (GPCs) remains unclear. Nevertheless, *in vitro* cultured GPCs remain clinically relevant for several reasons: (i) They contain phenotypic, transcriptomic and karyotypic information that mirrors the original patient tumor[11-12]; (ii) They re-establish orthotopic tumor xenografts that recapitulate the patient's original histopathology; and (iii) GPC-derived gene signatures contribute to disease progression and patient survival outcome independently of current clinical indicators such as age and histology[13-14], thereby underscoring the limitations of relying solely on morphology-based methods to diagnose and subsequently treat patients. These properties make GPCs a very attractive cellular tool for drug screening. However, because GPCs are slow-growing and are often a minority cellular subset, new endpoint measures need to be designed in such drug screens, which routinely rely on short-term viability assays. This forces a re-evaluation of criteria to define GPC activity[15], i.e. they must exhibit long-term self-renewal and the ability to form tumors that phenocopy the original primary tumor. Our work here describes the use of

GPCs in a small molecule screen to identify novel regulatory pathways, and we characterize a candidate gene, *PLK1* as a molecular target. Furthermore, we employ bio-informatical approaches to study the contribution of *PLK1*-associated pathways to patient survival and tumor progression. Collectively, our work sheds light on the role of PLK1 in gliomas.

1.1. Glioma classification

1.1.1. World Health Organization (WHO) grading

Histological grading is a means of predicting the biological behavior of a neoplasm. In the clinical setting, tumor grade is a key factor influencing the choice of therapies, particularly determining the use of adjuvant radiation and specific chemotherapy protocols. The WHO classification of tumors of the nervous system includes a grading scheme that is a "malignancy scale" ranging across a wide variety of neoplasms rather than a strict histological grading system[16-17]. It is widely used, but not a requirement for the application of the WHO classification.

1.1.2. Grading across tumor entities

Grade I applies to lesions with low proliferative potential and the possibility of cure following surgical resection alone. Neoplasms designated grade II are generally infiltrative in nature and, despite low-level proliferative activity, often recur. Some type II tumors tend to progress to higher grades of malignancy, for example, low-grade diffuse astrocytomas that transform to anaplastic astrocytoma and glioblastoma. Similar transformation occurs in oligodendroglioma and oligoastrocytomas. The designation WHO grade III is generally reserved for lesions with histological evidence of malignancy, including nuclear atypia and brisk mitotic activity. In most settings, patients with grade III tumors receive adjuvant radiation and/or chemotherapy. The designation WHO grade IV is assigned to cytologically malignant, mitotically active, necrosis-prone neoplasms typically associated with rapid pre- and postoperative disease evolution and a fatal outcome. Glioblastoma is an example of a grade IV disease. Widespread infiltration of surrounding tissue and a propensity for craniospinal dissemination characterize some grade IV neoplasms.

1.1.3. Grading of astrocytic tumors

Grading has been systematically evaluated and successfully applied to a spectrum of diffusely infiltrative astrocytic tumors. These neoplasms are graded in a three-tiered system similar to that of the Ringertz[18], St Anne-Mayo[19] and the previously published WHO schemes[17]. The WHO defines diffusely infiltrative astrocytic tumors with cytological atypia alone as grade II (diffuse astrocytoma), those also showing anaplasia and mitotic activity as grade III (anaplastic astrocytoma), and tumors additionally showing microvascular proliferation and/or necrosis as WHO grade IV. This system is similar to the St Anne/Mayo classification[19], with the only major difference being grade I; in the WHO system, grade I is assigned to the more circumscribed pilocytic astrocytoma, whereas the St Anne/Mayo classification assigns grade 1 to an exceedingly rare diffuse astrocytoma without atypia. Since the finding of a solitary mitosis in an ample specimen does not confer grade III behavior, separation of grade II from grade III tumors may be more reliably achieved by determination of MIB-1 labeling indices[20-22]. For WHO grade IV, some authors accept only the criterion of endothelial proliferation, i.e. an apparent multi-layering of endothelium. The WHO classification also accepts glomeruloid microvascular proliferations. Necrosis may be of any type; perinecrotic palisading need not be present.

1.1.4. Tumor grade as a prognostic factor

WHO grade is one component of a combination of criteria used to predict a response to therapy and outcome. Other criteria include clinical findings, such as age of the patient, neurologic performance status and tumor location; radiological features such as contrast enhancement; extent of surgical resection; proliferation indices; and genetic alterations. For each tumor entity, combinations of these parameters contribute to an overall estimate of prognosis. Despite these variables, patients with WHO grade II tumors typically survive more than 5 years and those with grade III tumors survive 2–3 years. The prognosis of patients with WHO grade IV tumors depends largely upon whether effective treatment regimens are available. The majority of glioblastoma patients, particularly the elderly, succumb to the disease within a year. For those with other grade IV neoplasms, the

outlook may be considerably better. For example, cerebellar medulloblastomas and germ cell tumors such as germinomas, both WHO grade IV lesions, are rapidly fatal if untreated, while state-of-the-art radiation and chemotherapy result in 5-year survival rates exceeding 60 and 80%, respectively.

1.2. Molecular heterogeneity of gliomas and the application of bioinformatical approaches

In 2006, the National Cancer Institute initiated an effort to deep profile, as one of the first cancers, glioblastoma multiforme, because of its dismal prognosis despite advanced surgical intervention and adjuvant chemotherapy and radiation treatment. This effort is predicated on the belief that histologically similar tumors can be molecularly heterogeneous, and that distinct pathways drive the biological phenotype. The first publication arising from The Cancer Genome Atlas (TCGA) effort showed that patients with GBM sustain mutations that can be grouped into three major signaling networks[23]: Receptor tyrosine kinases (RTKs), p53 and Retinoblastoma tumor suppressor pathways. Importantly, GBM tumors are molecularly heterogeneous, further highlighting the limitations of relying solely on morphology-based histological methods to diagnose and subsequently treat patients. A follow-up study then showed that GBM tumors can be molecularly classified into four subgroups (Proneural, Classical, Mesenchymal, Neural)[24], with each subgroup containing unique gene expression, genomic aberrations and clinical profile. A major inference from such studies is that GBM patients can now potentially be treated according to their molecular subclasses and pathway activation. Indeed, Wiedemeyer *et al*.[25] recently showed through pharmacological targeting in a panel of GBM cell lines that co-deletion of *CDKN2A* and *CDKN2C* served as a strong predictor of sensitivity to a selective inhibitor of CDK4/6. This mapped to similar patterns of *CDKN2A* and *CDKN2C* mutations in TCGA patients, leading to hyperactivated CDK4/6. The Wiedemeyer study thus demonstrates that the integration of genomic, functional and pharmacologic data can be exploited to inform the development of targeted therapy directed against specific cancer pathways. Importantly, the TCGA effort emphasizes that gene expression drives GBM disease progression and patient survival outcome.

In assessing the contribution of GPCs to the primary tumor phenotype, several studies have focused on analyzing common GPC marker expression in tissue paraffin sections, often with ambiguous data. This may be reconciled by the fact that GPC properties that sustain the tumor phenotype may reside in more than just specific marker profiles[4,26-29]. Consequently, pathway activation resembling those functioning in stem-like cells, represented by a set of genes, is more likely to correctly interrogate the clinical contribution of GPCs. An elegant study was carried out by Visvader and colleagues in *BRCA1* mutation-associated breast tumors[30]. The authors derived differentially regulated genes in subsets of epithelial cells and found that luminal progenitors were highly represented in *BRCA1* mutation-associated basal tumors, even more than the commonly anticipated stem cell population. This suggests that luminal progenitors are more likely the cells-of-origin for *BRCA1* mutation-associated breast cancers, later confirmed in a transgenic mouse model study. Such studies underscore the predictive ability of gene expression mapping of pathway activation, rather than focus on a specific marker identity. Separately, John Dick and colleagues recently demonstrated that serial tumor-propagating (and not marker-defined) acute myeloid leukemia stem cells contribute to disease progression and patient survival outcome[31], highlighting the importance of functionally defining the cancer stem cell. Two other more relevant studies demonstrated that GPCs contribute to GBM patient survival outcome, with preferential activation of core stem cell programs (hematopoietic, neural and embryonic stem cells)[14,32]. The key message from such studies is that cancer stem cells perpetuate tumors not merely in terms of their cell numbers, but more accurately reflected by their pathway activation. Consequently, the primary tumor phenotype is a manifest of cancer stem cell behavior and signaling.

1.3. Animal models of glioma

As previously discussed, high-grade gliomas are heterogeneous tumors both at the molecular and cellular levels. The complex biology of these tumors makes understanding glioma pathogenesis and the development of novel effective therapies extremely challenging. While using established glioma cell lines or primary glioma cultures to study glioma biology or test novel drugs *in vitro* can be of some benefit[33-35], these studies lack the ability to address the more complex issues related to gliomagenesis, the role of the tumor stroma and drug pharmacodynamics (i.e., efficacy and toxicity). Over the years, a number of strategies for creating *in vivo* mouse models of glioma have been developed that include tumor cell allograft and xenograft implantation models (Table-1).

Table-1. Mouse models of glioma

	Model	Pros	Cons
Classic human tumor xenografts	Subcutaneous/orthotopic implantation of established human glioma cell lines into athymic rodents	• Low breeding costs • Large numbers of tumor bearing mice can be generated • Bioluminescence monitoring of tumor growth	• Many do not recapitulate human histopathology or molecular character • Tumor-host immunological response is inhibited
Direct to xenograft human tumor implants	Orthotopic implantation of human glioma cells into athymic rodents	• More accurately mimics the response to therapy of human glioma • Histopathologically and moleculary relevant	• Tumor-host immunological response is inhibited
Genetically engineered mouse model (GEMMs)	Mice harboring genetic alterations that allow for gliomagenesis de novo	• Molecular and histologically similar to the human disease • Tumor-host immunological response intact • Several short latency high penetrance models are available • Bioluminescence monitoring of tumor growth	• Extensive breeding cost

1.3.1. Xenograft models

Classic xenograft models are generated by subcutaneously or orthotopically implanting established and commonly serum-grown, human glioma cell lines into athymic mice. Bioluminescence and green fluorescent protein have aided the utility of these models for drug discovery by allowing the visualization of tumors *in vivo*[36-39]. U87MG is one serum-grown, human cell line that has been used extensively because of the high rate of tumor take after implantation and the short survival time. A number of studies have been conducted using U87MG cells to assess the pharmacokinetics and treatment efficacy of a variety of novel therapies[40-41]. While this model provides a straight forward *in vivo* approach to preclinical testing, the major drawback of using cell lines is the lack of histologic similarity to the human disease[42]. These models have been of limited utility in predicting the efficacy of novel therapies in humans when used in preclinical studies[43-44]. Other xenograft models have been developed by taking tumor cells directly from the patient, or GPCs grown in serum-free condition, and implanting them into athymic mice resulting in a more invasive phenotype[2]. Genetically and histologically accurate models of human glioma have also been developed through creating genetically engineered mouse models (GEMMs) which appear to be the best models to date for investigating glioma pathogenesis. GEMMs of glioma can exhibit a similar survival response to therapy as patients and thus may be useful models in preclinical studies[43].

1.3.2. Genetically engineered model of glioma

Carcinogenesis is a process involving serial mutagenic events in genes involved in cell proliferation, survival and invasion. Human cancers primarily occur somatically and the cell type of origin dictates the character of the resulting tumor[45]. GEMMs that possess germ-line modifications of well-established oncogenes are usually heterozygous at the gene locus of interest as homozygous loss is often embryonic lethal. In these models, spontaneous loss of the second allele leads to tumor formation[46-47]. Thus, many germline transgenic models tend to be more reflective of a human tumor predisposition syndrome where the threshold for transformation is lower. Germ-line models can be combined with 'conditional' systems to allow for tumor induction in a temporal-spatial manner[48-49].

The use of the Cre-Lox and RCAS/tv-a systems are two examples of this approach. The Cre-Lox system allows for targeted deletion of a gene flanked by loxP sites (derived from the P1 bacteriophage) within a specific cell type when Cre recombinase is expressed under the control of the tissue-specific promoter. The replication competent avian leukosis virus splice acceptor (RCAS) viral vector can be used to deliver a gene of interest into targeted brain cells when the expression of TVA (avian leukosis virus receptor A; the RCAS receptor) is driven by a tissue-specific promoter[50]. Additionally, mice harboring germline aberrations in tumor suppressor genes such as INK4a/ARF have a decreased threshold for tumor formation and develop high penetrant malignant gliomas when additional tumor inducing lesions are introduced[51]. GEMMs have been developed by over-expressing components of signal transduction pathways that promote cell proliferation and survival. Disrupting normal function of components of the P13K/AKT/mammalian target of rapamycin and RAS/MAPK signaling pathways through aberrations in receptor tyrosine kinases or their ligands (i.e. EGFR and PDGFβ), over-expressing protein kinases (i.e. AKT, RAS) or by loss of tumor suppressors (i.e. NF1, TP53, Rb) can contribute to glioma formation. Although over-expression of AKT and RAS is observed in the human disease, it is not a result of a direct gene effect. Instead, gene over-expression is the result of the activation of upstream receptor tyrosine kinases and their ligands. Perhaps the more relevant models of glioma are those that model the newly identified molecular subclasses of human glioma. Generally speaking, these GEMMs can be considered as accurate models of the signaling abnormalities that occur in human glioma; however, one could argue that they simply confirm causality of tumor formation. It should be noted that even though glioma formation is driven by molecular anomalies that define the human subtypes (i.e., PDGF, EGFR, NF1), it is not yet known to what extent these tumors harbor other molecular characteristics contained in the subclasses that they theoretically represent. Recent gene expression studies of gliomas isolated from GEMMs have revealed that these tumors resemble the human disease at the molecular level[52-53].

1.4. Re-defining assay criteria for detecting GPCs

In our study, we sought to determine signaling pathways that regulate GPC survival, since they would be the most likely culprits of tumor recurrence. Specifically, we looked for compounds that could inhibit these GPCs, cultured *in vitro* as spherical structures. Conventional tumor cell screening typically involves short-term viability readouts of adherent, monolayer cells upon drug treatment. Undoubtedly, the use of serum-grown glioma cell lines facilitates drug screens due to their fast-growing nature. Also, phenotypic screens such as high content screening can be applied to these adherent monolayer cells. However, the use of these serum-grown glioma cells has to be taken with caution as they have been found to possess pronounced phenotypic and transcriptomic differences distinct from their primary tumors[54]. In dealing with GPCs, we recognized that *bona fide* self-renewal in slow-growing cells cannot be accurately detected in short-term viability assays as the latter also measure other transient-amplifying progenitors in the heterogeneous spheres[55]. Consequently, parameters such as sphere number over serial passages which reflects GPC frequency, and sphere size which indicates GPC-specific proliferation are measured. Sphere activity often correlates with *in vivo* tumor-initiating and sustaining capacity, thus is a reliable *in vitro* factor to monitor especially in the subset of GPCs that confer self-renewal with concomitant tumor-propagating ability. The extended period of such screens often complicates the experimental procedure, since regular replenishment of growth factors must take place to sustain the relatively undifferentiated state of GPCs as otherwise, induction of differentiation leads to loss of tumorigenic potential[56]. Additionally, we adapted the sphere assay to measure residual self-renewing activity upon drug removal from the medium over an extended period. This step would indicate if GPC frequency has been altered for a long-lasting inhibition. Of note, we identified several known regulators of GPC maintenance, as well as a potentially novel player, Polo-like kinase 1 (PLK1).

1.5. *PLK1* regulation and physiological role

1.5.1. *PLK1* regulation

PLK1 is involved in multiple roles during mitosis[57-59]. The general protein structure of all members of the Polo-like kinase family consists of an amino-terminal Serine/Threonine catalytic kinase domain and a carboxyl-terminal Polo-box domain (Figure-1). The expression, activity and cellular localization of PLK1 are strictly regulated throughout cell cycle, with its activity peaking during G2/M phase. Accordingly, PLK1 can be regulated at 2 levels; namely at transcriptional level during G_0-G1 phase where *PLK1* expression repressed[60-62], or at protein level[63]. In the regulation of PLK1, published literature has implicated the CDE/CHR (cell-cycle-dependent element/cell cycle gene homology region)[62] and retinoblastoma tumor suppressor (RB) pathway[64]. To-date, the mechanism behind repression of *PLK1* is largely unclear, although published literature has suggested CDF-1 (CDE/CHR binding factor1) in repression *PLK1* transciption[61]. Alternatively, the expression of p53-inducible cell cycle inhibitor $p21^{WAF21/CIP1/SDI1}$ has also been shown to interact with CDE/CHR, leading to transcriptional repression[65].

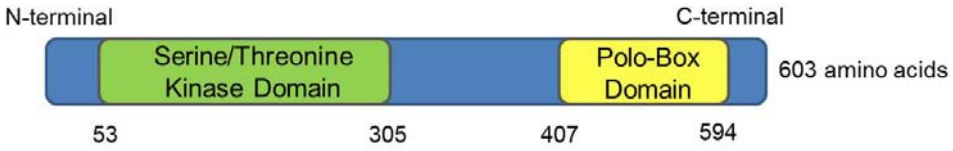

Figure-1. Domains of PLK1 protein. The N-terminal kinase domain spans from amino acid residues 53 to 305 while C-terminal Polo-Box domain spans from residues 407 to 594.

In the Rb pathway, *PLK1* repression is partially dependent on the E2F transcription factor family; specifically, E2F4, a repressor E2F[64]. E2F proteins have been established as important regulators of cell cycle, whereby their interaction with Rb proteins result in G_0-G1 repression of promoters alongside histone deacetylases[66-67]. Furthermore, Rb-mediated suppression of *PLK1* is been found to be dependent on SWI/SNF, a heterogeneous multi-subunit chromatin remodeling complex[64] (Figure-2). It was shown that loss of SWI/SNF does not disrupt the interactions of the Rb pocket

proteins (p107 and p130) and E2F4 at the *PLK1* promoter. Hence, the depletion of SWI/SNF abrogates Rb pathway suppression of *PLK1* in a hierarchical manner whereby: (1) The histone deacetylase fails to be recruited at the promoter, and (2) chromatin remains in the relaxed conformation for continuous transcription.

Another candidate known to positively regulate *PLK1* expression throughout cell cycle is FoxM1 (Foxhead Box M1)[68]. FoxM1 is a known substrate of PLK1 during cell division. The initial activation of FoxM1 is initiated by cyclin dependent kinase 1(CDK1), which enables binding to the polo-box domain (PBD) of PLK1, hence forming a complex where it gets hyperphosphorylated. Subsequently, FoxM1's transcriptional activity is activated and leads to an increase of expression of several mitotic regulators. PLK1 and FoxM1 work synergistically, creating a positive feedback loop which enhances each other's activity.

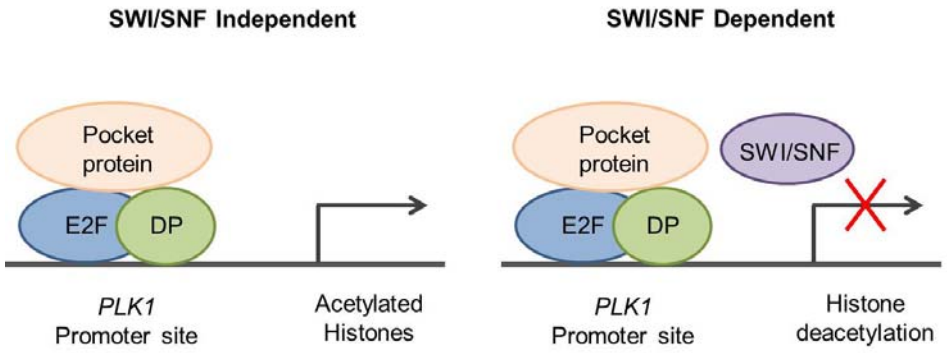

Figure-2. Schematic diagram of *PLK1* transcriptional regulation. In SWI/SNF-deficient cells, E2F4 and pocket proteins can still be recruited to *PLK1* promote while histones remain acetylated and the promoter retains activity. On the contrary, in the presence of SWI/SNF, recruitment of E2F4 and pocket proteins leads to deacetylation at *PLK1* promoter, and therefore promoter repression.

At protein level, PLK1 kinase activity highly depends on the activation of its catalytic domain at the threonine 210 (Thr210) residue[57,63,69]. Under normal circumstances, the structural conformation of PLK1 auto-inhibits itself and its subsequent activation requires cooperation between both Aurora kinase A (AurkA) and Bora. Briefly, the polo-box binding domain (PBD) of PLK1 interacts with its own kinase domain, forming a T-loop that hinders AurkA from accessing Thr210. As Bora binds to the PBD of PLK1, auto-inhibition is relieved and AurkA gains access to initiate phosphorylation on Thr210. Thereafter, PLK1 executes a series of phosphorylation events pertinent to mitosis; for

example, activation of cyclin dependent kinase 1 (Cdk1). Alongside, the activated PLK1 migrates to respective mitotic machinery to take on its role in cell cycle.

1.5.2. Physiological role of PLK1

At the onset of cell division, PLK1 assumes multiple essential roles to maintain normal mitosis (Figure-3). Of note, PLK1 localization is observed to be highly dynamic during cell division. The PBD has been found to be important in localizing the protein[70-71]. Inhibition of PBD using Poloxin, a synthetic derivative of thymoquinone presents severe impacts on cell cycle following mislocalization of PLK1, for instance, chromosome congression defects, mitotic arrest and apoptosis. A brief summary of PLK1's involvement is as follows:

i. M phase entry and G2 DNA checkpoint:

PLK1 initiates mitotic entry by activating Cdc25C[72-73] and inhibiting Wee1/Myt1. This results in the activation the Cyclin B/Cdk1 complex which in turn initiates mitosis. PLK1 activity is known to be inhibited after DNA damage[74]. Some targets of PLK1 involved in this checkpoint includes p53[75] and BRCA2[76] (breast cancer susceptibility protein, essential for DNA repair). Under normal conditions, these proteins are inhibited by PLK1 through phosphorylation. To proceed on, PLK1 activity is essential to repress their inhibition.

ii. Centrosome maturation and bipolar spindle formation:

Centrosome maturation needs PLK1 for the recruitment of various proteins such as γ-tubulin and also its separation to establish proper bipolar spindle[77]. The phosphorylation of the centrosome protein, Nlp by PLK1 is essential for microtubule nucleation, which otherwise, leads to failure in the formation of the mitotic spindle[78]. Also, PLK1 is found to phosphorylate α, β and γ-tubulins and the tubulin-stabilizing protein (TCTP)[79-80]. Collectively, PLK1 is required for establishment of bipolar spindle and regulates the activity of tubulins.

iii. Separation of sister chromatids:

Sister chromatids are kept intact by cohesin[81] till anaphase occurs. The phosphorylation of cohesin by PLK1 occurs twice during mitosis. At prophase (early mitosis), the cohesin subunit, SA2, is phosphorylated to allow dissociation from chromosome. Later on at the metaphase-anaphase juncture, PLK1 phosphorylates the cohesin subunit, Scc1, hence aiding its cleavage by separase.

iv. Chromosome alignment and kinetochore function:

PLK1 has been implicated in chromosome alignment as its mislocalization causes incomplete lining-up of chromosomes at the metaphase plate[82]. Furthermore, PLK1 has been shown to be involved in the stabilization of microtubule-kinetochore interactions and also the recruitment of kinetochore proteins such as Hec1/Ndc80 which aids in the attachment of microtubules to kinetochore at metaphase[83].

v. Activating Anaphase Promoting Complex/cyclosome (APC/C) and cytokinesis:

APC/C, an E3 ubiquitin ligase, is activated at metaphase-anaphase juncture once spindle checkpoint is cleared with proper alignment of chromosomes at the metaphase plate and attached to microtubules. PLK1 activates APC/C by two ways: (1) Phosphorylating subunits of APC/C, and (2) inducing destruction of Emi1, an APC/C inhibitor. The active APC/C promotes exit of cell division by initiating degradation of Cyclin B/Cdk1, also, by releasing separase that aids in sister chromatid separation.

At cytokinesis, PLK1 activity is important for proteins such as NudC (nuclear distribution gene C), MKlp2 (myosin kinase like protein 2) and RhoGEF ECT2 (Rho guanine nucleotide exchange factor ECT2) as its depletion results in cytokinesis failure, leading to multinucleated cells[70,84-85].

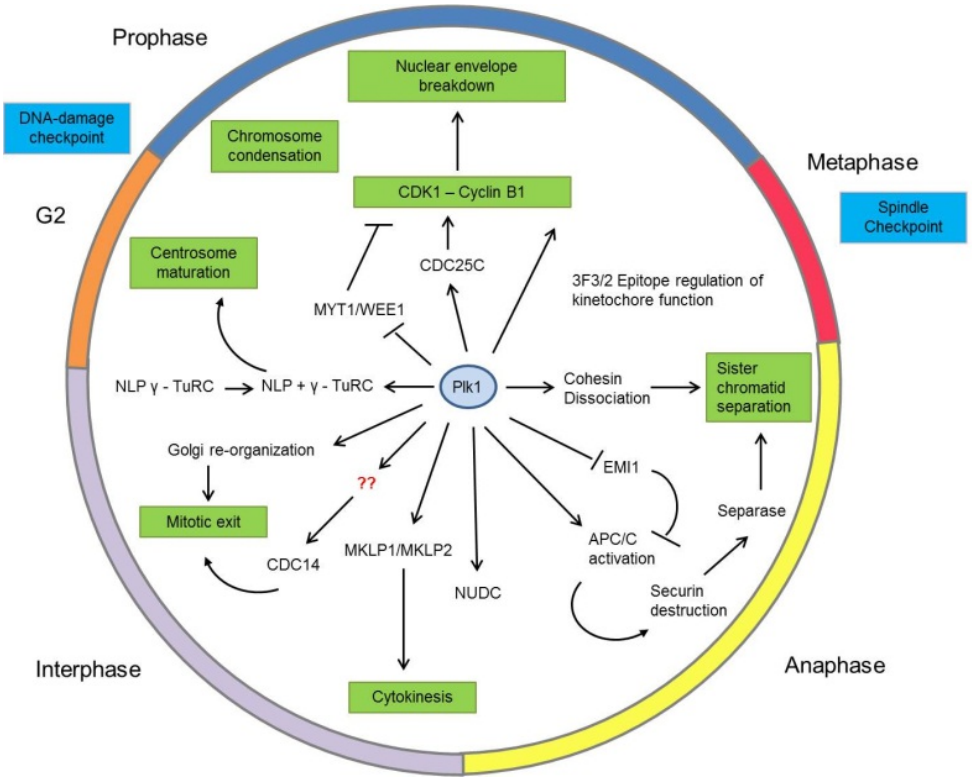

Figure-3. Schematic diagram illustrating the multiple roles of PLK1 during cell division. PLK1 activity is important at the various phases of mitosis to ensure proper cell division. It also serves as gatekeeper at both G2/M phase DNA-damage checkpoint and spindle checkpoint.

1.5.3. PLK1 and tumors

Elevation of PLK1 has been reported in several forms of cancers[86-91] and its upregulation has been proposed as a negative prognostic factor of the disease[92-94]. Given that PLK1 is heavily involved in mitosis, deregulation of PLK1 would inevitably result in mitotic catastrophe with the formation of multinucleated cells. Initial work has presented low levels of *PLK1* mRNA in mature cells such as the heart, lung, brain, liver, kidney, pancreas and skeletal muscles[95]. On the contrary, mitotically active normal cells derived from the colon and placenta show higher expression of *PLK1*, hence highlighting that only proliferating cells possess elevated *PLK1* levels. Subsequently, *Smith et al.*[96] demonstrated the malignant transformation of normal NIH 3T3 cells with over-expression of PLK1. Furthermore, PLK1 is also known to inhibit the p53 tumor suppressor via phosphorylation, therefore repressing the activation of p53-mediated apoptosis. Collectively, these observations support the notion of over-expression of PLK1 as a cause of tumorigenesis, instead of the effect of tumorigenesis.

Alternatively, PLK1 depletion potentially results in tumorigenesis too. Previously, missense mutations of PLK1 within its PBD were found to disrupt the interaction between PLK1 and HSP90[97]. HSP90 is a molecular chaperon vital for protein folding[98]. As a result, PLK1 expression is reduced due to instability of its mutant protein. Consequently, the PLK1 depletion inevitably contributes to mitotic defects and ultimately leading to tumorigenesis.

1.6. Scope of study

1.6.1 Hypothesis

We hypothesize that GPCs can be eradicated by targeting their regulatory pathways, resulting in tumor involution and long-lasting inhibition. Patients who demonstrate activation of such regulatory pathways through genomewide transcriptomic changes correlate with poor prognosis, and are likely more amenable to such pathway inhibitory small molecules.

1.6.2 Objectives

We will present a case study of a small molecule screen conducted with GPCs and explain how unique sphere activity assays were implemented to distinguish drug efficacies against the long-term, self-renewing fraction, as opposed to transient-amplifying progenitors, latter of which are detected in conventional viability assays. We identified Polo-like kinase 1 as a novel regulator of GPC survival. Finally, we will leverage on public glioma databases to illustrate GPC contribution to disease progression and patient survival outcome. Our study sheds light on the role of PLK1 in maintaining the brain tumor stem cell population, and combines bioinformatical approaches to interrogate PLK1-associated biological pathways in clinical databases. We provide evidence to illustrate GPC contribution to disease progression and patient survival outcome.

CHAPTER 2 - MATERIALS AND METHODS

2.1. Cell culture

2.1.1. Tissue collection and GPC neurosphere culture

Graded clinical brain tumor specimens (NNI-1, 4, 5, 8, and 12) were obtained through informed consent as part of a study protocol approved by the institutional review board. In this study, NNI-1 was from a patient with recurrent GBM (Grade IV) and had received radiation therapy, while NNI-4 and NNI-5 were from patients with primary GBM and treatment-naïve. Tumor samples were processed using methods established in our previous work[99]. Cells were seeded as free-floating spheres at a density of 2,500 cells per cm^2 in chemically defined serum-free selection growth medium consisting of basic fibroblast growth factor (bFGF, 20 ng/ml, PeproTech, New Jersey), epidermal growth factor (EGF, 20 ng/ml, PeproTech), heparin (5 μg/ml; Sigma-Aldrich, St Louis), and serum-free supplement (B27, 1x, Gibco, Grand Island, NY) in a 3:1 mix of Dulbecco's modified Eagle's medium (DMEM; Sigma-Aldrich) and Ham's F-12 Nutrient Mixture (F-12, Gibco). Also, final concentrations 100 Units/ml Penicillin-Streptomycin, 1 mM Non-Essential Amino Acid (NEAA, Gibco) and 1 mM Sodium Pyruvate (Gibco) were added. The cultures were incubated at 37°C in a water-saturated atmosphere containing 5% CO_2 and 95% air. To maintain the undifferentiated state of neurosphere cultures, growth factors were replenished every 2-3 days. Cultures were expanded by mechanical trituration using flame-drawn glass Pasteur pipettes, and cells were re-seeded at 100,000 cells per millilitre in fresh medium supplemented with growth factors.

2.1.2. ATCC glioma cell cultures

Human glioma cell lines (U251, T98G and U87-MG) and mouse astrocyte (C8-D1A) were purchased from ATCC (American Type Cell Culture, California, USA). Cells were maintained as adherent monolayer cultures in DMEM supplemented with 10% Fetal Bovine Serum (FBS, Gibco), together with Penicillin-Streptomycin, NEAA and Sodium Pyruvate.

Lenti-X 293T, a sub-clone of the transformed human embryonic kidney cell line, HEK 293, was purchased from Clontech (Clontech, California, USA). Cells were maintained as adherent monolayer cultures in DMEM supplemented with 10% FBS (Gibco) and 1mM Sodium Pyruvate (Gibco). The cultures were incubated at 37^{o}C in a water-saturated atmosphere containing 5% CO_2 and 95% air.

2.1.3. Normal Human Astrocytes (NHA) and Normal Human Neural Progenitor (NHNP)

Both NHA and NHNP were purchased from Lonza (Lonza Incorporation; Allendale, New Jersey, USA). NHA cells were maintained as adherent monolayer cultures with Clonetics™ Astrocyte Cell System (Lonza), a serum-based culture condition, according to manufacturer's instruction. NHNP cells were maintained as suspension cultures in Poietics™ Neural Progenital Cell System (Lonza), which is serum-free culture condition, according to manufacturer's instruction. The cultures were incubated at 37^{o}C in a water-saturated atmosphere containing 5% CO_2 and 95% air.

2.2. Cell viability assay

2.2.1. Determining half inhibitory concentrations (IC_{50}) of BI2536

BI2536 was purchased from Chemietek (Indianapolis, USA). GPC neurospheres were dissociated with Accutase™ (eBIOscience Inc., San Diego) and seeded into 96-well plates, at a density of 2,000 cells per well, with DMEM/F12 medium supplemented with growth factors. The neurospheres were allowed to recover over 3-4 days prior to drug treatment. For ATCC glioma lines, cells were seeded at a density of 662 cells per well into 96-well plates and allowed to recover overnight prior to treatment. Cell viability after drug treatment was assessed using alamarBlue® (Serotec, Oxford, UK). Briefly, cells were incubated with 10% culture volume of alamarBlue® for approximately 16 hours before absorbance readings were measured at 570 and 600 nm. Dose response curves for each line were generated using GraphPad Prism (GraphPad Software Inc., USA) and IC_{50} were computed from 12-point titration curves ranging from 10^{-4} to 10^{2} μm.

2.2.2. High-throughput Screen

GPC neurospheres were dissociated with Accutase™ (eBIOscience Inc.) and seeded into 96-well plates, at a density of 10,000 cells per well, with DMEM/F12 medium supplemented with growth factors. Cells were allowed to recover over 3-4 days prior to compound addition at 10 μm in HTS I or 0.1 μm HTS II respectively. Cell viabilities after drug treatments were assessed using alamarBlue® (Serotec).

2.2.3. Viability of cells after sh*PLK1* transduction

GPC neurospheres transduced with sh*PLK1* constructs were selected-out by replacing spent media with fresh complete media consisting 2 μg/ml puromycin (Sigma-Aldrich) at 72 hours after lentiviral transduction. Neurospheres were dissociated with Accutase™ (eBIOscience Inc.) after 48 hours of selection, stained with 7-Amino-Actinomycin Viability Dye D (7-AAD; BD Pharmingen™; USA), and seeded into 96-well plates, at a density of 2,000 live cells per well using BD FACSAria™ (BD Biosciences; New Jersey; USA) cell sorter. Thereafter, cell viability was assessed using alamarBlue® (Serotec) at Day 10 and 20 after lentiviral transduction.

ATCC glioma cell lines were lentivirally transduced for 48 hours prior to replacement with fresh media containing 2 μg/ml puromycin (Sigma-Aldrich). After 48 hours of puromycin selection, cells were harvested and re-seeded into 96-well plates at a density of 662 cells per well. Thereafter, cell viability was assessed by means of alamarBlue® (Serotec) at Day 5 and 10 after lentiviral transduction.

2.2.4. Viability assessment after PLK1 overexpression

Lentiviral transduced GPCs were subjected to cell sorting based on mCherry fluorescence, at a density of 2,000 cells per well. Cells were allowed to recover for 1 day prior to BI2536 (Chemietek) treatment. Thereafter, viability of cells were assessed using alamarBlue® (Serotec) at Day 3 post-drug treatment.

2.3. Western blot analysis

Cells were harvested and pelleted prior to lysis with lysis buffer [1x Igepal (Sigma Aldrich), 10% glycerol (Sigma Aldrich), 2 mM EDTA, 0.15 M NaCl, 50 mM Tris-HCl pH 7.2, Complete Mini Protease Inhibitor Cocktail Tablets (Roche; Indianapolis; USA), Phostop Phosphatase Inhibitor Cocktail Tablet (Roche)]. Approximately 40 µg of heat denatured protein lystates were resolved on 8% SDS polyacrylamide gel, transferred to polyvinylidene difluoride (PVDF) membrane (Millipore, Darmstadt, Germany), and probed with the following primary antibodies: anti-PLK (1:1000, Life Technologies, #37-700), anti-tubulin, beta III isoform (TuJ1, 1:1000, Millipore, MAB1637), anti-Glial Fibrillary Acidic Protein (GFAP, 1:4000, Dako, Denmark, Z0334) and β-actin antibody (1:20000, Sigma Aldrich, AC-15). Goat anti-mouse horseradish peroxidase (HRP)-conjugated secondary antibody (1:10000, ECL Amersham Biosciences, Buckinghamshire, UK) or goat anti-rabbit horseradish peroxidase (HRP)-conjugated secondary antibody (1:10000, ECL Amersham Biosciences, Buckinghamshire, UK) were used. All antibodies were diluted in blocking buffer [5% bovine serum albumin (PAA, Germany), 10 mM Tris-HCl pH 7.4, 100 mM NaCl, 0.1% Tween® 20 (Merck)]. Protein bands were visualized using chemiluminescence detection kit, SuperSignal West Pico (Thermo Scientific, Rockford, USA) or SuperSignal West Femto (Thermo Scientific) according to the manufacturer's instructions. Visualization of protein bands was done using a digital imaging system, SYNGENE G-Box, iChemXT. Protein expression was quantitated using Quantity One® software (Bio-Rad Laboratories, California, USA), normalized against actin levels.

2.4. Immunoprecipitation and kinase assay

Protein lysates were pre-cleared by incubating 1 mg of protein with sepharose beads (Protein A-Sepharose®; Zymed Laboratories Inc,, San Francisco; USA) for 30 minutes. Thereafter, protein lysates were incubated overnight with agitation at 4°C using 5 µg anti-Plk1 antibody (Life Technologies). Fresh sepharose beads were then added to the protein-antibody mixture and incubated at 4°C with agitation for another 3 hours for protein-antibody complex to bind to the beads. Sepharose beads were collected and washed 5 times with lysis buffer and finally, once with kinase assay buffer.

PLK1 kinase activity was determined using Z'LYTE™ Kinase Assay Kit (Life Technologies) that utilized Fluorescence Resonance Energy Transfer (FRET) between coumarin and fluorescein (FITC) of the peptide-based substrate. Reactions and quantitation were performed accordingly to manufacturer's instruction.

2.5. Flow cytometry analysis

Neurospheres were dissociated with Accutase™ (eBioscience), and blocked with FcR blocking reagent (Miltenyi Biotec, Bergisch Gladbach, Germany). For stemness analysis, cells were stained according to manufacturers' instructions with anti-CD133/2-allophycocyanin (Clone 293C, 1:10 Miltenyi Biotec, #130-090-854), anti-CD15 (1:10, BD Biosciences, #347423), anti-Nestin (1: 1000, Millipore, Massachusetts, USA, MAB5326). Aldehyde Dehydrogenase activity was determined using the AldeFluor™ kit (Stem Cell Technologies, Vancouver, Canada) according to manufacturer's instructions. For ascertaining apoptosis, cells were stained with anti-cleaved-PARP (1:10, BD Biosciences, #552933). A total of 10,000 events were acquired on FACSCalibur instrument (BD Biosciences). Data were analysed using FlowJo software (Tree Star; Ashland, OR).

2.6. Flow sorting of GPCs

To isolate GPCs based on their CD133 status, neurospheres were harvested and dissociated with Accutase™ (eBioscience), and blocked with FcR blocking reagent (Miltenyi Biotec), and stained with anti-CD133/2-allophyocyanin (Clone 293C, 1:10 Miltenyi Biotec, #130-090-854) and 7-AAD viability dye (BD Pharmingen™) prior to cell sorting using BD FACSAria™ (BD Bioscience). For mCherry-expressing GPCs, neurospheres were dissociated and stained with 7-AAD viability dye prior to sorting.

2.7. Tumor neurosphere assay

For each GPC line, cells were sorted based on CD133 status using BD FACSAria™ (BD Bioscience). Thirty live cells were seeded per well in 96-well plate. Cells were sorted based on their CD133 status. Each well contained DMEM/F12 culture medium supplemented with growth factors. Cells were allowed to recover for 3-4 days, then treated with DMSO or BI2536 (Chemietek), and maintained until 21 days post-treatment at 37^{o}C, in 5% CO_2 humidified incubator. Drugs and growth factors were replenished twice a week. Neurosphere number and size were determined at day 7, 14 and 21 respectively. A *bona fide* neurosphere is defined as a single sphere of diameter exceeding 20 μm. Scoring and diameter measurements were performed using Nikon Eclipse Ti Microscopy, accompanied with digital camera (DS-Qi1) and NIS-Element Imaging Software (Nikon Instruments Inc., New York, USA).

For evaluation of long-term BI2536 inhibition, 30 cells were seeded per well of 96-well plate with fresh media supplemented with only growth factors. Replenishment of growth factors was done twice weekly. Neurosphere number and their size were determined at day 7, 14 and 21 post-drug removal.

2.8. Cell cycle analysis

Cells were harvested and fixed in cold 70% ethanol. Subsequently, cells were stained with cocktail consisting 4 μg/ml Propidium Iodide (Sigma-Aldrich) and 100 μg/ml RNase A (Sigma-Aldrich). Data acquisition was performed using FACSCalibur instrument (BD Biosciences) and analysed using FlowJo software (Tree Star).

2.9. Imunofluorescence analysis

Neurospheres were dissociated enzymatically and seeded on laminin-coated (Sigma-Aldrich) 8-well culture slides (BD Biosciences) at a density of 1.5 x 10^4 cells per well. Cells were fixed with 4% paraformaldehyde (Sigma-Aldrich) for 10 minutes, permeabilized with 0.1% Triton X-100 (Sigma-Aldrich) for 10 minutes, blocked with 5% FBS for 1 hour and stained for the following

markers: Nestin (1:300, Chemicon, MAB5326), Oct4 (1:100, Santa Cruz Biotechnology Inc., California, USA, H-134), Musashi-1 (1:100, Chemicon, AB5977), TuJ1 (1:200, Chemicon, MAB5326), GFAP (1:4000, Dako, Z0334), and oligodendrocyte marker (O4; 1:50, Chemicon, MAB345) . Secondary detection antibodies conjugated to Alexa-Fluor 488 or 594 (1:200, Molecular Probes, Life Technologies) were used. Finally, the culture slides were mounted with Vectashield® mounting media with DAPI (4,6-diamidino-2-phenylindole) (Vector Laboratories Inc., California, USA). Images were acquired with Olympus Fluoview 1000 confocal microscope (Olympus American Inc., Pennsylvania, USA).

2.10. Differentiation of GPCs with BI2536

GPCs were rescreened in a similar fashion as the initial high throughout screen. Concentrations that induced signs of differentiation in each GPC lines were determined and subsequent immunofluorescence analysis were performed using that concentration. GPCs were dissociated and seeded on laminin-coated (Sigma-Aldrich) 8-well culture slides (BD Biosciences) at a density of 1.5 x 10^4 cells per well. The media was removed and replaced with fresh media containing either DMSO or BI2536 at the concentration that induced differentiation. Fresh media with drugs were replaced every 4 days. At Day 10 post-treatment, cells were fixed with 4% paraformaldehyde and subjected to immunofluorescence analysis as described above. Scoring was performed using images captured on Nikon Eclipse Ti Microscope (Nikon Instruments Inc.).

2.11. Lentiviral transduction

PLK1 knockdown was achieved through pLKO.1-based vectors purchased from Open Biosystems (sh*PLK1* #1: TRCN0000006247; #2: TRCN0000121074, TurboGFP positive control vector: SHC003, Non-target shRNA control: SHC002). Viral particles were packaged using the Lenti-X™ HTX Packaging System according to manufacturer's instruction (Clontech). Virus titer of

supernatant collected was determined using Lenti-X™ p24 Rapid Titer Kit (Clontech) according to manufacturer's instructions.

PLK1 overexpression was achieved by utilizing pReceiver-mCherry or pReceiver-mCherry-*PLK1* lentiviral vectors (GeneCopoeia Inc., Maryland, USA). Viral particles were packaged using GeneCopoeia Lenti-Pac™ FIV Expression Packaging Systems (GenCopoeia Inc.) while virus titer was determined with Quicktiter™ Lentivirus Quantitation kit (Cell Biolabs Inc., San Diego, USA), according to manufacturer's instruction.

2.12. *In vivo* subcutaneous flank model of Balb/c nude mice

Mice were handled according to the guidelines of the Institutional Animal Care and Use Committee, National Neuroscience Institute, Singapore. Approximately 2 million U87 glioma cells in 200 μL of Phosphate Buffered Saline (PBS) were subcutaneously injected into the right flank of 6-8 weeks old, female Balb/C nude mice (Animal Resource Center, Australia). Tumor dimensions were measured every 2 days using a vernier caliper, and the respective volumes were calculated using the following formula: Length x (Width^2) x $\pi/6$. Mice were randomly put into 2 treatment groups; with saline control or BI2536 (Chemietek) treatment, at 50 mg/kg, 10 mL/kg body mass. BI2536 was reconstituted in 0.1N HCl diluted with 0.9% NaCl. Treatments were initiated when tumor volumes reached 0.5 cm^3. For each treatment cycle, mice were given injections on 2 consecutive days per week. Maximum duration spanned 4 cycles from initiation of treatment. Tumor xenografts were harvested from mice at various cycles and paraffin wax-embedded for further analysis.

2.13. Stereotaxic intracranial implantation of NOD-SCID gamma (NSG) mouse

Animal experimentation was performed according to protocols approved by the Institutional Animal Care and Use Committee. Implantations were carried out as previously described[99] using NOD.Cg-*Prkdcscid Il2rgtm1Wjl*/SzJ NOD-SCID gamma mice (The Jackson Laboratory). The following coordinates were used: antero-posterior, +1.0 mm; medio-lateral, +2 mm; dorso-ventral, -2.5 mm. Mice were euthanized by means of transcardiac perfusion with 4% paraformaldehyde upon

presentation of neurological deficits with ataxia, cachexia, lethargy or seizure. Hematoxylin-and-eosin (H&E) staining and immunohistochemistry were performed on 5 μm-thick paraffin sections.

2.14. Karyotypic analysis of tumor neurospheres (conducted by Dr. SH Leong and A/Professor OL Kon, National Cancer Centre)

Two million cells from dissociated neurospheres were cultured in T-25 flask (BD Biosciences). The cells were then treated within 3-5 days with 0.1 μg/ml colcemid (Life Technologies) for 24 hours. Metaphase-arrested cells were pelleted (180 g for 10 minutes) and treated with hypotonic solution of 0.075 M potassium chloride. Chromosomes were fixed in methanol:acetic acid (3:1) , re-centrifuged and resuspended in fixative. Twelve μl of the fixed cell suspension was dropped on a clean, moistened glass slide and placed on a hot plate at 48^{o}C to obtain chromosome spreads. Spectral karyotyping (SkyPaint, Applied Spectral Imaging, Israel) was performed on metaphases according to the manufacturer's instructions.

2.15. Immunohistochemical staining of tumor tissues

Both orthotopic and flank xenografts from mice were fixed in 4% paraformaldehyde, embedded in paraffin wax (Microm AP280-2, Zeiss), and sectioned (4 μm) using a microtome (Microm HM360, Zeiss). Hematoxylin and eosin (H&E) staining was performed as described in our previous work[99]. For antibody staining, we adapted protocols from Gritti *et al.*[100]. Briefly, sections were mounted on poly-L-lysine coated slides and subsequently processed for heat-induced epitote retrieval. Sections were blocked with 5% goat serum for 1 hour at room temperature and stained with Nestin (Chemicon, MAB5326) antibodies overnight, followed by incubation with HRP-conjugated secondary antibodies. Detection was performed using the ChemMate Detection Kit (Dako); a positive reaction was indicated by brown coloration using DAB (3,3'-Diaminobenzidine), and counterstained with hematoxylin. TUNEL assay was executed according to manufacturer's instructions (Millipore).

2.16. Microarray data acquisition of tumor neurospheres

For each sample, total RNA was isolated from neurosphere cells using TRI Reagent (Molecular Research Center, Cincinnati, OH). Thereafter, RNA samples were hybridized to Affymetrix GeneChip® Human Genome U133 Plus 2.0 Array using 3' IVT express kit (Affymetrix Inc, Santa Clara, California). Data was deposited at private reviewer URL: http://www.ncbi.nlm.nih.gov/geo/query/acc.cgi?token=ztaxraywcqwkcbo&acc=GSE36782

2.17. Bioinformatics analysis on public datasets (conducted by Edwin Sandanaraj, Singapore Institute for Clinical Sciences, A*STAR)

Since brain tumors are driven by gene expression[24], we sought to determine *PLK1*-associated pathway networks by tapping into 2 public glioma datasets, REMBRANDT[101] and Gravendeel[102]. Raw cel files were downloaded from REMBRANDT application and gene expression omnibus (GEO) databases (GSE16011). The probe signals were processed using mas5 algorithm and non-exonic probes were removed. The probeset signals were consolidated to derive a unique gene-wise matrix as described in the genefilter package from R/bioconductor[103]. Briefly, the pre-processing approach restricted for probesets having entrez gene identifier and assigned the highest signaling probeset for the genes with multiple probesets. Pairwise interaction for the genes was measured using a rank-based correlation method. The *PLK1* co-expressed genes were selected based on a cut-off coefficient (r_s) of +/- 0.5. The same strategy was applied to both glioma datasets and the *PLK1* co-expressed genes with consensus were selected as the *PLK1* co-expressed gene module. The *PLK1* co-expressed gene module was allowed to self-cluster among the glioma patients and the stratification pattern was dissected using cutree option in R. The self-clustered patient groups based on the *PLK1* gene module were correlated for the survival pattern using the log-rank test. A Cox Regression model accounting for critical clinical covariates (age and histology) was built to assess the independent association of *PLK1*-based subgroups and survival. All statistical analyses were performed using R/bioconductor packages.

2.18. Pathway analysis (conducted by Edwin Sandanaraj, Singapore Institute for Clinical Sciences, A*STAR)

The biological relevance of the *PLK1* co-expressed module was investigated by 2 different approaches. Metacore from GeneGo was explored to identify the significantly enriched biological pathways. Pathways with significant enrichment P-values of less than 0.05 were reported as significantly enriched networks. In addition, we used Gene Set Enrichment Analysis (GSEA) to test the gene module with the molecular signature database using GSEA tool downloaded from the Broad Institute portal[104]. We pre-selected 181 genesets related to stemness behaviour from the molecular signatures database (MSigDB)[105]. The *PLK1* co-expressed gene module was tested for the enrichment with stemness signature gene sets. The significantly enriched associations were summarized as enrichment and the statistical scores were reported. A FDR cut-off of less than 25% was selected.

2.19. Quantitative real-time reverse transcription polymerase chain reaction

Extraction of RNA of NHA, NHNP and GPCs (NNI-1, 4, 5, 8 and 12) was performed using TRI Reagent® (Life Technologies) according to manufacturer's instruction. Following on, approximately 5 µg of RNA was converted to cDNA using Superscript III First-Strand Synthesis System (Life Technologies). Subsequently, quantitative real-time reverse transcription polymerase chain reaction (qRT-PCR) was carried out using Power SYBR Green PCR Master Mix (Applied Biosystems, Life Technologies) together with a standardized amount of 25 ng cDNA for each sample. The cycle parameters on ABI 700HT (Applied Biosystems) were 40 cycles of 95^{o}C of 30 seconds, 55^{o}C at 30 seconds and 72^{o}C at 30seconds. Each qRT-PCR was performed in triplicates and the expression of each gene was determined relative to the normalizer gene Hypoxanthine-guanine phosphoribosyltransferase (HPRT). Primer sequences are described on page 120, Supplementary Table-4.

2.20. Mutational analysis of TP53 at codon 72

Genomic DNA from NHA, NHNP and GPCs (NNI-1, 2, 4, 5, 8, 11, 12 and 14) were extracted using DNeasy Blood and Tissue Kit (Qiagen, Duesseldorf, Germany). The genetic variation in codon 72 in exon 4 of the *p53* gene was determined first by polymerase chain reaction (PCR) followed by BstU1 restriction enzyme digestion. Briefly, 100 ng of genomic DNA was used in PCR with 40 cycles of 95^{o}C of 30 seconds, 58^{o}C at 30 seconds and 72^{o}C at 1 minute. Thereafter, PCR products were purified using QIAquick PCR purification kit (Qiagen) and subjected to 1 hour of BstU1 digestion at 60^{o}C. After digestion, DNA electrophoresis was done on 2% agarose gel for analyses.

2.21. Statistical Analysis

Data are expressed as means ± SD (standard deviation) or SEM (standard error of mean) of at least three independent experiments. Student's *t*-test of the Mann-Whitney *U* test was used where appropriate. Values of $p \leq 0.05$ were taken as statistically significant.

CHAPTER 3: PLK1 AS A CANDIDATE REGULATOR OF GLIOMA-PROPAGATING CELL GROWTH

3.1. GPCs phenocopy the primary tumor

Several works have previously shown that GPCs cultured as spherical structures in serum-free medium supplemented with growth factors contain phenotypic, transcriptomic and karyotypic profiles that mirror the patient's original tumor[11-12]. Moreover, GPCs can be stably maintained by *in vivo* serial passage in immune-compromised mice[2]. However, it is unclear if GPCs contribute directly to disease progression and patient survival outcome. If so, it would be crucial to determine GPC regulatory pathways so as to design better therapeutics to effectively target the slow-growing but essential tumor-initiating and sustaining fraction.

In our study, we first verified our GPC collection according to our previous publication[99]. Essentially, we showed that GPCs re-establish orthotopic xenograft tumors that recapitulate the patient's original histopathology, including the presentation of pseudopalisading cells interspersed with areas of necrosis and vascularization (Figure-4A). In addition, these cells contain karyotypic hallmarks commonly found in the original tumor, such as amplification of chromosome 7 (where epidermal growth factor receptor lies) and deletion of chromosome 10 (where *PTEN* lies) (Figure-4B). Since large genomic efforts such as The Cancer Genome Atlas[23] and REMBRANDT[101] have demonstrated that brain tumors can be molecularly classified, we sought to characterize our GPCs molecularly by: (i) Relying on a previous GPC molecular classification scheme[106], and (ii) Determining the subgroup of our GPCs together with other investigators' GPCs. This approach would offer the advantage of profiling a larger and unique collection of GPCs with insight to their relation to the original primary tumor. Accordingly, we applied the molecular classification scheme in Lottaz *et al*.[106] and assessed our GPCs with that of Gunther *et al*.[107] and Pollard *et al*.[108]. Our data showed that our GPCs could be grouped into Proneural (NNI-1 to 5, 8, 12, 13) and Mesenchymal (NNI-9 to 11) classes (Figure-4C). The knowledge of such classes is important because they are enriched in distinct signaling pathways, thus targeting these pathways may offer therapeutic benefit by eradicating GBM

at its root. For example, Mesenchymal GPCs are typified by the TGFβ response pathway[106,109], latter previously shown to maintain GPC survival and tumor-propagation[110-111], and for which several TGFβ signaling inhibitors are in clinical trials[112]. Our findings validate our GPC collection.

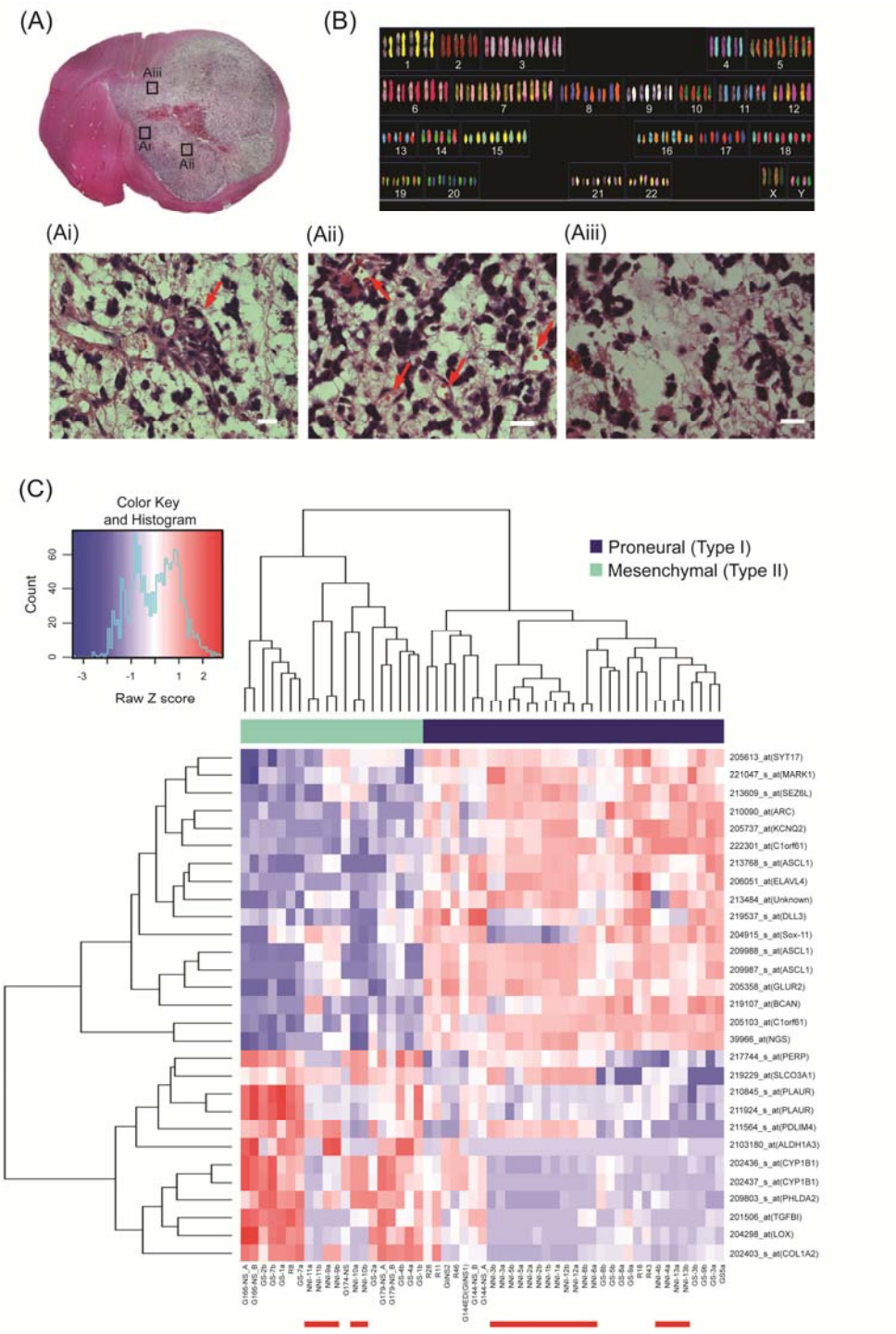

Figure-4. GPCs cultured in serum-free condition retain primary tumor phenotype. (A) Tumor xenografts phenocopied the patient's original histopathology. Notably, **(i)** pseudopalisading cells interspersed with areas of **(ii)** vascularisation and **(iii)** necrosis were observed. **(B)** Cytogenetic analysis revealed retention of glioblastoma karyotypic hallmark; of note, amplification of chromosome 7 and loss of chromosome 10. **(C)** A 24-gene signature derived from Lottaz *et al*. classified our GPC collection (underlined with red), along with several other groups GPCs, into 2 molecular subtypes – Proneural and Mesenchymal.

3.2. Small molecule screen identifies inhibitors of GPC proliferation

To identify regulators of GPC survival, we adapted the screen design of Diamandis *et al.*[113] Briefly, to facilitate an initial, higher throughput screen of 50 small molecules targeting various oncologic pathways accessed from Eli Lilly pharmaceutical company, we carried out 2 steps: (i) We assayed for viability after 5 days of treatment with compounds at 10 μM using 4 GPC lines (Figure-5A). Compounds that reduced viability by more than 80% were subjected to, (ii) A second screen conducted at 0.1 μM compound (Figure-5B). We then prioritized candidates that showed selectivity ratios > 2 in at least 1 GPC line (Table-2). The selectivity ratio represents % viability in normal mouse astrocytes (C8-D1A) / % viability in GPC; consequently a higher ratio reflects selectivity of GPC over normal astrocytic cells, latter of which characterizes the predominant cell type in glioma. Mouse astrocytes were utilized as fetal cells of human origin posed ethical issues for Eli Lilly. Notably, 3 compound classes were identified that have already been implicated in GPC survival, thus validating our screening method; PI3K/AKT, GSK3β, CDK1, 9 and TAK1 inhibitors[114-115]. Interestingly, a compound targeting PLK1 emerged, potentially identifying PLK1 as a novel regulator of GPC survival.

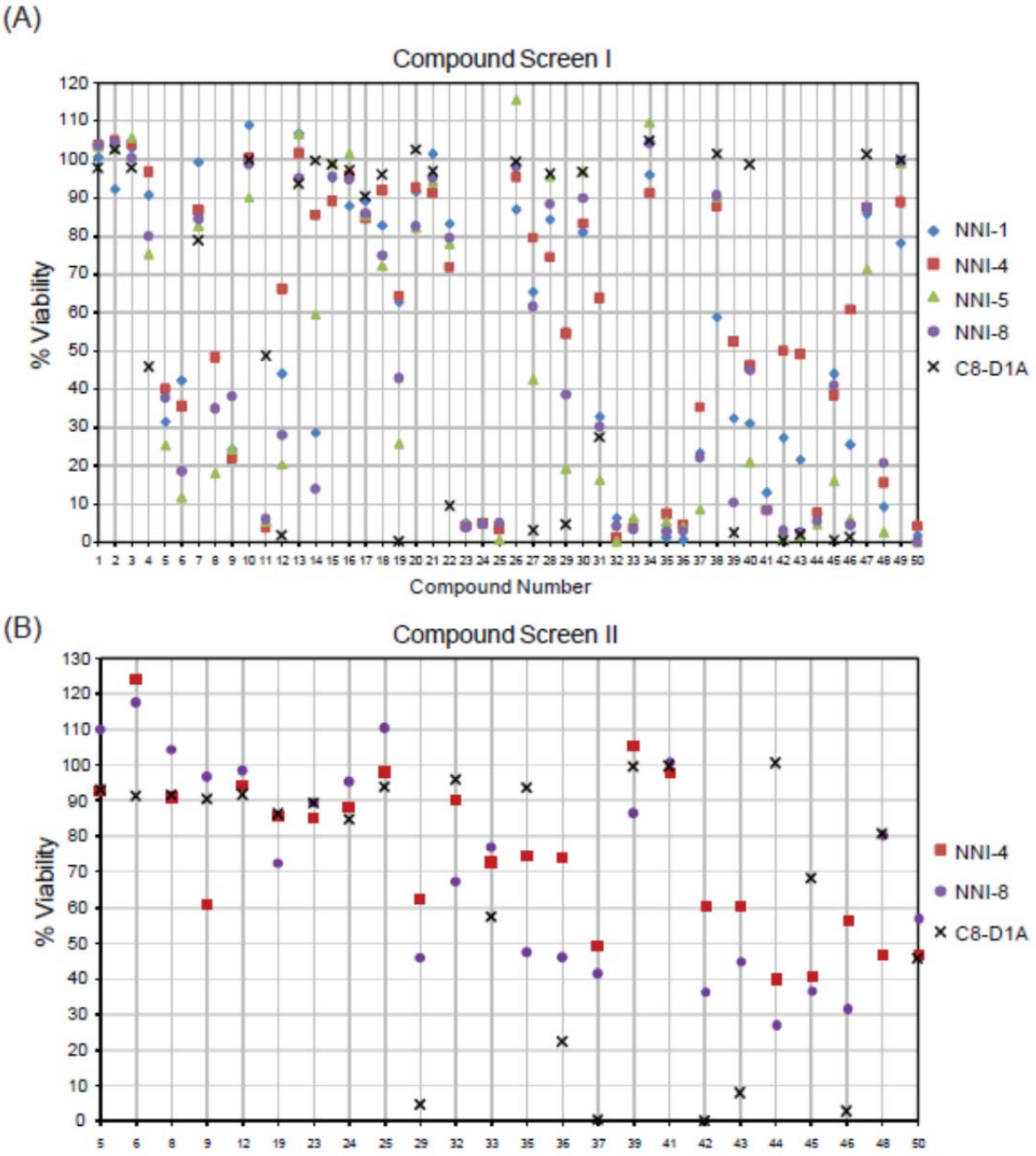

Figure-5. High-throughput screen identifies GPC inhibitory compounds. GPCs (NNI-1, 4, 5 and8) and mouse astrocytes (C8-D1A) were subjected to drug treatment at **(A)** 10 µM and **(B)** 0.1 µM. Compounds with viability selectivity ratio > 2 in at least 1 GPC line were selected.

Table-2. List of prioritized compounds from high-throughput screen. Compounds were selected based on viability selectivity ratio ($\%Viability_{C8\text{-}D1A}$ / $\%Viability_{GPCs}$).

Screen	Compound No.	Compound Target	Viability Selectivity Ratio			
			NNI-1	NNI-4	NNI-5	NNI-8
I	11	P70s8,PKAα,AKT	10.8	12.6	8.9	7.9
	14	GSK3β	3.5	1.2	1.7	7.2
	40	CDK1,9,TAK1	3.2	2.1	4.7	2.2
II	35	PLK1	-	1.2	-	2.0
	44	CDK9	-	2.5	-	3.7
	45	CDK9	-	1.7	-	1.9

3.3. *PLK1* mRNA expression is elevated in glioma tumors

PLK1 over-expression is common in several cancers of the breast[116], ovaries[117], prostate[118] and skin[119]. In addition, PLK1 protein expression has been documented to associate with higher glioma tumor grades[86]. We first verified *PLK1* mRNA expression in 2 large, independent glioma clinical databases, REMBRANDT[101] and Gravendeel[102]. We showed that *PLK1* mRNA expression is elevated in gliomas, especially GBM, when compared to adjacent non-tumor tissue (Figure-6A). This verification is important as it sets the stage for addressing the clinical relevance of GPCs in primary tumors using gene expression. Next, we assessed *PLK1* mRNA and protein expression in several GPC lines compared to normal human astrocytes (NHA) and normal human neural progenitor cells (NHNP). Our data indicated that PLK1 expression is likewise elevated in GPCs (Figure-6B), thus lending support to our hypothesis that PLK1 can present a viable therapeutic target via eradication of long-term, self-renewing GPCs.

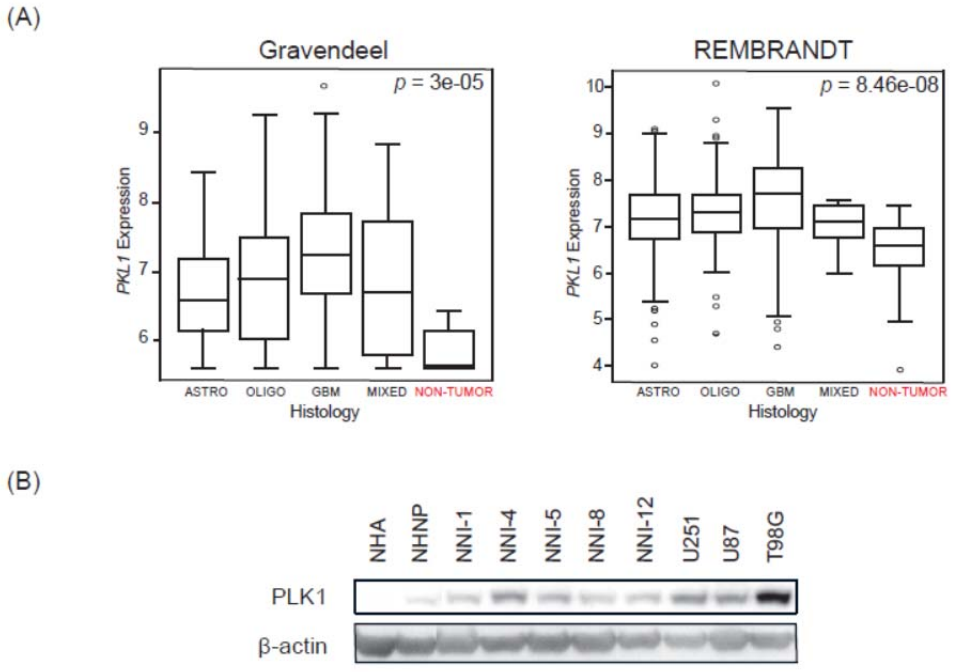

Figure-6. PLK1 is over-expressed in gliomas. (A) Expression of *PLK1* is significantly higher in GBM compared to adjacent non-tumor tissue in glioma databases Gravendeel and REMBRANDT. ANOVA test was applied to compare the means of *PLK1* expression from patients with different histological subtypes and non-tumor samples. **(B)** GPCs and ATCC glioma lines expressed higher levels of PLK1 protein compared to non-tumor lines NHA and NHNP. U251, U87 and T98G represent commercially procured, serum-grown glioma cells (American Type Culture Collection).

CHAPTER 4: USING BI2536 TO STUDY PLK1 INHIBITION IN GLIOMA-PROPAGATING CELLS

4.1. Verification of BI2536 efficacy in an *in vitro* kinase assay

PLK1 is a mitotic kinase which plays multiple roles in mitosis. PLK1 expression is cell cycle-regulated, where its expression peaks at G2/M phase[60]. During G2/M transition, Aurora A and Bora work synergistically to activate PLK1 by phosphorylating Threonine 210 (Thr210) at its kinase domain[63]. Thereafter, PLK1 elicits a series of phosphorylation events leading to mitotic entry and eventually its own degradation mediated by the anaphase-promoting complex (APC)[58]. Several examples of downstream targets of PLK1 include cohesin[120], BRCA2[76], CDC25C[72], Cyclin B[121] and kinesin-like motor protein[122]. The failure of PLK1 in phosphorylating these targets would thus lead to cell cycle defects.

To characterize PLK1 inhibition in GPCs, we relied on a well-published PLK1 small molecule inhibitor with known specificity that is currently in clinical trials for various oncologic diseases[123], BI2536 (Supplementary Figure-1 and Supplementary Table-1). We first verified that our commercially procured BI2536 is comparable with published activity by determining its ability to inhibit phosphorylation of human recombinant PLK1 in a kinase assay. Our results showed that the inhibitory concentration which reduced phosphorylation by 50% was approximately 0.79 nM, which is comparable to published data[123] (Figure-7). Thus, we verified that our source of BI2536 was reliable.

(A)

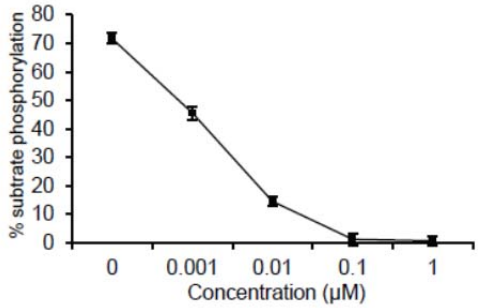

(B)

BI2536 Concentration (μM)	% Phosphorylation
0	71.70
0.001	45.60
0.010	14.50
0.100	1.20
1.000	0.60

Figure-7. BI2536 treatment abrogates PLK1 kinase activity. (A) *In vitro* kinase activity of recombinant human PLK1 was markedly reduced with BI2536 treatment. An IC_{50} of approximately 0.79 nM was derived. **(B)** PLK1 kinase activity expressed as % substrate phosphorylation versus positive control provided in assay kit.

4.2. BI2536 selectively inhibits GPCs over normal human neural cells

Next, we determined the compound's selectivity for GPCs over normal human neural cells by utilizing the selectivity ratio method as previously described[113]. We determined inhibitory concentrations which reduced viability by 50% (IC_{50}) for each GPC, compared to NHA and NHNP cells (Supplementary Figure-S2). Collectively, we showed that BI2536 displayed a selectivity ratio of 25 to 9621in GPCs compared to NHNP cells; while displaying a selectivity ratio of 1.4 to 560 when compared to NHA cells (Table-3). We rationalized that the significant differences between comparing to NHA and NHNP cells may lie in the fact that both are cultured under very distinct conditions: NHNP in serum-free medium supplemented with growth factors; and NHA in serum-containing medium. NHNP by virtue of being expanded under similar condition with GPCs may thus present a more reliable comparator cell. Taken together, we show that BI2536 acts selectively to inhibit GPCs.

Table-3. IC_{50} concentrations and selectivity ratios of BI2536. BI2536 demonstrated at least 24.6-fold and 1.4-fold higher selectivity for GPCs using NHNP and NHA as the comparator cell line respectively.

Cells	IC_{50} (μM)	IC_{50} Selectivity Ratio	
		NHNP / GPC lines	NHA / GPC lines
NHA	3.399	-	-
NHNP	58.3600	-	-
NNI-1	1.2780	45.7	2.7
NNI-4	0.0889	656.3	38.2
NNI-5	1.8990	30.7	1.8
NNI-8	0.0125	4672.5	272.2
NNI-12	2.3690	24.6	1.4
U251	0.0061	9594.7	558.8
U87	0.1047	557.4	32.5
T98G	0.0061	9620.8	560.3

4.3. BI2536 abolishes PLK1 kinase activity in GPCs and serum-grown glioma cells

We assessed kinase activity in patient-derived GPCs, as well as a panel of commercially available glioma cells namely U251MG, T98G and U87MG. In the experimental setup, cells treated with nocodazole were used as the positive control; reason being nocodazole arrests cells at G2/M phase[124] and maximal PLK1 activity would be expected. DMSO was also included as the solvent control for unsynchronized cells. Upon BI2536 treatment, we observed that PLK1 kinase activity was markedly reduced in all cell lines when compared to nocodazole-treated and DMSO controls (Figure-8). Notably, at least 70% reduction in kinase activity was recorded compared to the maximal activity in nocodazole-arrested cells. Our data illustrate that BI2536 effectively abolishes PLK1 activity in target cells.

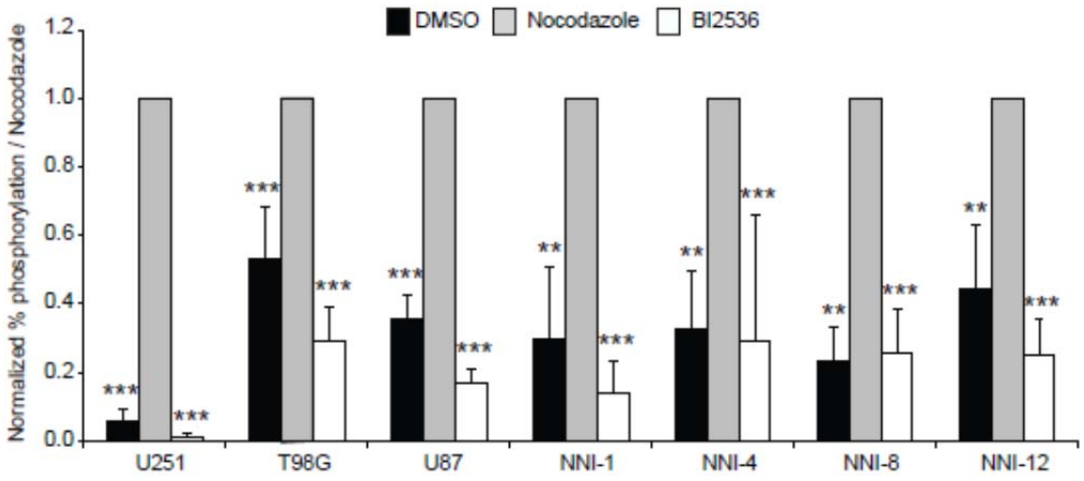

Figure-8. BI2536 treatment abrogates PLK1 kinase activities of GPCs and glioma cell lines. *In vitro* kinase activities of GPCs and glioma cell lines were significantly reduced with BI2536 treatment. $^{**}p < 0.01$, $^{***}p < 0.001$.

4.4. BI2536 induces cell cycle effects in GPCs and serum-grown glioma cells

Next, we studied the effect of BI2536 on cell cycle profiles of GPCs and serum-grown glioma cells. We observed in serum-grown cells, an at least 2.5-fold increase in G2/M cells compared to DMSO-treated cells, consistent with the mechanism of BI2536; and an increase in sub-G_0 cells at 48 hours post-treatment, indicative of apoptosis (Figure-9). Similarly in GPCs, we noted an at least 2-fold increase in G2/M cells compared to DMSO-treated cells (Figure-10). In addition, the sub-G_0 cells increased steadily with time. In normal cells, p53-mediated apoptosis would be activated to remove effete polypoid cells; however, our glioma cells have been verified to possess mutated *TP53* at codon 72 (proline to arginine mutation)[125] (Figure-11), thus explaining that BI2536 likely effected cellular apoptosis through p53-independent mechanisms. This is consistent with bioinformatical analysis in The Cancer Genome Atlas clinical database that revealed that PLK1 is frequently over-expressed in p53 mutant cells and are synthetically lethal[126]. We have further confirmed BI2536-induced apoptosis by flow cytometry using an antibody against cleaved poly[ADP-ribose] polymerase (PARP) (Figure-12A). In addition, as flow cytometry allows for multiparameter monitoring in single cells, we assessed the levels of cleaved PARP in both CD133(+) and CD133(-) cellular fractions of GPCs (Figure-12B).

CD133 is frequently implicated as one of the GPC markers[4], however, it should be noted that some gliomas can arise from CD133(-) cells[27-28]. Nevertheless, our data indicate that CD133(-) cells were more susceptible to BI2536-induced apoptosis when compared to CD133(+) cells across all GPC lines. This data may be explained in light of previous literature showing that CD133(+) cells have an activated DNA damage repair mechanism, possibly explaining for their survival advantage[5,7].

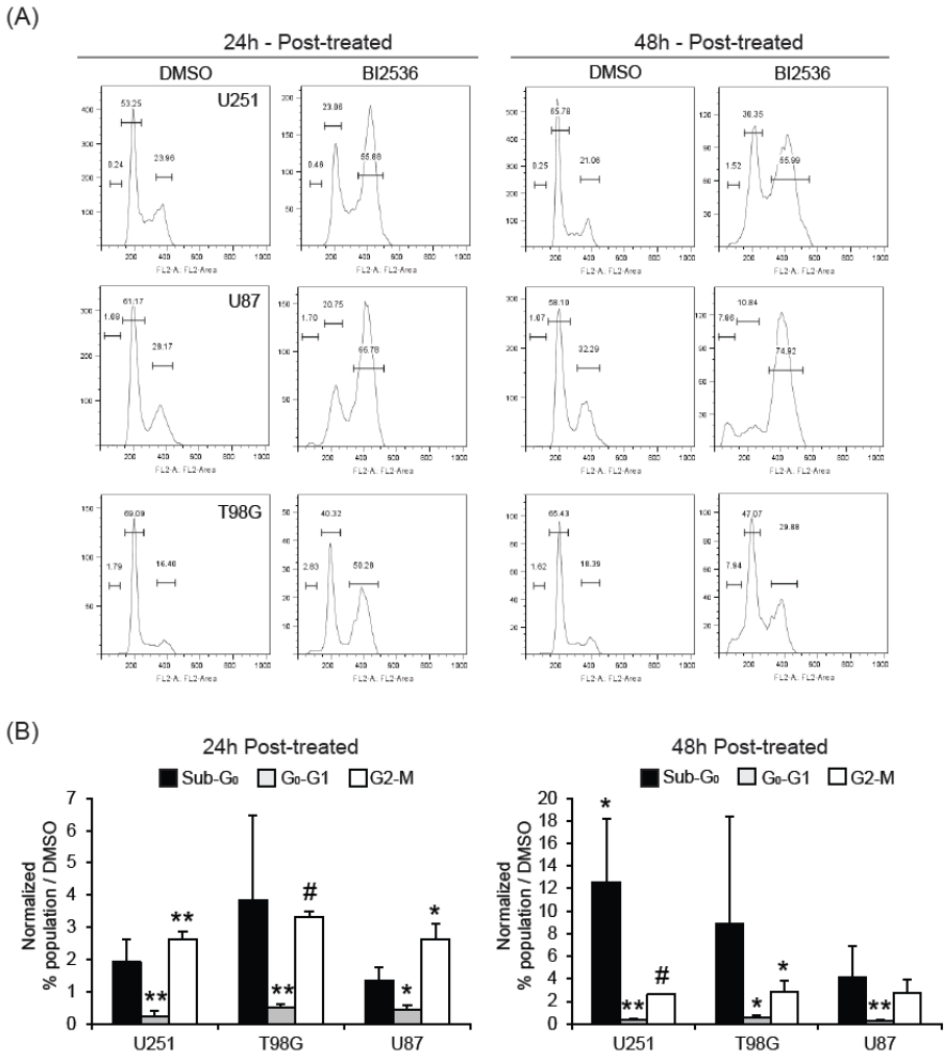

Figure-9. BI2536 causes G2/M phase cell cycle arrest in glioma lines. (A) Representative FACS plots of BI2536-treated serum-grown glioma lines after 24h and 48h. **(B)** Bar charts representing averages of cell cycle FACS results (n=3). Notably, BI2536 induced G2/M phase cell cycle arrest with concomitant apoptosis as reflected by sub-G_0 population. *$p < 0.05$, **$p < 0.01$, #$p < 0.001$.

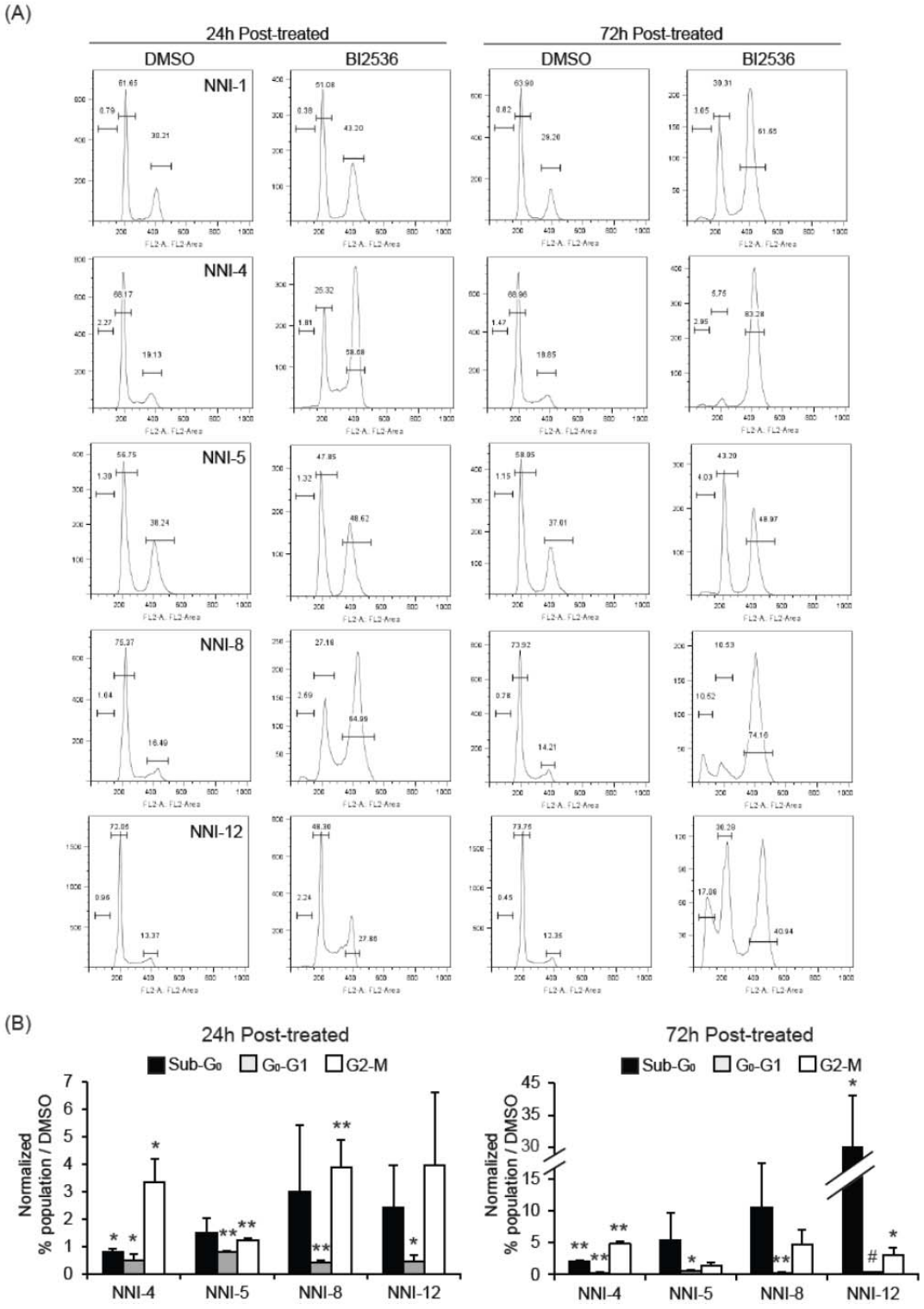

Figure-10. BI2536 causes G2/M phase cell cycle arrest in GPCs. (A) Representative FACS plots of BI2536-treated GPCs after 24h and 72h. **(B)** Bar charts representing averages of cell cycle FACS results (n=3). Notably, BI2536 induced G2/M phase cell cycle arrest with concomitant apoptosis as reflected by sub-G_0 population. *$p < 0.05$, **$p < 0.01$, #$p < 0.001$.

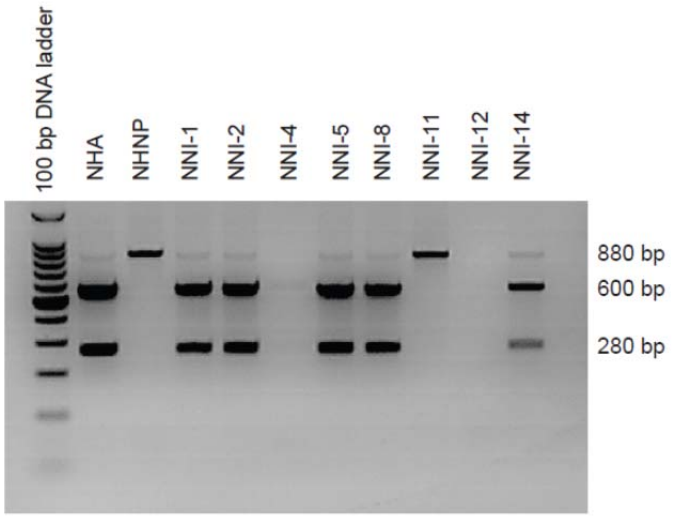

Figure-11. GPCs harbor *TP53* mutation at codon 72. A single fragment of 880 bp after BstU1 digestion indicates *pro/pro* expression of codon 72. Fragment sizes of 600 and 280 bp represent *arg/arg* while 880, 600 and 280 bp are *arg/pro* heterozygotes.

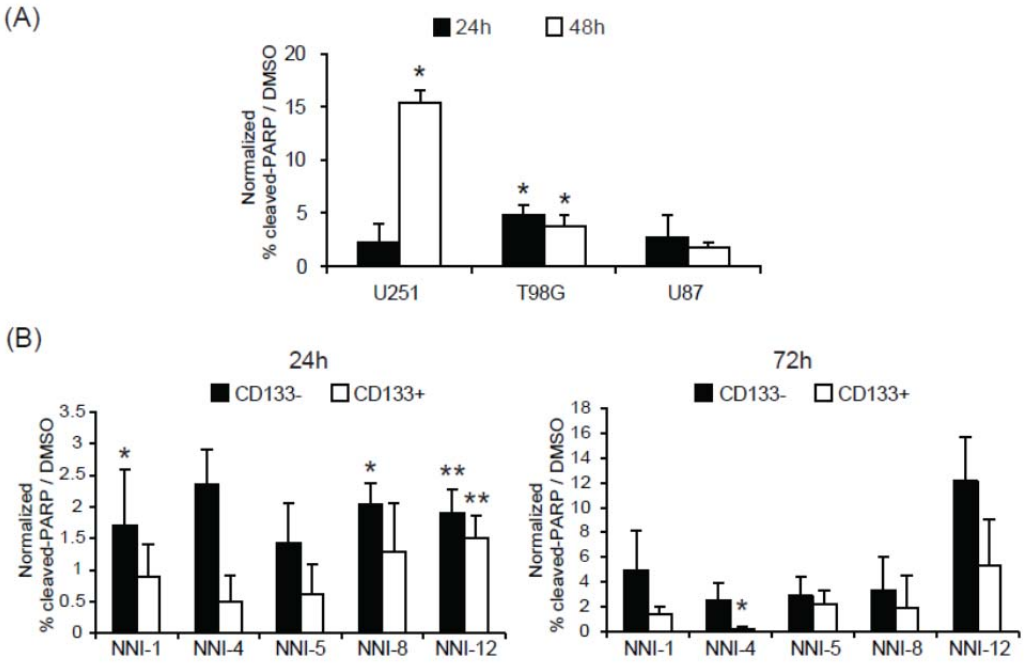

Figure-12. BI2536 induces apoptosis in GPCs and glioma cell lines. Expression of cleaved-PARP was assessed by flow cytometry. **(A)** Cleaved-PARP expression was elevated in glioma cell lines at 24h and 48h post-treatment. **(B)** In GPCs, CD133(-) cells were more susceptible to BI2536-induced apoptosis in comparison to CD133(+). *$p < 0.05$, **$p < 0.01$.

4.5. BI2536 abrogates clonogenicity of GPCs

Bearing in mind that GPC sphere cultures are heterogeneous, conventional short-term viability assays more than often produce erroneous results as they include readouts of majority cells such as the transient-amplifying progenitors[55,127]. True GPCs are slow-growing and the majority active cells mask their presence. We thus adapted the neurosphere assay which estimates *bona fide* tumor stem cell frequency, while sphere size indicates proliferative capacity[113,128]. This assay provides an *in vitro* readout of tumor stem cell activity that often correlates with survival outcome in orthotopic mouse models[110,128].

We first determined sphere-forming ability of BI253-treated GPCs. To distinguish the effects in CD133(+) and CD133(-) subpopulations, we flow-sorted the cells and seeded at clonal densities to prevent cellular aggregation which leads to inaccuracy in determining *bona fide* spheres arising from stem cell self-renewal[127]. Based on the number of seeded cells in each well of a 96-well plate (n=30), we tabulated the percentage of neurospheres formed, as well as measured diameters of all spheres. In general, across all GPC lines used, we observed a decrease in sphere numbers in all 3 flow-sorted groups [total sorted, CD133(+) and CD133(-)] (Figure-13). Except for NNI-1, all other lines displayed at least 40% reduction in percentage of neurospheres formed at day 7 post-treatment. Subsequently, all cell lines displayed less than 20% sphere-forming activity by day 21. This data indicates that the tumor stem cell frequency was significantly reduced upon BI2536 treatment. Although we had previously shown that CD133(+) cells were more resistant to apoptosis by cleaved PARP analysis (Figure-12), the trend in the neurosphere assay was less clear. Sphere-forming ability in all total sorted, CD133(+) and CD133(-) fractions were similarly targeted. We also observed an increased percentage of smaller spheres in BI2536-treated GPCs regardless of their CD133 status (Figure-14). This is an indication of reduced proliferation or disintegration of the bigger spheres in response to BI2536 treatment. These data are not surprising considering that several other GPC markers besides CD133 have been shown to contribute to GPC survival and tumor propagation (e.g. CD15, nestin, aldehyde dehydrogenase [ALDH][26,29]). While it is important to derive drugs that eradicate tumor-initiating cells, other majority bulk tumor cells do play crucial roles in providing a suitable

microenvironmental niche that supports growth[129]. Thus, taken together, BI2536 shows efficacy at depleting the GPC frequency.

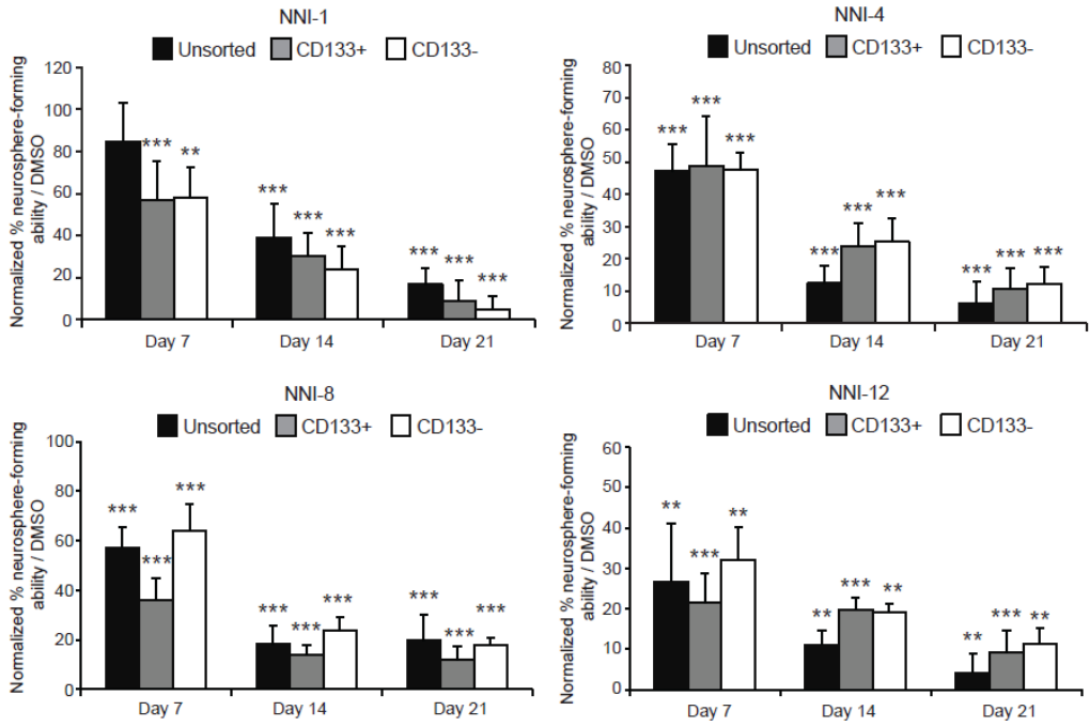

Figure-13. BI2536 reduces tumor stem cell frequency. BI2536 treatment reduced neurosphere-forming ability of GPCs. Notably, both CD133(+) and CD133(-) were equally targeted. *$p < 0.05$, **$p < 0.01$, ***$p < 0.001$.

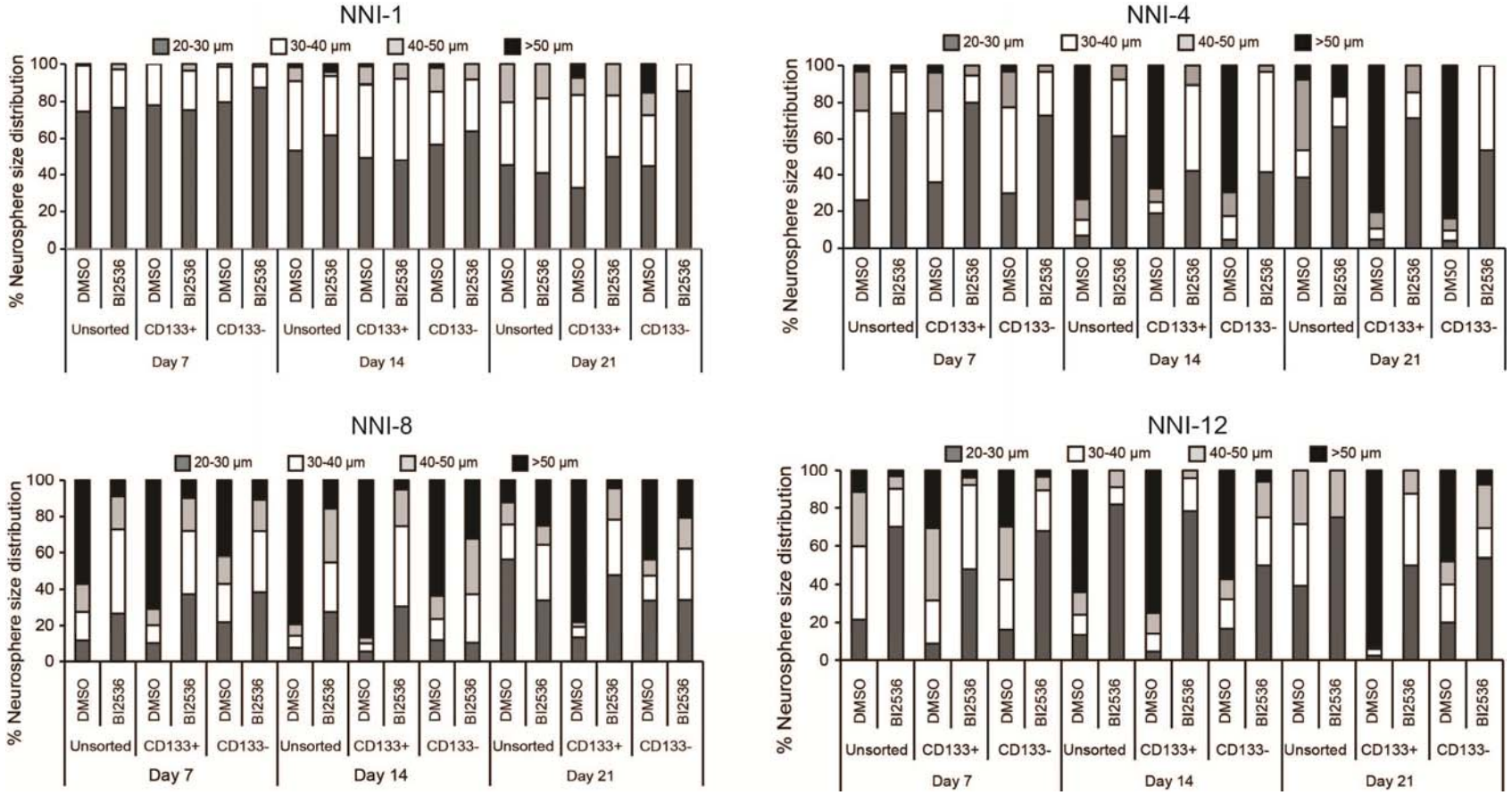

Figure-14. BI2536 reduces proliferation of GPCs. BI2536-treated GPCs showed an increased percentage of smaller spheres compared to DMSO-treated cells. The reduction in sphere size is indicative of reduced proliferation of GPCs. Notably, both CD133(+) and CD133(-) were equally targeted.

4.6. PLK1 inhibition abrogates long-term self-renewal capability of GPCs

We expect that drugs truly effective against GPCs would not allow for recovery over a prolonged period. We therefore modified the neurosphere assay in which we withdrew BI2536 treatment over 21 days, following the initial 14 days of drug treatment. This, we reasoned, would allow us to detect remnant self-renewal ability over the extended duration. To eliminate loss of tumorigenic potential due to cellular differentiation[56], we replenished growth factors twice weekly to maintain GPCs in their relatively undifferentiated "stem" state.

We observed by day 7 post-drug withdrawal the following: A significant reduction in the number of spheres formed across all GPC lines (Figure-15) where there was at least a 70-90% reduction in number of spheres formed; by day 21 post-drug withdrawal, most BI2536-treated GPCs showed no signs of recovery as indicated by the progressive drop in sphere number and total eradication in NNI-8 and NNI-12; and sphere sizes indicating proliferative capacity were significantly reduced. Collectively, we show that BI2536 effectively abrogates *bona fide* long-term self-renewal ability of GPCs.

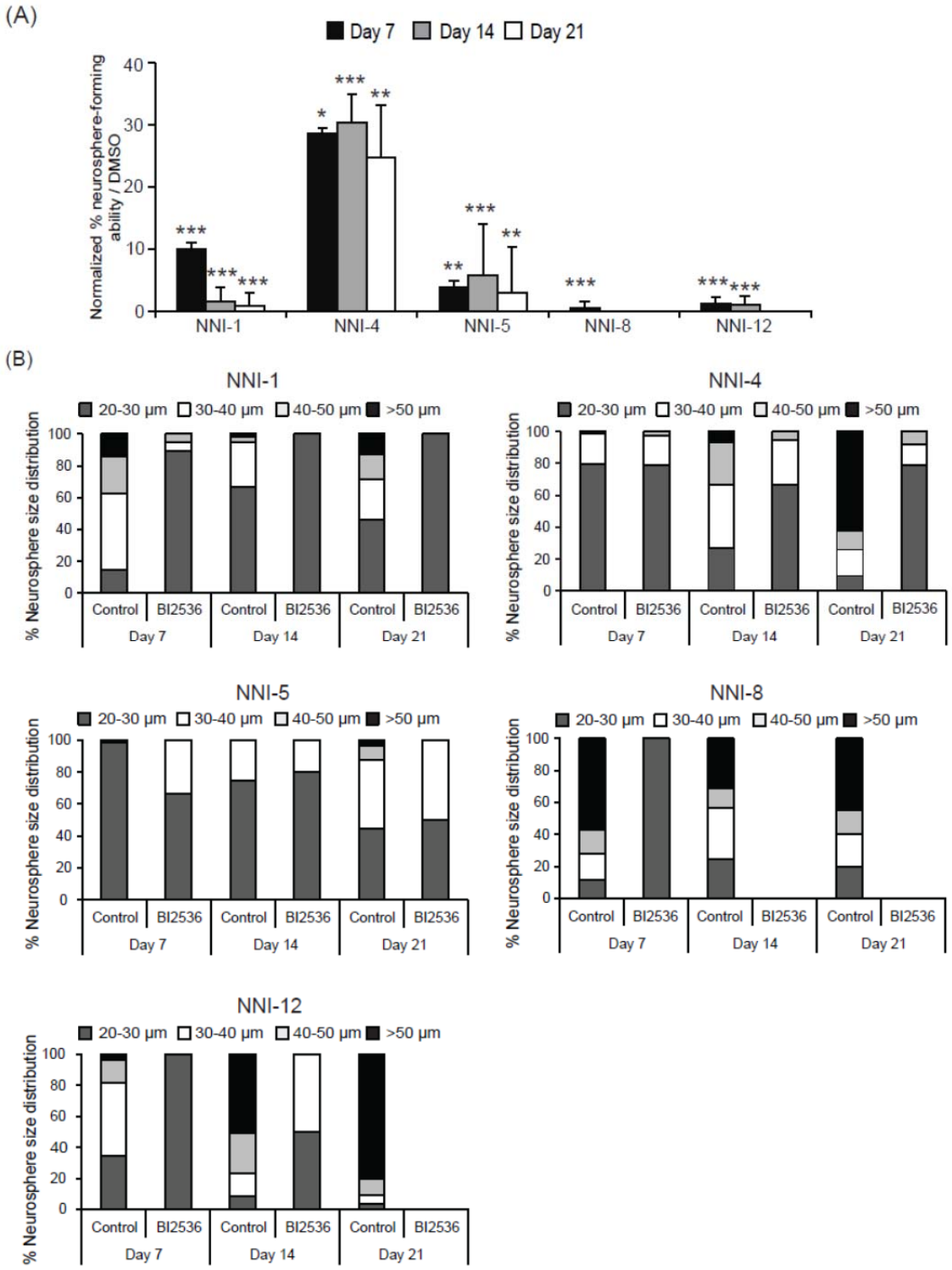

Figure-15. BI2536 effectively abrogates *bona fide* long-term self-renewal ability of GPCs. (A) Neurosphere-forming ability of GPCs remained minimal with drug withdrawal. **(B)** Distribution of neurosphere sizes showing smaller sphere sizes compared to DMSO-treated cells. In NNI-8 and NNI-12, GPCs were totally depleted by Day 21. *$p < 0.05$, **$p < 0.01$, ***$p < 0.001$.

4.7. PLK1 inhibition alters GPC stemness expression

Recent findings provide insight into the role of cell fate in relation to tumorigenicity of GPCs[56]. Relatively undifferentiated tumor stem cells retain tumor-initiating and propagating activity while the more lineage-committed, differentiated progenitors exit mitosis and senesce, thus resulting in tumor involution[56]. Induction of differentiation in GPCs has thus been proposed as a viable therapeutic strategy. Accordingly, we sought to determine if BI2536 induced differentiation of GPCs. To-date, there is no single marker that clearly defines *bona fid*e GPCs. Besides CD133, other genes commonly associated with stemness or self-renewal include CD15 (SSEA-1), nestin, *SOX2*, *OCT-4* and Musashi-1 (Msi-1)[26,29,99]. Such marker expression often generates conflicting data; moreover, their expression can be altered by experimental conditions[130] and disease state[131]. Hence, we probed for a panel of 4 stemness-associated markers; namely CD133, CD15, ALDH and nestin, upon BI2536 treatment. We observed that across all GPC lines, CD133 expression was reduced by at least 2-fold compared to DMSO-treated cells (Figure-16). Changes in CD15, ALDH and nestin expression were less obvious. In NNI-1 and NNI-5, CD15 expression doubled after BI2536 treatment. Taken together, these results suggest that PLK1 inhibition alters the GPC stemness profiles to varying extent. Our data underscores the limitation of relying solely on marker expression to characterize the GPC, thus forcing a re-evaluation of criteria to focus on functional activities such as self-renewal over extended periods[132].

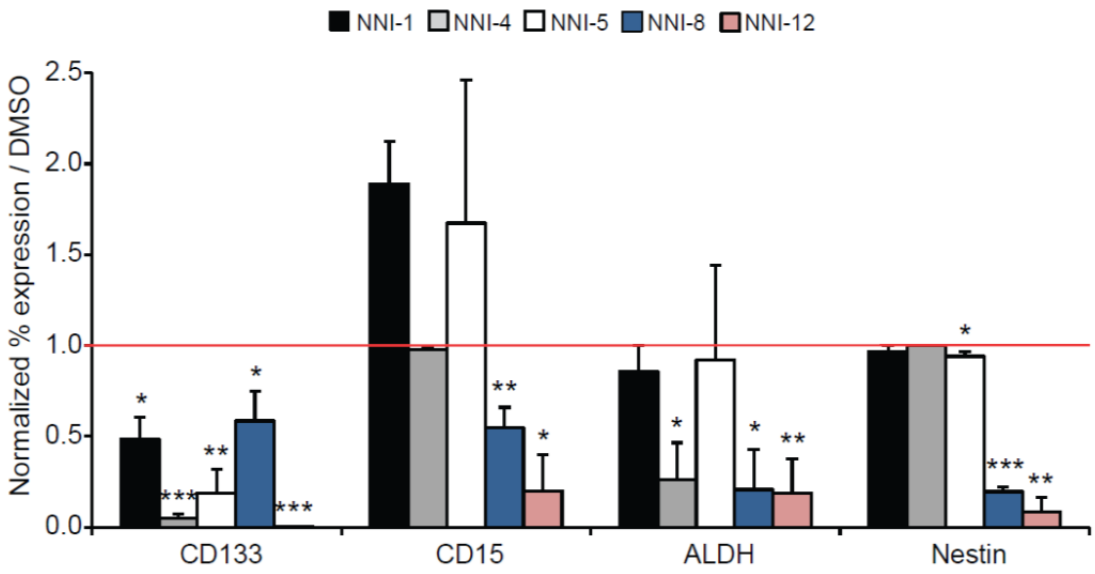

Figure-16. PLK1 inhibition alters stemness profile of GPCs. Stemness profile of GPCs was assessed using a panel of stemness-associated markers, CD133, CD15, ALDH and Nestin. Across 5 GPCs, CD133 expression was significantly reduced with PLK1 inhibition. *$p < 0.05$, **$p < 0.01$, ***$p < 0.001$.

4.8. BI2536 treatment induces cellular differentiation

To further substantiate our evaluation of BI2536 on stemness and differentiation profiles, we examined BI2536-treated GPCs at concentrations below their IC_{50} values to rule out non-specific drug effects (Table-4). We stained the cells with antibodies against nestin, Msi-1, Oct-4, glial fibrillary acidic protein (GFAP, astrocytes), β-tubulin III (TuJ1, neurons) and O4 (oligodendrocytes)[99]. Preliminary analyses indicated that 4 out of 7 GPC cells displayed neurite outgrowth, indicative of differentiation (Figure-17). In general, all GPCs showed significant increases in differentiated cells although to varying extent with GFAP, TuJ1 or O4 (Figure-18). The stemness phenotype was not significantly altered, consistent with previous reports on tumorigenic GPCs exhibiting both differentiated and self-renewal expression[2,133], often indicative of aberrant neural developmental cues.

Summary

Collectively, our data provides strong evidence that BI2536 targets GPCs via PLK1 inhibition. This results in cell cycle arrest with concomitant apoptosis. Additionally, GPCs are induced to differentiate. These effects may explain the feasibility of PLK1 as a therapeutic target in gliomas.

Table-4. BI2536 concentrations that induced GPC differentiation.

GPC line	BI2536 concentrations inducing differentiation (μM)
NNI-1	0.0100
NNI-4	0.0001
NNI-5	0.2000
NNI-12	0.2000

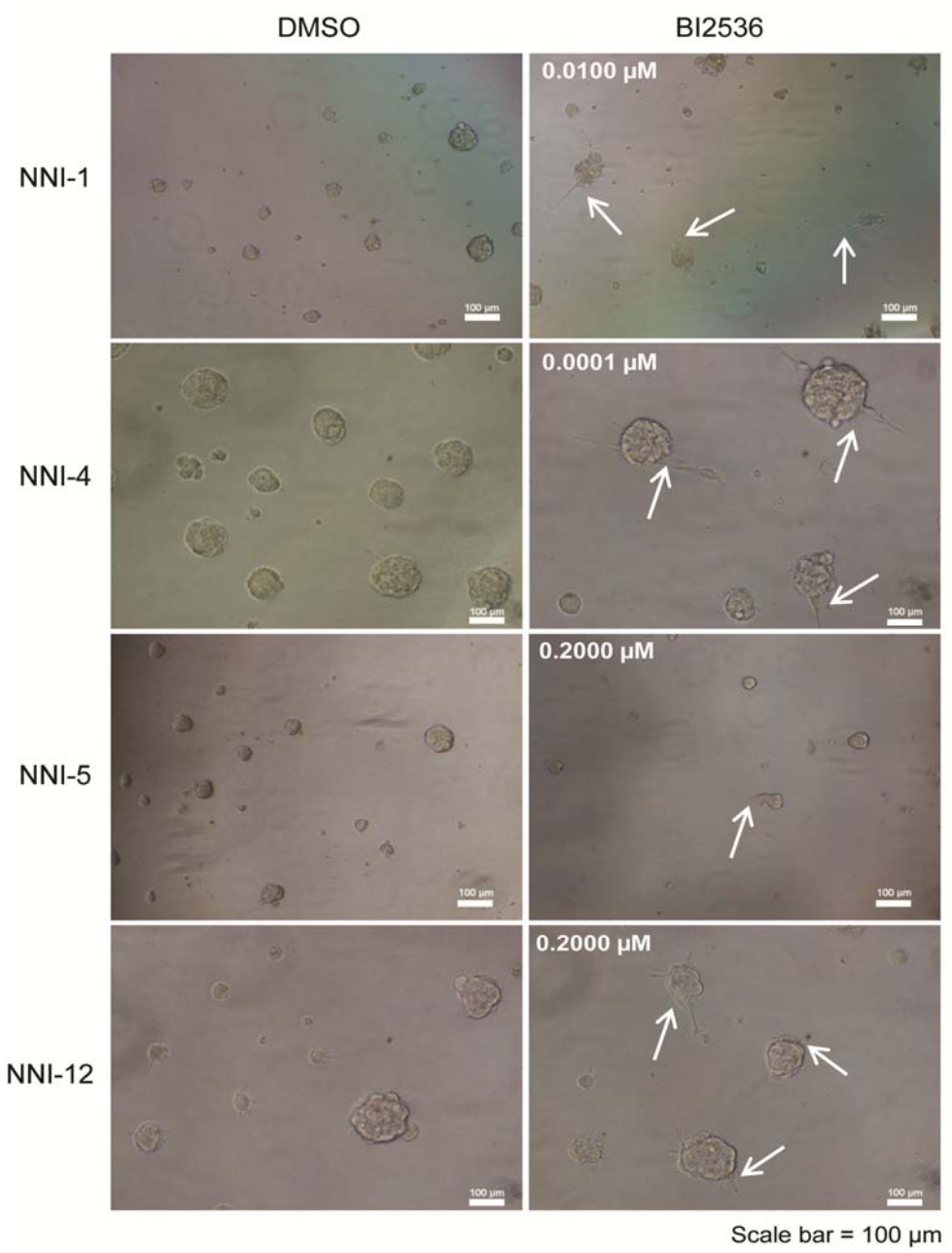

Figure-17. PLK1 inhibition by BI2536 induces cellular differentiation in GPCs. Neurite outgrowth (arrows), indicative of cellular differentiation were observed at lower concentrations of BI2536 treatments. Scale bar denotes 100 µm.

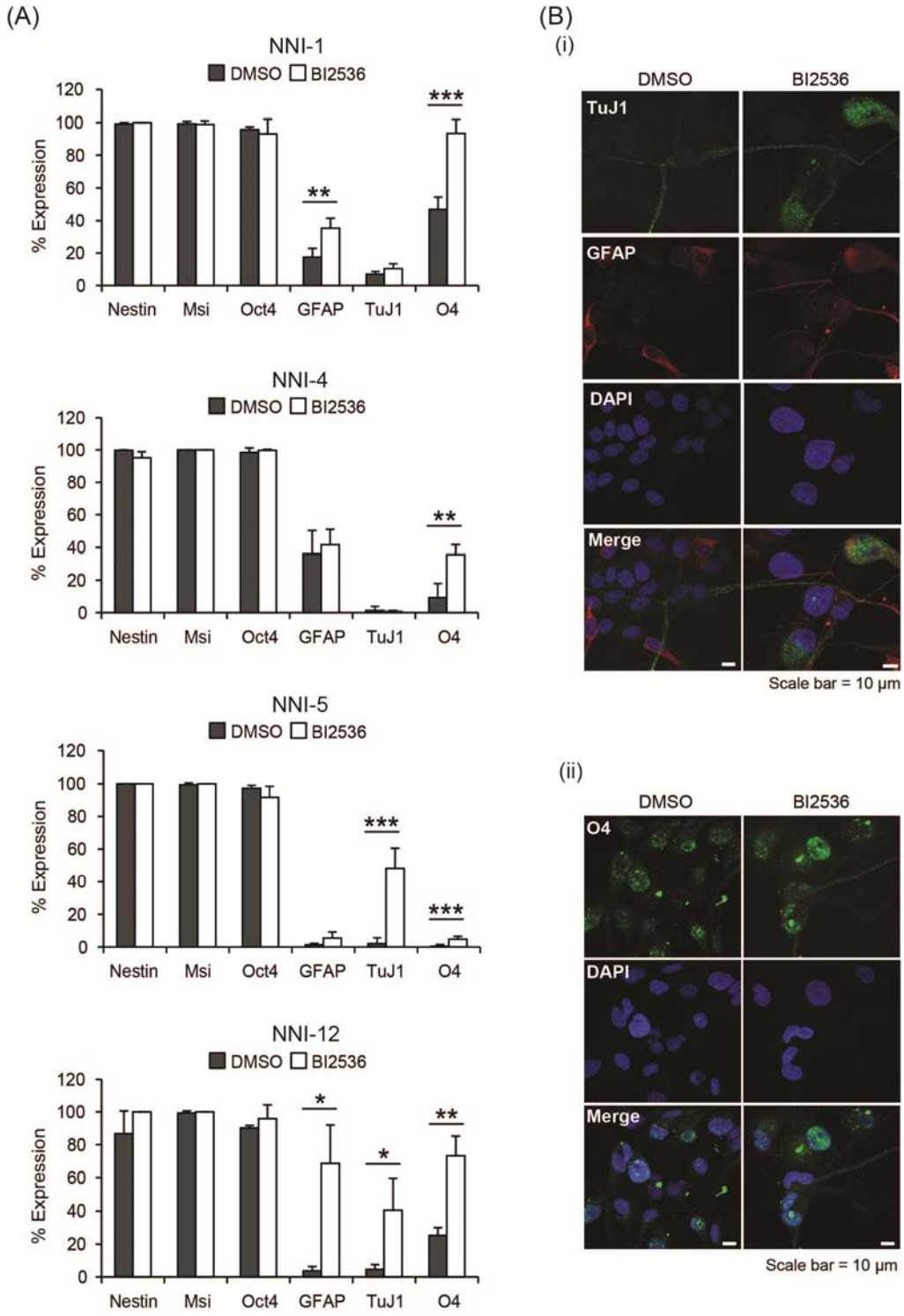

Figure-18. BI2536 induces differentiation of GPCs. (A) Four GPC lines showed increased expression of differentiation markers with BI2536 treatment. **(B)** Representative immunofluorescence images of NNI-4 subjected to DMSO or BI2536. **(i)** Co-staining of TuJ1, GFAP and DAPI, **(ii)** O4 with DAPI only. Nuclei were enlarged with BI2536 treatment. *$p < 0.05$, **$p < 0.01$, ***$p < 0.001$, scale bar denotes 10 µm.

CHAPTER 5: GENETIC KNOCKDOWN OF *PLK1* MITIGATES GLIOMA CELL GROWTH

5.1. GPCs are effectively transduced by lentiviruses

To rule out non-specific effects of BI2536, we performed lentiviral-mediated knockdown (sh*PLK1*) to implicate PLK1 in maintaining GPC survival. Lentiviral transductions are efficient genetic manipulation tools. They infect both dividing and quiescent cells equally well, integrating into the host genome to sustain prolonged expression of the gene construct[134]. This makes them ideal for genetic manipulations in slowly-dividing stem-like GPCs.

Using the pLKO.1-puro-based vector (Figure-19), we performed *PLK1* knockdown. To monitor transduction efficiency, we carried out, in parallel, transduction with clone SHC003, a TurboGFP-containing, non-targeting lentiviral vector of similar backbone as pLKO.1. This allows visualization of the green fluorescent protein which can be quantified by immunofluorescent methods. Figure-20 shows that by day 5 post-transduction, most GPCs expressed green fluorescence. Moreover, GFP expression was sustained till at least day 10, indicating that *PLK1* knockdown was likely sustained.

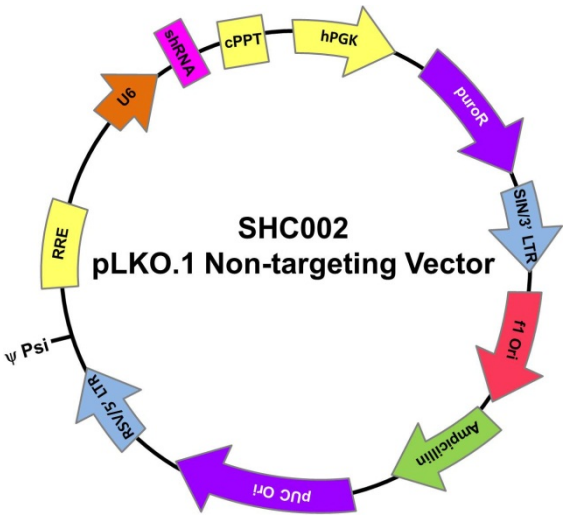

Figure-19. Vector map of pLKO.1 lentiviral backbone. Vector is driven by the U6 promoter and contains puromycin selection marker for establishment of stable clones.

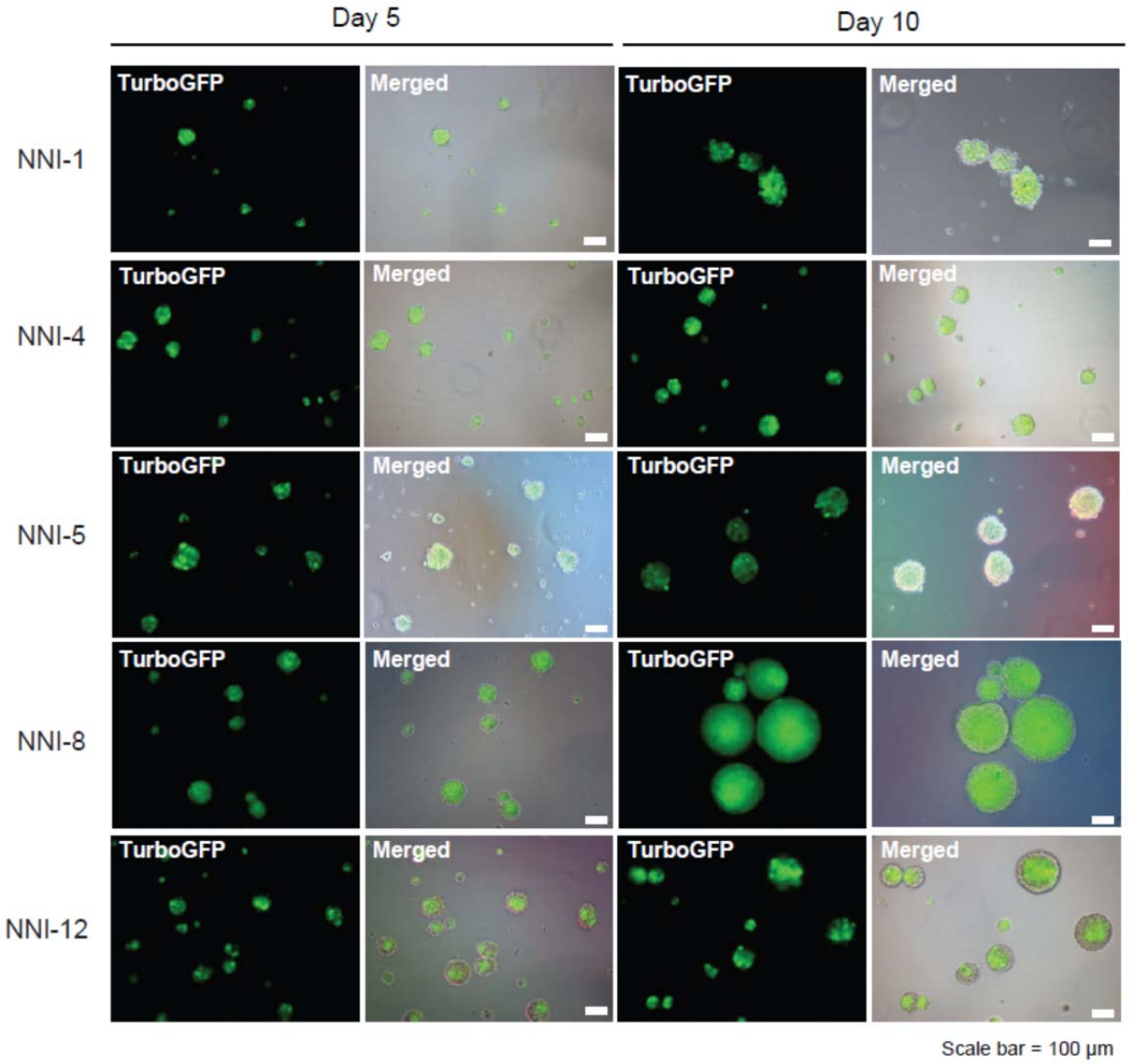

Figure-20. GPCs are effectively transduced by lentivirus. Successfully transduced GPCs were maintained in puromycin media for at least 10 days. Scale bar denotes 100 µm.

5.2. *PLK1* knockdown levels are significantly reduced in GPCs and serum-grown glioma cells

We quantified the extent of PLK1 knockdown by immunoblot analysis (Figure-21). We observed a varying extent but consistent trend of reduced PLK1 protein across most glioma cells, indicating that in most instances, *PLK1* knockdown was successfully achieved.

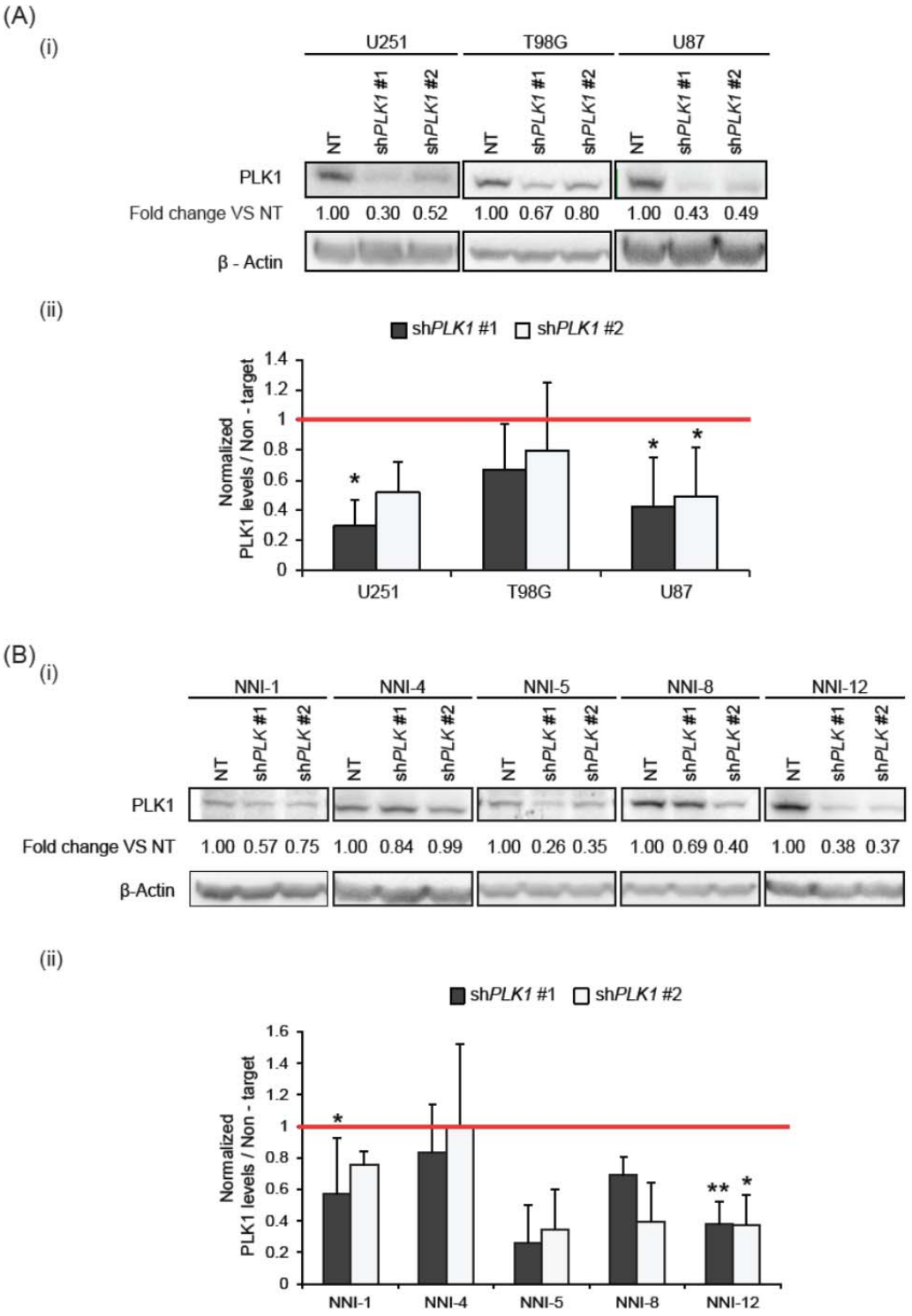

Figure-21. *PLK1* knockdown levels are significantly reduced in GPCs and glioma cell lines. (A)(i) Representative western blot analysis of glioma cell lines after sh*PLK1* knockdown. **(ii)** Bar chart representing averages of protein levels after sh*PLK1* knockdown. **(B)(i)** Representative western blot analysis of GPCs after sh*PLK1* knockdown. **(ii)** Bar chart representing averages of protein levels after sh*PLK1* knockdown. *$p < 0.05$, **$p < 0.01$, n=3.

5.3. PLK1 depletion reduces GPC viability and self-renewal capability

Next, we assessed the viability of glioma cells upon *PLK1* knockdown at 2 time-points post-transduction (Figure-22). We observed in both sh*PLK1* clones used that all glioma cell lines (patient-derived as well as commercially procured, serum-grown cells) exhibited significant reduction in viability. Our data suggests that PLK1 regulates glioma cell proliferation.

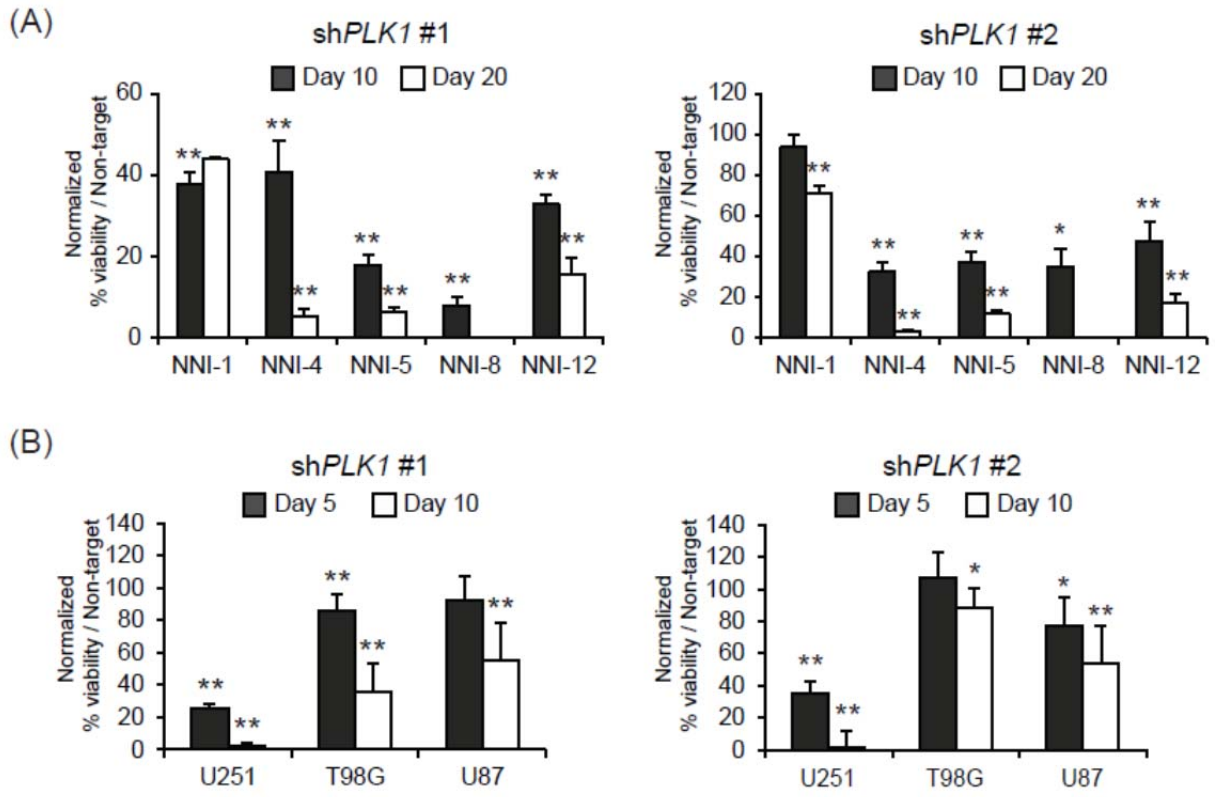

Figure-22. *PLK1* depletion reduces GPC viability and self-renewal capability. (A) Viability of GPCs at Day 10 and 20 post-transduction. **(B)** Viability of glioma cell lines at Day 5 and 10 post-transduction. *$p < 0.05$, ** $p < 0.01$.

5.4. *PLK1* knockdown mitigates GPC clonogenicity

We quantified the effects of *PLK1* knockdown on sphere-forming capacity, an indicator of GPC frequency and self-renewal. Our results showed that over an extended period of 21 days post-transduction, sphere formation was greatly reduced, with concomitant reduction in sphere size, latter being an indicator of GPC proliferation (Figure-23). These data support our hypothesis that PLK1 is a viable molecular target at eradicating self-renewing GPCs.

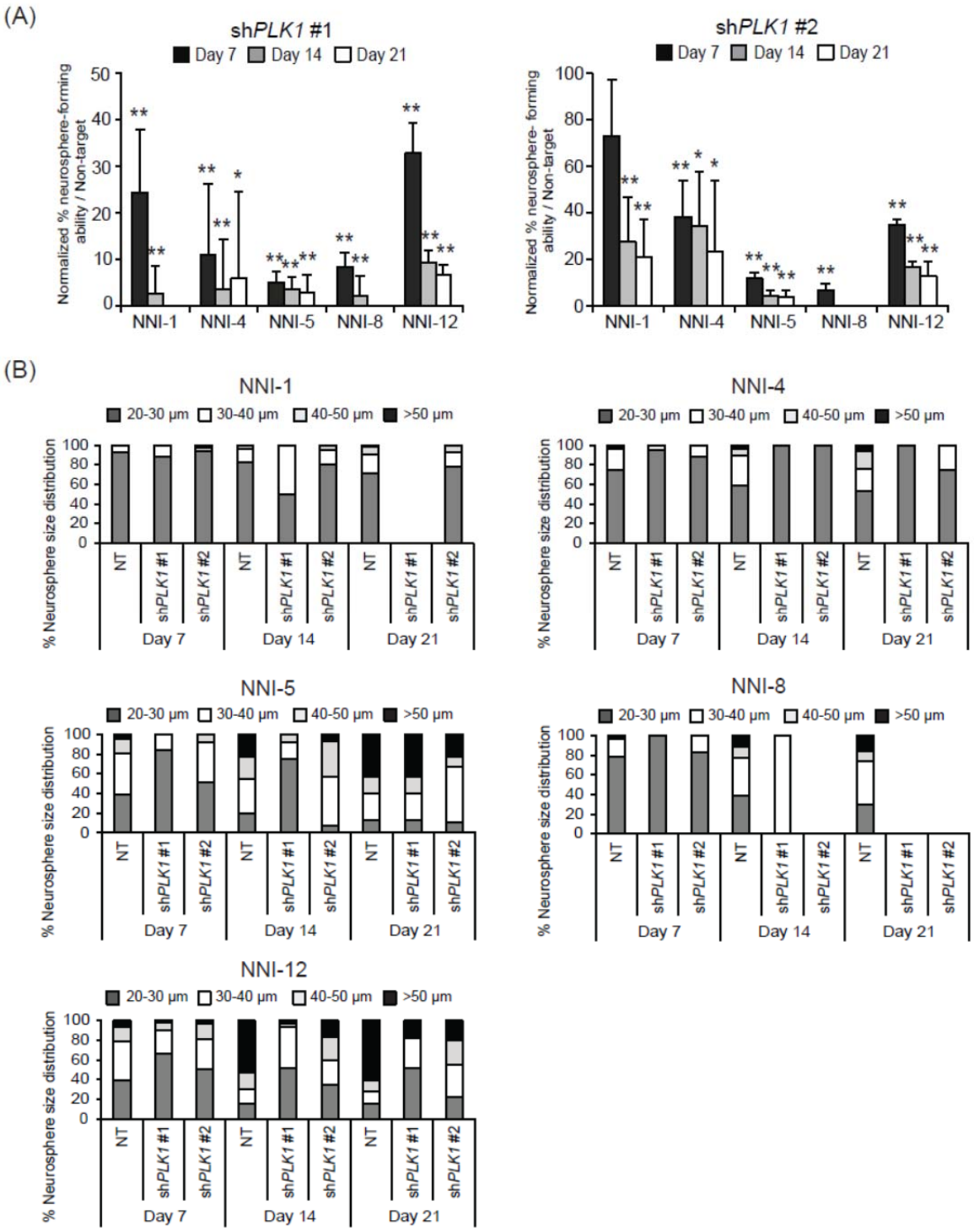

Figure-23. *PLK1* knockdown mitigates GPC clonogenicity. Both sh*PLK1* clones reduced self-renewal ability of GPCs effectively. **(A)** *PLK1* depletion reduced tumor stem cell frequency of GPCs as depicted by a decrease in percentage neurospheres formed. **(B)** Distribution of neurosphere sizes for each GPC line. Smaller spheres were more prominent in sh*PLK1* knocked down samples compared to their respective controls. In NNI-8, GPCs were totally depleted by Day 14. *$p < 0.05$, **$p < 0.01$.

5.5. *PLK1* knockdown has moderate effects on stemness and differentiation profiles

We next examined *PLK1* knockdown on the stemness and differentiation profiles of GPCs. We assessed the levels of CD133, CD15, ALDH and nestin (stemness markers); and TuJ1, GFAP (differentiation markers) at day 5 post-transduction. Figure-24 demonstrates that no major changes in stemness expression were observed. Contrary to our earlier BI2536 data, we could not detect signs of differentiation. We verified this by immunoblot analysis of GFAP and TuJ1 expression (Figure-25). Collectively, our data suggests that PLK1 depletion effects cell death by apoptosis, and may have moderate roles in determining cell fate. Our genetically acquired data differed from BI2536 data with respect to stemness and differentiation profiles, likely due to the non-specific action of BI2536.

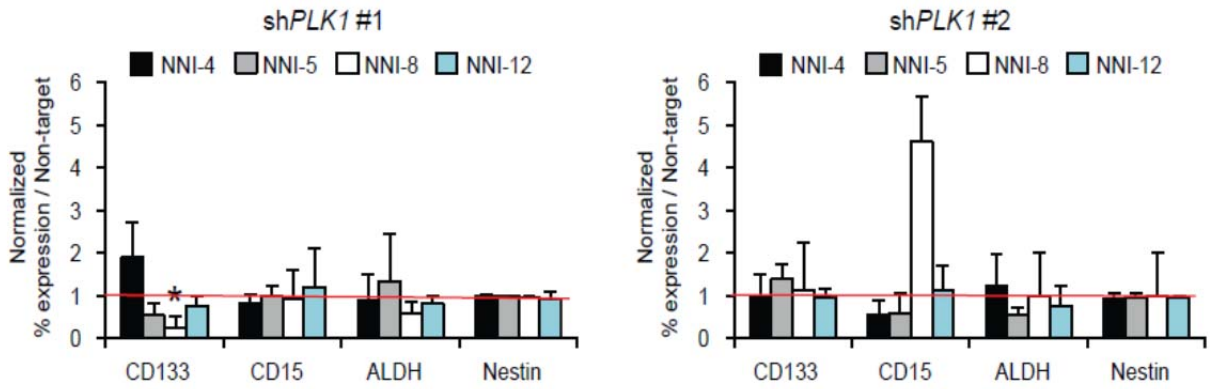

Figure-24. *PLK1* knockdown has moderate effects on stemness profiles of GPCs. No significant change in expression of stemness markers was observed. *$p < 0.05$.

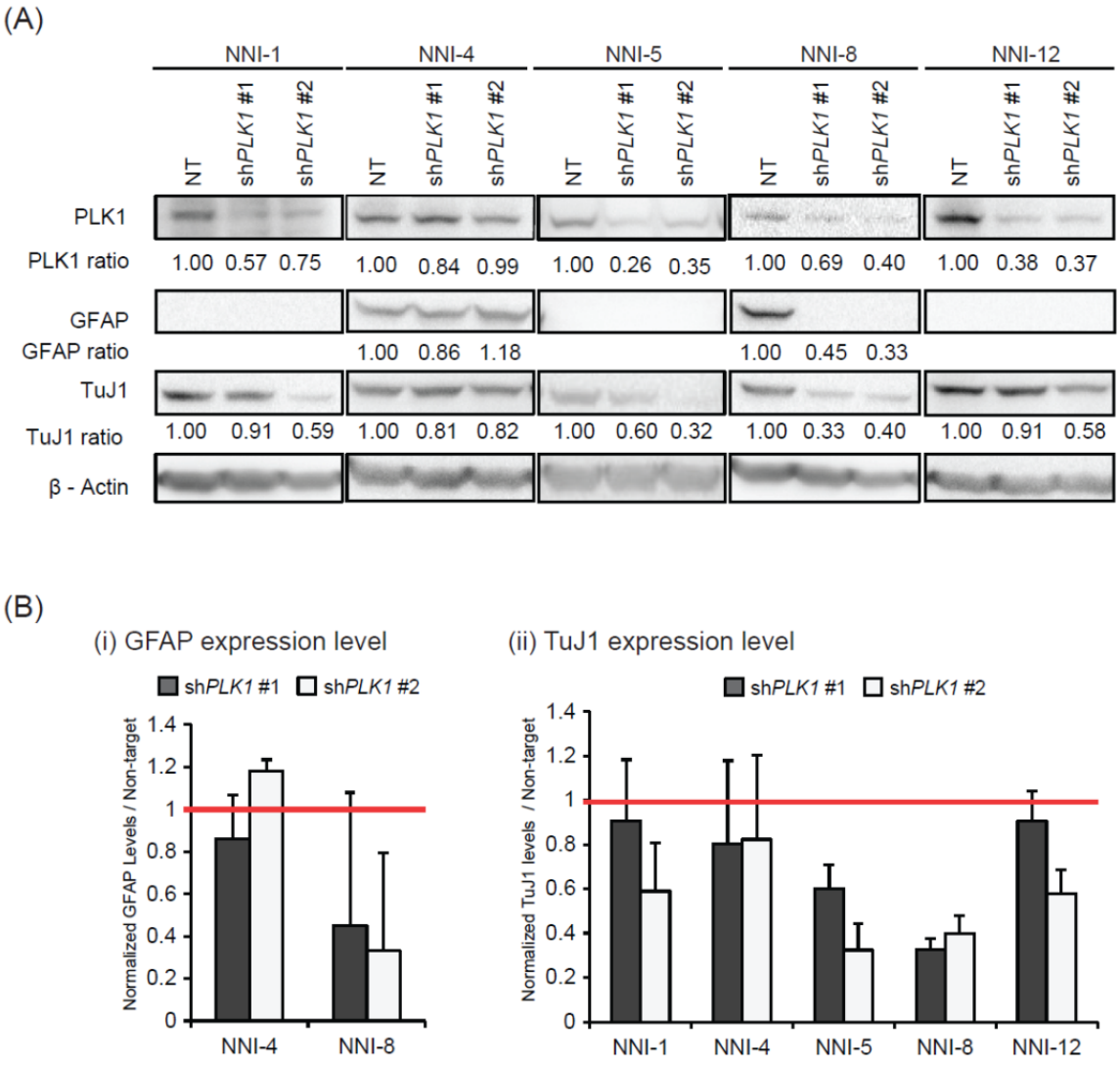

Figure-25. Western blot analysis demonstrates reduction of differentiation markers with *PLK1* knockdown. Differentiation markers GFAP and TuJ1 were probed in western blot analysis. **(A)** Representative western blots of sh*PLK1* GPC lines. **(B)** Bar charts representing average expression of **(i)** GFAP and **(ii)** TuJ1, (n=2). GFAP protein was undetectable in NNI-1, 5 and 12.

5.6. **PLK1 over-expression rescues BI2536 inhibition**

To gain insight into the molecular mechanism behind BI2536 inhibition of glioma cell growth, we proceeded to over-express PLK1 in a lentiviral vector, and then determine its ability to rescue growth inhibition in transduced cells upon BI2536 treatment. This approach would definitively implicate PLK1 in BI2536 inhibition mechanism and support that previous *in vitro* observations are most likely attributed to specifically PLK1 inhibition.

Accordingly, we lentivirally transduced GPCs with either vector control or PLK1-over-expressing vector, both bearing mCherry as a visualization marker for assessing transduction efficiency (Figure-26). Lentiviral transduction was previously demonstrated to be an effective genetic manipulation tool in slow-growing, non-dividing stem-like cells[128]. We then treated the cells with BI2536 and determined cell viability after 3 days. First, we observed that despite using similar multiplicity of infection (MOI), GPC lines varied in transduction efficiencies for both vectors, further confirmed by FACS analysis (Figure-27). This is likely due to individual patient line variations typically seen in studies involving clinical specimens[110-111]. In addition, PLK1 over-expression is known to cause cellular transformation[96] and may thus affect the perpetuation of PLK1-over-expressing clones. Secondly, since transduction efficiencies differed and may confound data interpretation, we flow-sorted and analyzed equal numbers of mCherry-positive cells from both control and PLK1-over-expressed cells. Immunoblot analysis confirmed the over-expression of PLK1 (Figure-28). Our data showed that across all GPC lines tested, PLK1 over-expression was sufficient to nearly fully rescue BI2536 inhibitory effects on cell proliferation (Figure-29).

Summary

Our data provides evidence that PLK1 inhibition accounts for the inhibitory effect of BI2536 in GPC cell viability and clonogenicity. This provides firm basis for PLK1 as a therapeutic target.

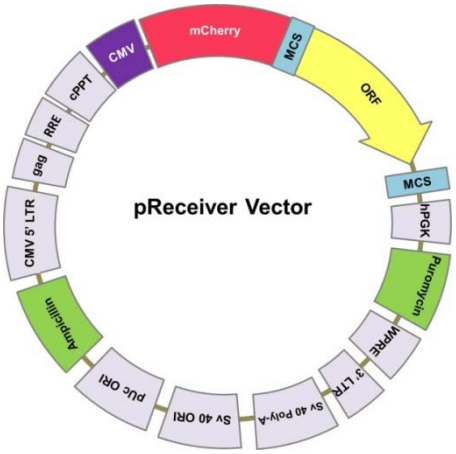

Figure-26. Vector map of pReceiver lentiviral backbone. Vector is driven by CMV promoter, contains mCherry fluorescence marker for visual tracking and puromycin selectable marker for establishment of stable clones.

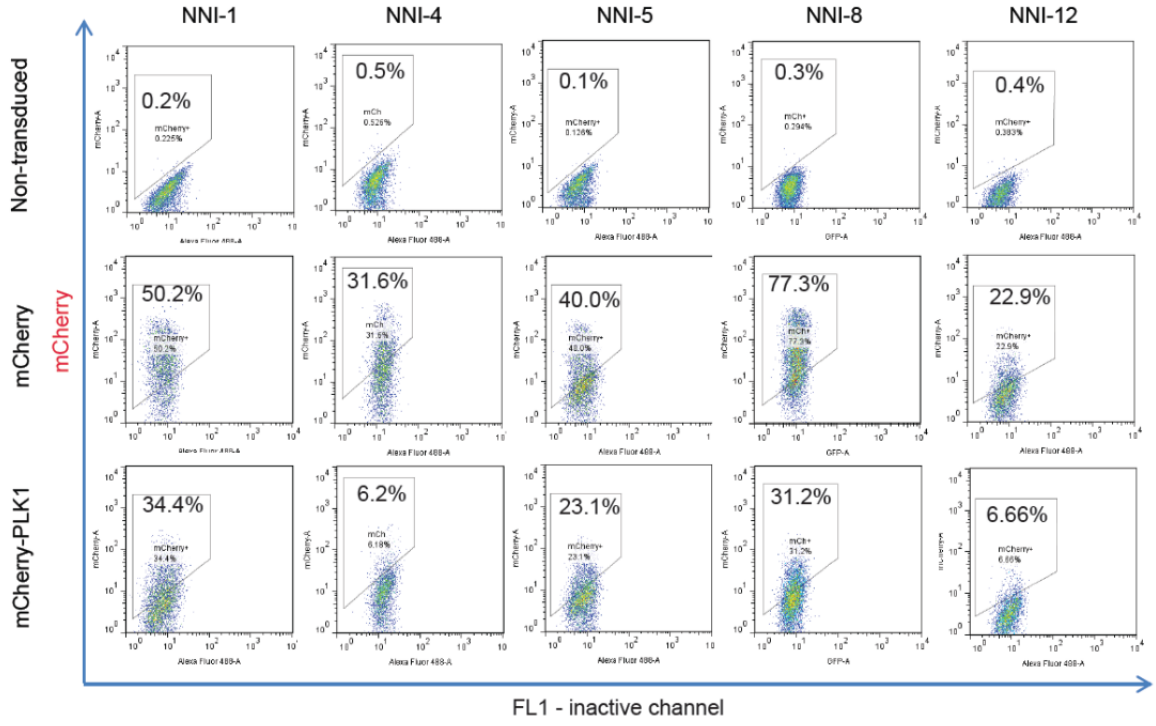

Figure-27. Transduction efficiency varies among GPC lines with pReceiver lentiviral backbone. Representative FACS plots of GPCs transduced with mCherry or mCherry-*PLK1* constructs. Differing percentages of mCherry+ signal were observed, suggesting variation in patient lines.

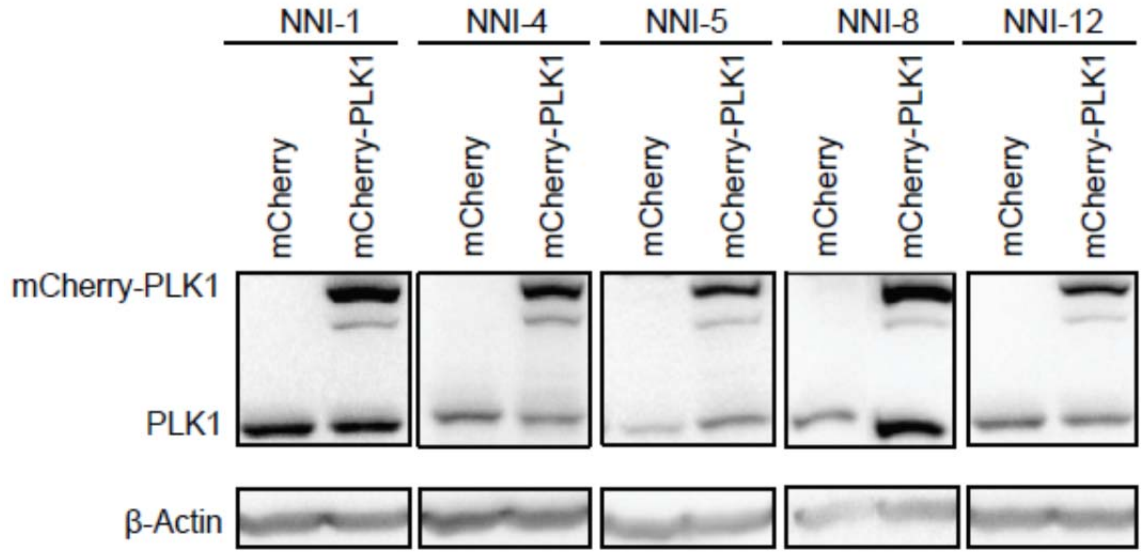

Figure-28. PLK1 is over-expressed in lentivirally transduced GPCs. Representative western blots of GPCs transduced with mCherry or mCherry-*PLK1* constructs.

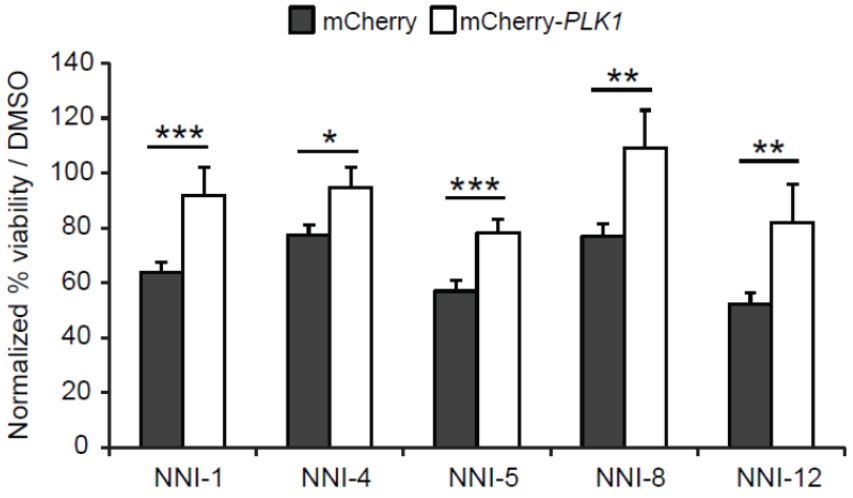

Figure-29. PLK1 over-expression rescues BI2536 inhibition. PLK1 over-expression resulted in near complete rescue of cell viability after BI2536 treatment. *$p < 0.05$, **$p < 0.01$, ***$p < 0.001$.

CHAPTER 6: BI2536 TREATMENT MITIGATES GLIOMA GROWTH IN MOUSE XENOGRAFT MODEL

6.1. BI2536 treatment mitigates glioma growth

Due to the reproducibility and experimentally feasible, short-term latency of U87MG glioma cells, together with the finding that they possess a tumor-initiating and sustaining GPC-like fraction[135], we decided to evaluate the effects of BI2536 in subcutaneous xenografts of BALB/c nude mice, a system which allows for relative ease in monitoring tumor volume changes. The efficacy of PLK1 small molecule inhibitors including BI2536 have already been demonstrated in several other tumor systems[123,136-138].

Accordingly, we implanted U87MG cells into the flanks of nude mice and monitored tumor volume and weight of mouse. When tumors reached 0.5 cm^3, we subjected the mice to either vehicle control or BI2536 intravenous tail-vein injections[123]. Tumor volume was measured every 2 days until termination of experiment where maximal tumor size was humanely possible. By 2 cycles of treatment, BI2536-treated animals exhibited reduced tumor volumes although not significant (Figure-30). By 3 cycles of treatment, BI2536-treated animals displayed significantly reduced tumor volumes by more than 2-fold compared to vehicle-treated animals (BI2536, n=16; vehicle, n=8); however, no significant difference was observed when compared to the initial tumor size at 0 cycle. Also, the average body weight of mice was reduced by approximately 10%, suggesting that BI2536 was tolerated with minimal toxicity. Our data provides evidence that BI2536 mitigates glioma growth via a cytostatic effect.

(A)

(B)

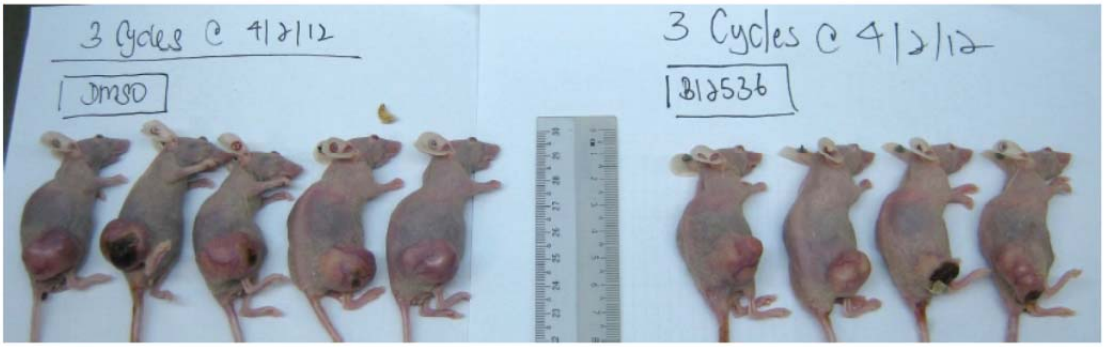

(C)

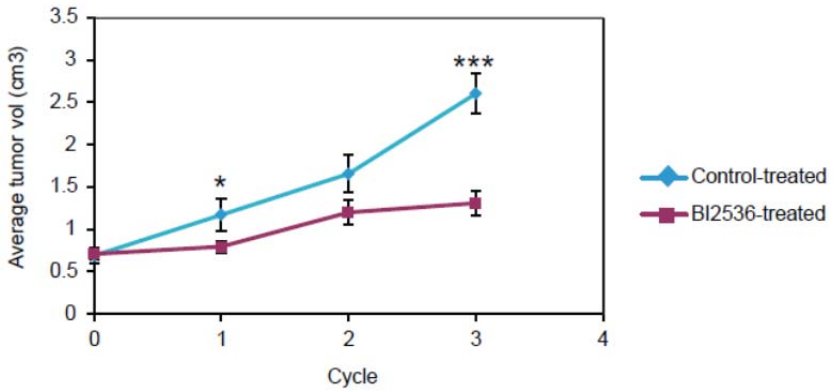

Figure-30. BI2536 treatment mitigates glioma growth. Photographs of control and BI2536-treated mice after **(A)** 2 cycles and **(B)** 3 cycles of treatment. **(C)** Average tumor volume of BI2536-treated mice was significantly smaller than control-treated after 3 cycles of treatment. Reduced rate of tumor growth indicated cytostatic effects of BI2536 treatment. *$p < 0.05$, ***$p < 0.001$.

6.2. BI2536 induces apoptosis

Next, we analyzed the mouse tumors by immunohistochemistry using the Terminal deoxynucleotidyl transferase dUTP nick End Labeling (TUNEL) assay that detects cell death by apoptosis. Consistent with the role of PLK1 inhibitors at inducing mitotic arrest with concomitant apoptosis[123,136-138], we observed that BI2536-treated tumors displayed significantly increased number of TUNEL-positive cells (Figure-31). These data suggest that BI2536 induces cell death by apoptosis, likely a contributing factor to the reduced tumor volumes.

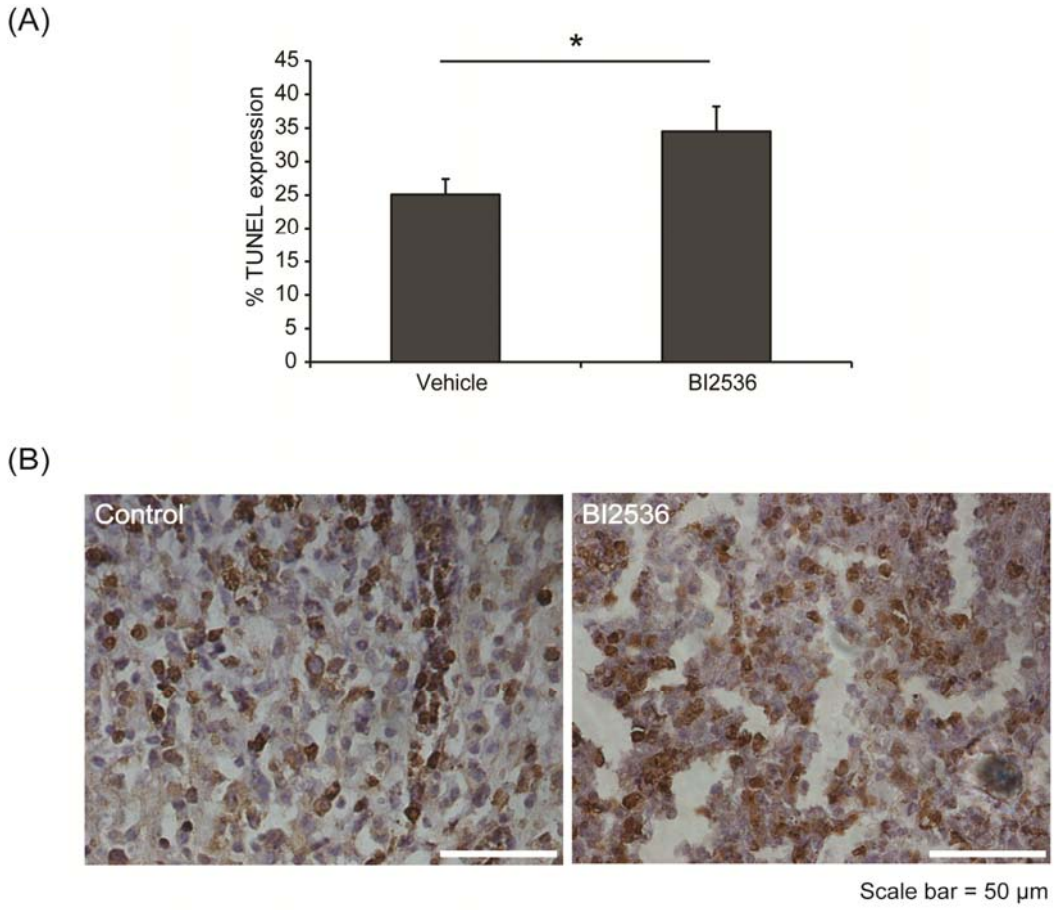

Figure-31. BI2536 induces apoptosis. BI2536-treated mice presented higher percentage of TUNEL+ cells, indicative of apoptosis. *$p < 0.05$, scale bar denotes 50 µm.

6.3. BI2536 targets Nestin-expressing glioma cells

One of the most important findings of our *in vitro* experiments points to the specific targeting of GPCs via the PLK1 signaling mechanism. Although most standard animal oncology models utilize tumor volume changes or survival as endpoints for determining the efficacy of treatments, these measures do not reveal the changes within GPCs, typically forming the minority cellular fraction but crucial for tumor-initiating and sustaining activity. In other words, tested treatments may inhibit majority, fast-growing cells but miss targeting the essential slow-growing, tumor-propagating fraction. The cancer stem cell hypothesis forces a re-evaluation of such endpoints for measuring inhibition of GPCs[132]. Accordingly, we determined the number of Nestin-positive cells in our tumor xenografts. Nestin frequently marks early neural precursors[139] and has been shown to be vital for glioma-propagating activity[26]. We observed that BI2536-treated tumors displayed significantly reduced but moderate number of Nestin-positive cells compared to vehicle-treated tumors by the third cycle of treatment (Figure-32). CD133 was not analyzed in the immunohistochemical sections due to inconsistencies arising from the choice of antibody clones used[140]. Our data suggests that BI2536 targets Nestin-expressing neural precursors.

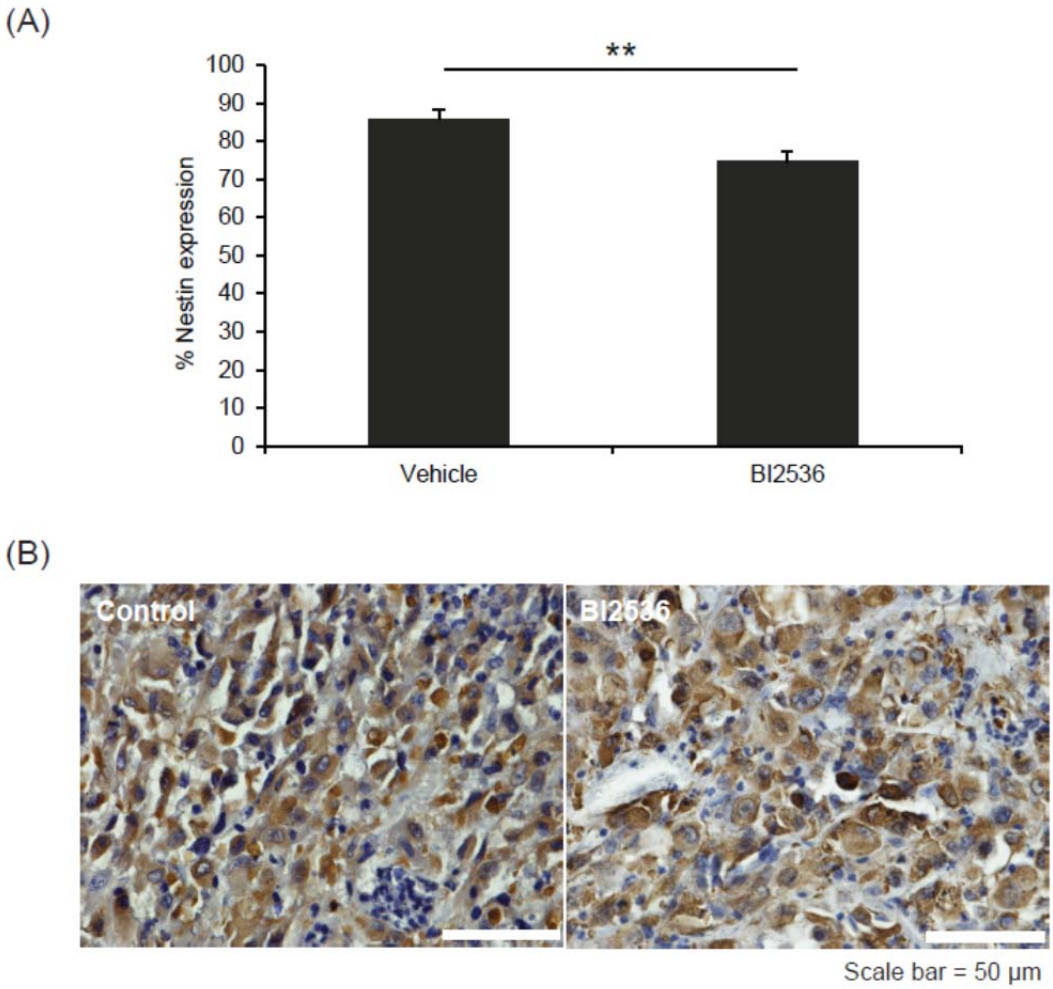

Figure-32. BI2536 targets Nestin-expressing glioma cells. BI2536-treated mice presented marginally lower percentage of Nestin-positive cells. $^{**}p < 0.01$, scale bar denotes 50µm.

Summary

Our animal model illustrates a cytostatic effect of BI2536 via apoptosis, and that Nestin-expressing GPCs are targeted. Although our data are moderately significant, nonetheless, they imply that combinational therapy to inhibit both self-renewing GPCs and bulk tumor cells may present a more effective therapeutic approach.

CHAPTER 7: *PLK1*-HIGH GENE SIGNATURE PORTENDS POOR PROGNOSIS

(Conducted by Edwin Sandanaraj, Singapore Institute for Clinical Sciences, A*STAR)

As our *in vitro* observations and animal model by no means represent perfect recapitulations of the tumorigenic process, we sought to analyze *PLK1* pathway relevance in patient clinical databases to substantiate our hypothesis. Our earlier data demonstrated that high *PLK1* mRNA expression in glioma patients (Figure- 6). Others have similarly observed that high PLK1 protein expression is present in higher tumor grades of clinical specimens, correlating with poorer survival[86]. Although the role of PLK1 in brain tumors is not new, we emphasize that our approach seeks to establish the direct link between patient-derived GPCs and disease progression and survival outcome. This is an important endeavor for the following reasons: (i) GPCs are controversial cells as their cell-of-origin in clinical specimens cannot be identified. Consequently, their clinical relevance and utility are questionable. Our effort will show that these cells contribute molecularly to patient survival outcome; (ii) We will show that brain tumors are molecularly heterogeneous and that the *PLK1*-high gene signature functions as an independent negative prognostic factor in brain tumors, considering current clinical indicators such as age and histology; and importantly, (iii) Our work will highlight the limitations of relying solely on morphology-based histological methods to diagnose and subsequently treat patients.

7.1. A *PLK1* gene signature is generated

Accordingly, we utilized 2 of the largest brain tumor clinical databases, REMBRANDT[101] (N=298) and Gravendeel[102] (N=276), to generate a "*PLK1* gene signature". In this process, we looked for genes that are significantly co-expressed with *PLK1* mRNA expression (Supplementary Table 2, correlation coefficient of ±0.5). We generated a list of 175 genes which intersected the 2 databases, of which, 171 genes that are positively correlated to *PLK1* expression and 4 inversely correlated. Collectively, these 175 genes represent our *PLK1* gene signature. A pathway network analysis on *PLK1* gene signature using GeneGo revealed that mainly cell cycle signaling modules are enriched (Figure-33), consistent with the role of PLK1 in cell cycle[58].

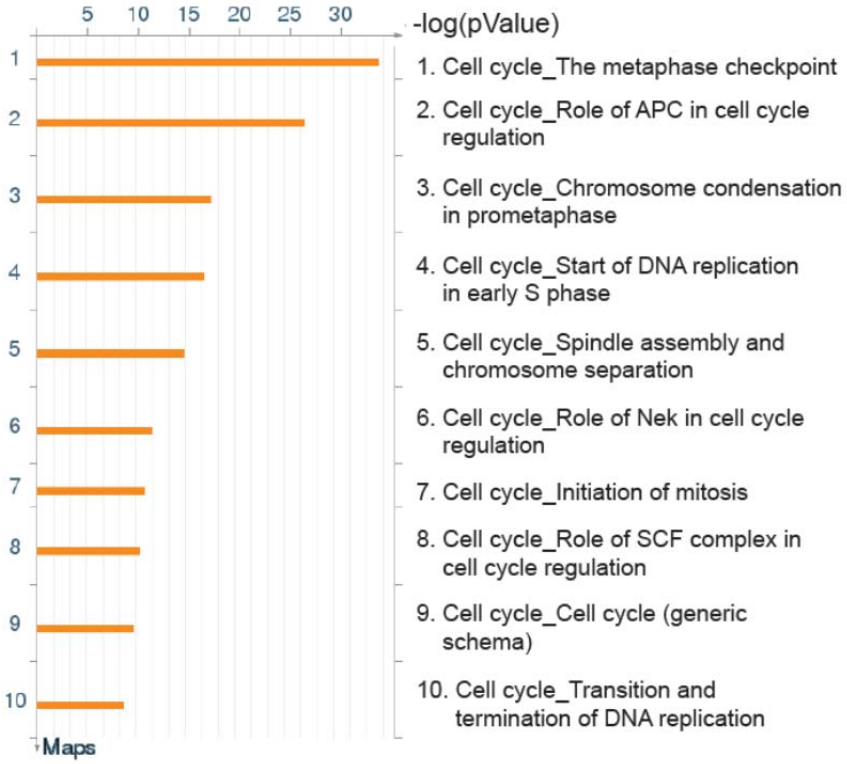

Figure-33. GeneGo pathway network associated with *PLK1* gene signature. Genes associated with high and low *PLK1* expression are mainly cell cycle-related networks.

7.2. *PLK1* gene signature stratifies brain tumor patient survival

Next, we asked if patient survival varied between the *PLK1*-high and –low groups. We performed self-clustering of the *PLK1* gene signature and observed that it significantly stratified patients' survival (REMBRANDT, p=2e-06; Gravendeel, p=1e-10) (Figure-34). Poorly surviving patients were enriched in the *PLK1*-high gene signature while patients with better prognosis tended to fall into the *PLK1*-low group. Furthermore, multivariate analysis indicated that the *PLK1* gene signature predicted survival independently of age and histology (Table-5; REMBRANDT, p=7.11e-05; Gravendeel, marginal insignificance, p=0.0721), suggesting that the gene signature defines molecular heterogeneity in the tumors that cannot be accounted for by current clinical indicators.

As several efforts have shown that gene expression drives molecular subgrouping of brain tumors[24,102,141-142], furthermore with each subgroup showing unique genomic, karyotypic and clinical profiles, we sought to examine closer the *PLK1*-high and –low expression patient tumors. We observed that *PLK1*-high tumors tended to exhibit Mesenchymal features of higher grades, typified by highly aggressive and recurrent tumors[142] (Figure-34). In contrast, *PLK1*-low tumors displayed Proneural molecular features, consistent with lower tumor grades[142]. The ability to draw connections between the *PLK1*-stratified patient groups and tumor molecular features is an important advance as it allows us to study primary tumor features that cannot be predicted by age and histology alone. This has significant implications as now, no 2 patient tumors are viewed alike based on molecular features, even though their histologies may be identical. This molecular heterogeneity may thus account for the frequently observed inter-patient variability to treatment response.

To further substantiate that GPC-like properties may account for *PLK1*-high and –low primary tumor behavior, we used Gene Set Enrichment Analysis[143] to determine if core stem cell programs can be enriched in the *PLK1*-stratified tumors. The core stem cell programs include signatures derived from embryonic, hematopoietic and neural stem cells and were utilized in a previous cancer stem cell-based approach by Nevins and colleagues[32]. This is a reasonable approach for us as both embryonic and neural stem cell modules have previously been shown to modulate brain tumor progression[128]. Accordingly, we observed that the *PLK1*-high patient tumors are enriched in

key stem cell modules signaling extensive self-renewal and proliferation (Supplementary Table-3). Interestingly, both Nanog[128] and Myc[144] were previously implicated as regulators of GPC sustenance. To verify that our bioinformatical predictions about *PLK1*-associated genes are valid in GPCs, we first filtered out neural stem cell modules and then investigated the expression of several well-known cell cycle-related genes which have been implicated in tumorigenesis. They include NIMA (never in mitosis gene-a)-related kinase 2 (*NEK2*), DNA topoisomerase 2-alpha, (*TOP2A*), protein regulator of cytokinesis 1 (*PRC1*), Epithelial Cell Transforming Sequence 2 (*ECT2*) and Forkhead box protein M1 (*FOXM1*). Our data consistently showed up-regulation of these genes in GPCs as compared to NHA cells (Figure-35). These data suggest that our GPCs represent biologically relevant cellular models of PLK1-over-expressed tumorigenic cells.

Collectively, our data provide strong evidence that stem cell-like traits are important in conferring the *PLK1*-high primary tumor phenotype, and consequently poor patient survival.

Summary

Our data provides strong evidence for the role of GPC-like traits in conferring the poor prognosis outcome of *PLK1*-high patients. These traits comprise extensive self-renewal and proliferating capabilities. In addition, our *PLK1* gene signature highlights the molecular heterogeneity of brain tumors that cannot be accounted for by current clinical indicators, age and histology. This finding forces a re-evaluation of the use of morphology-based pathological analyses to diagnose and subsequently treat patients, and paves the way for genome-informed targeted therapeutic design.

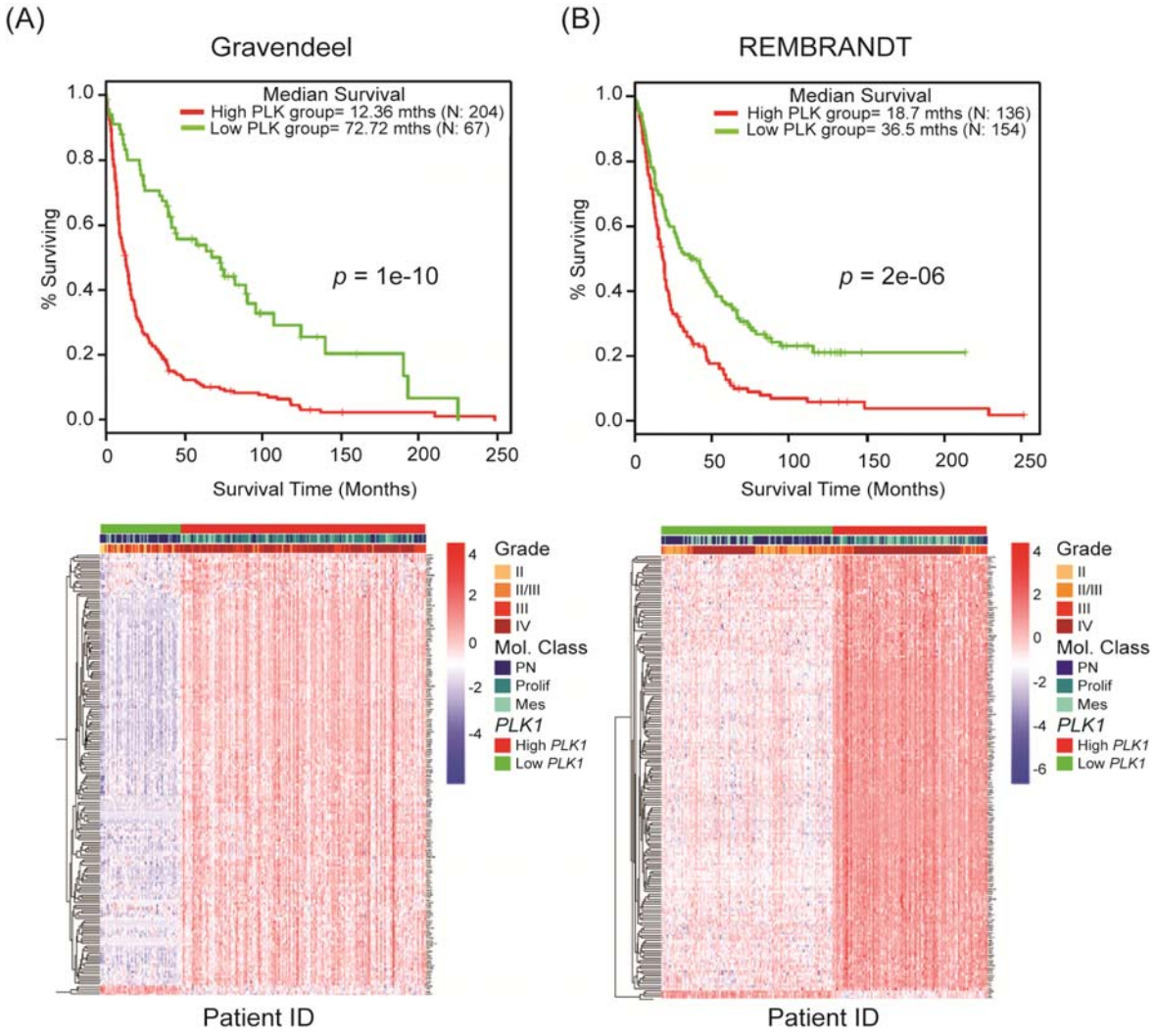

Figure-34. *PLK1* gene signature stratifies patient survival. From glioma databases **(A)** Gravendeel **(B)** REMBRANDT, *PLK1*-high group portends poorer survival and comprises the more aggressive tumor subtypes, namely Proliferative and Mesenchymal. Kaplan-Meier plots were drawn to show the cumulative probability of survival over the time from *PLK1* subgroups. A log-rank test p-value was computed to determine the significant difference between *PLK1* subgroups.

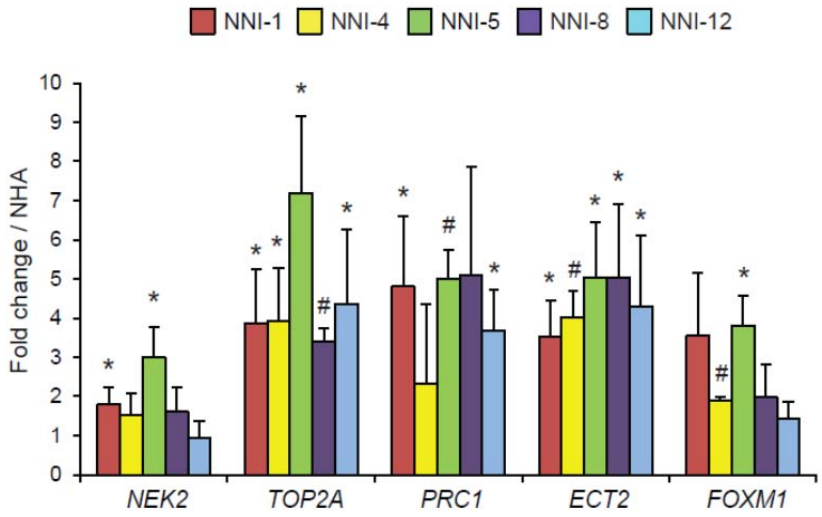

Figure-35. Quantitative real-time qRT-PCR analysis demonstrates up-regulation of cell cycle-related gene in GPCs. Cell cycle-related genes *NEK2*, *TOP2A*, *PRC1, ECT2 and FOXM1* were up-regulated in GPCs relative to NHA cells. **p*-value < 0.05, # *p*-value < 0.01.

Table-5. Multivariate Cox regression analysis of *PLK1* gene signature with age and histology.

Gravendeel

Covariates	Exp (coeffient)	Std error	95% CI	p-value
PLK1 Signature PLK1 Low	0.4676	0.1914	[0.3214-0.6804]	7.11E-05
Histology GBM	1.1131	0.2452	[0.6884-1.7997]	0.6621
Histology MIXED	0.2807	0.2986	[0.2807-0.9051]	0.0218
Histology OLIGODENDROGLIOMA	0.3042	0.2767	[0.1769- 0.5232]	1.70E-05
Age	1.0432	0.00554	[1.0319-1.0546]	2.36E-14

REMBRANDT

Covariates	Exp (coeffient)	Std error	95% CI	p-value
PLK1 Signature PLK1 Low	0.7694	0.1458	[0.5782-1.024]	0.0721
Histology GBM	2.4566	0.1832	[1.7156-3.518]	9.27E-07
Histology MIXED	0.9702	0.4694	[0.3866-2.435]	0.9487
Histology OLIGODENDROGLIOMA	0.9468	0.2448	[0.5860-1.530]	0.8233
Age	1.0129	0.0047	[1.0036-1.022]	0.0063

CHAPTER 8 – GENERAL DISCUSSION

One of the central tenets in cancer stem cell biology is understanding the cellular heterogeneity of tumors, and consequently what impact it has on experimental designs. Traditional short-term viability assays are fast methods in high-throughput screens; however, they often do not reflect effects on *bona fide* self-renewing cells in a surrounding of transient-amplifying progenitors. Thus, small molecule screens based on cancer stem cells must take into account the need to incorporate assays that measure long-term self-renewal in slow-growing cells. This is an important concept as small molecule candidates may, through viability assay prioritization, eradicate bulk tumors without inhibiting the most essential, tumor-initiating and sustaining fraction. Consequently, tumor recurrence is inevitable. To design better therapeutic strategies against these highly infiltrative and recurrent gliomas, the targeting of GPCs is essential. Here, we show that the well-developed neurosphere assay in neural stem cell biology provides a reliable method to assay for self-renewal[145]; in addition when combined with serial transplantation in mice, tumor-initiating and sustaining activity is measured. The prioritization of small molecule candidates based on the selectivity ratio enables GPC-specific targeting to be delineated from toxicity to normal cells.

In vivo efficacy of BI2536 in reducing tumor cell proliferation has been demonstrated by several groups[90,123,146-148]. We therefore tested *the* efficacy of BI2536 in Balb/C nude mice engrafted with U87MG serum-grown glioma cells, previously shown to contain a stem-like population responsible for tumor initiation[135]. Our results showed cytostatic effects on glioma growth. Conceivably, differences in experimental parameters such as choice of cell lines and onset of treatment might have contributed to the moderate effects. Also, further *in vivo* assessment of pharmacodynamics is desired as it will shed light on BI2536 levels within the tumor and animal body. Nonetheless, BI2536 has already shown promising results in clinical studies, together with various PLK1 inhibitors such as BI6727, ON01910 and GSK461364[149-152]. Furthermore, these compounds have shown favorable toxicity profiles in patients receiving the treatment.

We have seen that bioinformatics analyses revealed higher *PLK1* expression in GBM tissue compared to normal brain, thus validating our initial screen design on selectivity ratios to prioritize

compounds. While preparing this thesis and manuscript, an article was published on the novel role of PLK1 in regulating survival of GBM GPCs, thus validating our approach and conclusions[90]. Our work extends upon their findings by querying the contribution of GPCs to patient survival outcome, thus providing a direct relationship between these cells and the primary tumor phenotype; consequently validating their use as an *in vitro* cellular screening system tailored towards stem cell-specific parameters. Admittedly, such extended and in-depth sphere assays would not be amenable to high throughput screening in the traditional sense (i.e. thousands of compounds) but we wish to emphasize a re-evaluation of screening criteria to detect long-term self-renewing GPCs.

Cancer stem cells are controversial cells mainly because they have been shown to initiate tumors in mice at varying frequencies depending on tumor subtype and experimental conditions, indicating that the tumor-initiating capacity, a central theme in cancer stem cells, may actually be an artefactual consequence of experimental parameters[27,130]. This forces a re-definition of cancer stem cells to focus on the most important criteria: Long-term self-renewal and the ability to recapitulate the primary tumor pathophysiology. Still, the question remains as to whether such cells are clinically meaningful if they constitute an often small fraction of the tumor mass. Here, we have tapped into large, public glioma databases to evaluate the prognostic value of *PLK1* gene expression. Although our conclusions are not entirely novel in that previous works have indeed implicated high PLK1 in GBM specimens and cell lines[86]; moreover *PLK1* is synthetically lethal with *TP53* mutation in GBM[126], we show that genes associated with *PLK1* high patient cohort encompass several stem cell-like candidates, several of which contribute to clinical outcome in other cancers[31-32,153]. Noteworthy, our *PLK1* high expression is enriched for the Proliferative and Mesenchymal molecular subclasses in glioma databases comprising various tumor grades and histologies. Such findings imply that the choice of patient databases/histologies and conceivably molecular heterogeneity of primary tumors affect the assignment of *PLK1* high and low groups. Furthermore, it shows that although the *PLK1* gene signature has a prognostic role, its true predictive value would have to be determined using a prospectively collected patient cohort subjected to PLK1 inhibition therapy.

These data collectively highlight the value of GPCs in determining disease progression and patient outcome, and that by inference; their targeting should present a long-lasting, effective cure. The additional understanding that PLK1 targeting occurs at the level of GPCs should therefore prioritize the development of this class of compounds in glioma therapy. Our findings also suggest that *PLK1* expression predicts molecular heterogeneity that cannot be accounted for by histology alone. This highlights the limitation of morphology-based approaches in patient diagnosis and consequently impacting on treatment decision. Our work further supports that patients with elevated *PLK1* signaling pathway may thus be amenable to PLK1 inhibition therapies. In summary, we show the relevance of GPCs as a valuable *in vitro* screening platform, and further validate their prognostic significance in disease progression and patient survival outcome.

8.1. Future directions

Our work sheds light on the role of PLK1 in mitigating GPC survival, and importantly, in tumor growth in a nude mouse model. Ideally, we would like to conduct BI2536 dose efficacy studies using orthotopic mouse models of glioma established from patient-derived GPCs, and treating the animals by oral gavage to simulate actual patient scenarios. The feasibility of this approach has recently been demonstrated in glioma biology[90].

In addition, we would like to explore deeper the mechanism behind PLK1 inhibition. Conceivably, we could subject GPCs transduced with non-targeting and sh*PLK1* lentiviral clones to genome-wide gene expression analysis. We could then define a differential gene list, and interrogate its pattern of association in patient gene expression data. We showed recently that the Connectivity Map offers a technically feasible method to carry out this gene association study[13,154-155]. Such a method has several advantages: (i) It allows data from various platforms to be integrated and analyzed in association with each other through the common language of gene expression, previously shown to drive glioma disease progression; (ii) it allows us to determine patient cohorts likely to receive treatment benefit through PLK1 inhibition; and (iii) it allows us to identify patient genetic characteristics associated with a favorable response, as these patient databases contain deep sequencing information. Such an endeavor would enable us to draw a connection between our *in vitro* PLK1 inhibition-induced tumor cell death, and patient treatment profiles. Our work will redefine the utility of molecularly driven, genome-informed decisions in tailoring therapies for glioma patients.

Finally, we recently showed that GPCs from major glioma variants phenocopy their original patient's biological and transcriptomic programs, and contributed to different signaling pathway activation in patient cohorts[13]. This work has significant implications as it means we can now tap into our patient-derived GPCs to establish orthotopic xenograft tumors for preclinical drug testing. Our GPCs thus represent patient-mouse tumor replicas that can be prospectively mined for drug responses, yet have retrospective clinical history and deep sequencing information for correlation studies.

8.2. Conclusion

GPCs are clinically relevant tools which reflect the biology and transcriptomic programs of the patient's original primary tumor. We provide evidence that PLK1 is a viable therapeutic target and its inhibition abrogates glioma growth. Our bioinformatical analysis highlights that the *PLK1* high signature is a negative prognostic factor; furthermore, correlates with highly aggressive, infiltrative and recurrent tumors. Our work highlights the limitation of relying solely on morphology-based histological methods to diagnose and subsequently treat patients. Gliomas are thus viewed as molecularly heterogeneous cancers[24,102,142,156]. With the advances of public efforts in gathering deep sequencing information of patient primary tumors[23,101], glioma biology is now well-poised to interrogate the feasibility of genome-informed treatment strategies. Our study here provides the first steps in combining such bench research with animal models and patient resources.

BILIOGRAPHY

1. Louis, D. N., Ohgaki, H., Wiestler, O. D., Cavenee, W. K., Burger, P. C., Jouvet, A., Scheithauer, B. W. & Kleihues, P. The 2007 WHO classification of tumours of the central nervous system. ***Acta Neuropathol*** 114, 97-109 (2007).

2. Galli, R., Binda, E., Orfanelli, U., Cipelletti, B., Gritti, A., De Vitis, S., Fiocco, R., Foroni, C., Dimeco, F. & Vescovi, A. Isolation and characterization of tumorigenic, stem-like neural precursors from human glioblastoma. ***Cancer Res*** 64, 7011-7021 (2004).

3. Singh, S. K., Clarke, I. D., Terasaki, M., Bonn, V. E., Hawkins, C., Squire, J. & Dirks, P. B. Identification of a cancer stem cell in human brain tumors. ***Cancer Res*** 63, 5821-5828 (2003).

4. Singh, S. K., Hawkins, C., Clarke, I. D., Squire, J. A., Bayani, J., Hide, T., Henkelman, R. M., Cusimano, M. D. & Dirks, P. B. Identification of human brain tumour initiating cells. ***Nature*** 432, 396-401 (2004).

5. Bao, S., Wu, Q., McLendon, R. E., Hao, Y., Shi, Q., Hjelmeland, A. B., Dewhirst, M. W., Bigner, D. D. & Rich, J. N. Glioma stem cells promote radioresistance by preferential activation of the DNA damage response. ***Nature*** 444, 756-760 (2006).

6. Eramo, A., Ricci-Vitiani, L., Zeuner, A., Pallini, R., Lotti, F., Sette, G., Pilozzi, E., Larocca, L. M., Peschle, C. & De Maria, R. Chemotherapy resistance of glioblastoma stem cells. ***Cell Death Differ*** 13, 1238-1241 (2006).

7. Liu, G., Yuan, X., Zeng, Z., Tunici, P., Ng, H., Abdulkadir, I. R., Lu, L., Irvin, D., Black, K. L. & Yu, J. S. Analysis of gene expression and chemoresistance of CD133+ cancer stem cells in glioblastoma. ***Mol Cancer*** 5, 67 (2006).

8. Alcantara Llaguno, S., Chen, J., Kwon, C. H., Jackson, E. L., Li, Y., Burns, D. K., Alvarez-Buylla, A. & Parada, L. F. Malignant astrocytomas originate from neural stem/progenitor cells in a somatic tumor suppressor mouse model. ***Cancer Cell*** 15, 45-56 (2009).

9. Liu, C., Sage, J. C., Miller, M. R., Verhaak, R. G., Hippenmeyer, S., Vogel, H., Foreman, O., Bronson, R. T., Nishiyama, A., Luo, L. & Zong, H. Mosaic Analysis with Double Markers Reveals Tumor Cell of Origin in Glioma. ***Cell*** (2011).

10. Zheng, H., Ying, H., Yan, H., Kimmelman, A. C., Hiller, D. J., Chen, A. J., Perry, S. R., Tonon, G., Chu, G. C., Ding, Z., Stommel, J. M., Dunn, K. L., Wiedemeyer, R., You, M. J., Brennan, C., Wang, Y. A., Ligon, K. L., Wong, W. H., Chin, L. & DePinho, R. A. p53 and Pten control neural and glioma stem/progenitor cell renewal and differentiation. ***Nature*** 455, 1129-1133 (2008).

11. Lee, J., Kotliarova, S., Kotliarov, Y., Li, A., Su, Q., Donin, N. M., Pastorino, S., Purow, B. W., Christopher, N., Zhang, W., Park, J. K. & Fine, H. A. Tumor stem cells derived from glioblastomas cultured in bFGF and EGF more closely mirror the phenotype and genotype of primary tumors than do serum-cultured cell lines. ***Cancer Cell*** 9, 391-403 (2006).

12. Wakimoto, H., Mohapatra, G., Kanai, R., Curry, W. T., Jr., Yip, S., Nitta, M., Patel, A. P., Barnard, Z. R., Stemmer-Rachamimov, A. O., Louis, D. N., Martuza, R. L. & Rabkin, S. D. Maintenance of primary tumor phenotype and genotype in glioblastoma stem cells. ***Neuro Oncol*** (2011).

13. Ng, F. S., Toh, T. B., Ting, E., Koh, G. R., Sandanaraj, E., Phong, M., Wong, S. S., Leong, S. H., Kon, O. L., Tucker-Kellogg, G., Ng, W. H., Ng, I., Tang, C. & Ang, B. T. Progenitor-Like Traits Contribute to Patient Survival and Prognosis in Oligodendroglial Tumors. ***Clin Cancer Res*** (2012).

14. Yan, X., Ma, L., Yi, D., Yoon, J. G., Diercks, A., Foltz, G., Price, N. D., Hood, L. E. & Tian, Q. A CD133-related gene expression signature identifies an aggressive glioblastoma subtype with excessive mutations. ***Proc Natl Acad Sci U S A*** 108, 1591-1596 (2011).

15. Rich, J. N. & Eyler, C. E. Cancer Stem Cells in Brain Tumor Biology. ***Cold Spring Harb Symp Quant Biol*** (2009).

16. Kleihues, P., Burger, P. C. & Scheithauer, B. W. The new WHO classification of brain tumours. ***Brain Pathol*** 3, 255-268 (1993).

17. Zulch, k. j. e. Histological typing of tumours of the central nervous system. World Health Organization, Geneva. (1979).

18. Ringertz, j. Grading of gliomas. Acta Pathol Microbiol Scand 27:51-64. (1950).

19. Daumas-Duport, C. & Varlet, P. Dysembryoplastic neuroepitheilial tumors. ***Rev Neurol (Paris)*** 159, 622-636 (2003).

20. Giannini, C., Scheithauer, B. W., Steinberg, J. & Cosgrove, T. J. Intraventricular perineurioma: case report. ***Neurosurgery*** 43, 1478-1481; discussion 1481-1472 (1998).

21. Huang, C. I., Chiou, W. H. & Ho, D. M. Oligodendroglioma occurring after radiation therapy for pituitary adenoma. ***J Neurol Neurosurg Psychiatry*** 50, 1619-1624 (1987).

22. Neder, L., Colli, B. O., Machado, H. R., Carlotti, C. G., Jr., Santos, A. C. & Chimelli, L. MIB-1 labeling index in astrocytic tumors--a clinicopathologic study. ***Clin Neuropathol*** 23, 262-270 (2004).

23. Atlas, T. C. G. Comprehensive genomic characterization defines human glioblastoma genes and core pathways. ***Nature*** 455, 1061-1068 (2008).

24. Verhaak, R. G., Hoadley, K. A., Purdom, E., Wang, V., Qi, Y., Wilkerson, M. D., Miller, C. R., Ding, L., Golub, T., Mesirov, J. P., Alexe, G., Lawrence, M., O'Kelly, M., Tamayo, P., Weir, B. A., Gabriel, S., Winckler, W., Gupta, S., Jakkula, L., Feiler, H. S., Hodgson, J. G., James, C. D., Sarkaria, J. N., Brennan, C., Kahn, A., Spellman, P. T., Wilson, R. K., Speed, T. P., Gray, J. W., Meyerson, M., Getz, G., Perou, C. M. & Hayes, D. N. Integrated genomic analysis identifies clinically relevant subtypes of glioblastoma characterized by abnormalities in PDGFRA, IDH1, EGFR, and NF1. ***Cancer Cell*** 17, 98-110 (2010).

25. Wiedemeyer, W. R., Dunn, I. F., Quayle, S. N., Zhang, J., Chheda, M. G., Dunn, G. P., Zhuang, L., Rosenbluh, J., Chen, S., Xiao, Y., Shapiro, G. I., Hahn, W. C. & Chin, L. Pattern of retinoblastoma pathway inactivation dictates response to CDK4/6 inhibition in GBM. ***Proc Natl Acad Sci U S A*** 107, 11501-11506 (2010).

26. Bar, E. E., Chaudhry, A., Lin, A., Fan, X., Schreck, K., Matsui, W., Piccirillo, S., Vescovi, A. L., DiMeco, F., Olivi, A. & Eberhart, C. G. Cyclopamine-mediated hedgehog pathway inhibition depletes stem-like cancer cells in glioblastoma. ***Stem Cells*** 25, 2524-2533 (2007).

27. Beier, D., Hau, P., Proescholdt, M., Lohmeier, A., Wischhusen, J., Oefner, P. J., Aigner, L., Brawanski, A., Bogdahn, U. & Beier, C. P. CD133(+) and CD133(-) glioblastoma-derived cancer stem cells show differential growth characteristics and molecular profiles. ***Cancer Res*** 67, 4010-4015 (2007).

28. Sakariassen, P. O., Prestegarden, L., Wang, J., Skaftnesmo, K. O., Mahesparan, R., Molthoff, C., Sminia, P., Sundlisaeter, E., Misra, A., Tysnes, B. B., Chekenya, M., Peters, H., Lende, G., Kalland, K. H., Oyan, A. M., Petersen, K., Jonassen, I., van der Kogel, A., Feuerstein, B. G., Terzis, A. J., Bjerkvig, R. & Enger, P. O. Angiogenesis-independent tumor growth mediated by stem-like cancer cells. ***Proc Natl Acad Sci U S A*** 103, 16466-16471 (2006).

29. Son, M. J., Woolard, K., Nam, D. H., Lee, J. & Fine, H. A. SSEA-1 is an enrichment marker for tumor-initiating cells in human glioblastoma. ***Cell Stem Cell*** 4, 440-452 (2009).

30. Lim, E., Vaillant, F., Wu, D., Forrest, N. C., Pal, B., Hart, A. H., Asselin-Labat, M. L., Gyorki, D. E., Ward, T., Partanen, A., Feleppa, F., Huschtscha, L. I., Thorne, H. J., Fox, S. B., Yan, M., French, J. D., Brown, M. A., Smyth, G. K., Visvader, J. E. & Lindeman, G. J. Aberrant luminal progenitors as the candidate target population for basal tumor development in BRCA1 mutation carriers. ***Nat Med*** 15, 907-913 (2009).

31. Eppert, K., Takenaka, K., Lechman, E. R., Waldron, L., Nilsson, B., van Galen, P., Metzeler, K. H., Poeppl, A., Ling, V., Beyene, J., Canty, A. J., Danska, J. S., Bohlander, S. K., Buske, C., Minden, M. D., Golub, T. R., Jurisica, I., Ebert, B. L. & Dick, J. E. Stem cell gene expression programs influence clinical outcome in human leukemia. ***Nat Med*** 17, 1086-1093 (2011).

32. Shats, I., Gatza, M. L., Chang, J. T., Mori, S., Wang, J., Rich, J. & Nevins, J. R. Using a stem cell-based signature to guide therapeutic selection in cancer. ***Cancer Res*** 71, 1772-1780 (2011).

33. Alley, M. C., Scudiero, D. A., Monks, A., Hursey, M. L., Czerwinski, M. J., Fine, D. L., Abbott, B. J., Mayo, J. G., Shoemaker, R. H. & Boyd, M. R. Feasibility of drug screening with panels of human tumor cell lines using a microculture tetrazolium assay. ***Cancer Res*** 48, 589-601 (1988).

34. Bleau, A. M., Hambardzumyan, D., Ozawa, T., Fomchenko, E. I., Huse, J. T., Brennan, C. W. & Holland, E. C. PTEN/PI3K/Akt pathway regulates the side population phenotype and ABCG2 activity in glioma tumor stem-like cells. ***Cell Stem Cell*** 4, 226-235 (2009).

35. Momota, H., Nerio, E. & Holland, E. C. Perifosine inhibits multiple signaling pathways in glial progenitors and cooperates with temozolomide to arrest cell proliferation in gliomas in vivo. ***Cancer Res*** 65, 7429-7435 (2005).

36. Dinca, E. B., Sarkaria, J. N., Schroeder, M. A., Carlson, B. L., Voicu, R., Gupta, N., Berger, M. S. & James, C. D. Bioluminescence monitoring of intracranial glioblastoma xenograft: response to primary and salvage temozolomide therapy. ***J Neurosurg*** 107, 610-616 (2007).

37. Hashizume, R., Ozawa, T., Dinca, E. B., Banerjee, A., Prados, M. D., James, C. D. & Gupta, N. A human brainstem glioma xenograft model enabled for bioluminescence imaging. ***J Neurooncol*** 96, 151-159 (2010).

38. Yang, M., Baranov, E., Jiang, P., Sun, F. X., Li, X. M., Li, L., Hasegawa, S., Bouvet, M., Al-Tuwaijri, M., Chishima, T., Shimada, H., Moossa, A. R., Penman, S. & Hoffman, R. M.

Whole-body optical imaging of green fluorescent protein-expressing tumors and metastases. ***Proc Natl Acad Sci U S A*** 97, 1206-1211 (2000).

39. Yang, M., Baranov, E., Moossa, A. R., Penman, S. & Hoffman, R. M. Visualizing gene expression by whole-body fluorescence imaging. ***Proc Natl Acad Sci U S A*** 97, 12278-12282 (2000).

40. Carcaboso, A. M., Elmeliegy, M. A., Shen, J., Juel, S. J., Zhang, Z. M., Calabrese, C., Tracey, L., Waters, C. M. & Stewart, C. F. Tyrosine kinase inhibitor gefitinib enhances topotecan penetration of gliomas. ***Cancer Res*** 70, 4499-4508 (2010).

41. Moroz, M. A., Huang, R., Kochetkov, T., Shi, W., Thaler, H., de Stanchina, E., Gamez, I., Ryan, R. P. & Blasberg, R. G. Comparison of corticotropin-releasing factor, dexamethasone, and temozolomide: treatment efficacy and toxicity in U87 and C6 intracranial gliomas. ***Clin Cancer Res*** 17, 3282-3292 (2011).

42. Candolfi, M., Curtin, J. F., Nichols, W. S., Muhammad, A. G., King, G. D., Pluhar, G. E., McNiel, E. A., Ohlfest, J. R., Freese, A. B., Moore, P. F., Lerner, J., Lowenstein, P. R. & Castro, M. G. Intracranial glioblastoma models in preclinical neuro-oncology: neuropathological characterization and tumor progression. ***J Neurooncol*** 85, 133-148 (2007).

43. Sharpless, N. E. & Depinho, R. A. The mighty mouse: genetically engineered mouse models in cancer drug development. ***Nat Rev Drug Discov*** 5, 741-754 (2006).

44. Voskoglou-Nomikos, T., Pater, J. L. & Seymour, L. Clinical predictive value of the in vitro cell line, human xenograft, and mouse allograft preclinical cancer models. ***Clin Cancer Res*** 9, 4227-4239 (2003).

45. Kinzler, K. W. & Vogelstein, B. Lessons from hereditary colorectal cancer. ***Cell*** 87, 159-170 (1996).

46. Van Dyke, T. & Jacks, T. Cancer modeling in the modern era: progress and challenges. ***Cell*** 108, 135-144 (2002).

47. Zhu, Y., Guignard, F., Zhao, D., Liu, L., Burns, D. K., Mason, R. P., Messing, A. & Parada, L. F. Early inactivation of p53 tumor suppressor gene cooperating with NF1 loss induces malignant astrocytoma. ***Cancer Cell*** 8, 119-130 (2005).

48. Gu, H., Marth, J. D., Orban, P. C., Mossmann, H. & Rajewsky, K. Deletion of a DNA polymerase beta gene segment in T cells using cell type-specific gene targeting. ***Science*** 265, 103-106 (1994).

49. Kuhn, R., Schwenk, F., Aguet, M. & Rajewsky, K. Inducible gene targeting in mice. ***Science*** 269, 1427-1429 (1995).

50. Federspiel, M. J., Bates, P., Young, J. A., Varmus, H. E. & Hughes, S. H. A system for tissue-specific gene targeting: transgenic mice susceptible to subgroup A avian leukosis virus-based retroviral vectors. ***Proc Natl Acad Sci U S A*** 91, 11241-11245 (1994).

51. Tchougounova, E., Kastemar, M., Brasater, D., Holland, E. C., Westermark, B. & Uhrbom, L. Loss of Arf causes tumor progression of PDGFB-induced oligodendroglioma. ***Oncogene*** 26, 6289-6296 (2007).

52. Chow, L. M., Endersby, R., Zhu, X., Rankin, S., Qu, C., Zhang, J., Broniscer, A., Ellison, D. W. & Baker, S. J. Cooperativity within and among Pten, p53, and Rb pathways induces high-grade astrocytoma in adult brain. ***Cancer Cell*** 19, 305-316 (2011).

53. Lei, L., Sonabend, A. M., Guarnieri, P., Soderquist, C., Ludwig, T., Rosenfeld, S., Bruce, J. N. & Canoll, P. Glioblastoma models reveal the connection between adult glial progenitors and the proneural phenotype. ***PLoS One*** 6, e20041 (2011).

54. De Witt Hamer, P. C., Van Tilborg, A. A., Eijk, P. P., Sminia, P., Troost, D., Van Noorden, C. J., Ylstra, B. & Leenstra, S. The genomic profile of human malignant glioma is altered early in primary cell culture and preserved in spheroids. ***Oncogene*** 27, 2091-2096 (2008).

55. Reynolds, B. A. & Rietze, R. L. Neural stem cells and neurospheres-re-evaluating the relationship. ***Nat Methods*** 2, 333-336 (2005).

56. Piccirillo, S. G., Reynolds, B. A., Zanetti, N., Lamorte, G., Binda, E., Broggi, G., Brem, H., Olivi, A., Dimeco, F. & Vescovi, A. L. Bone morphogenetic proteins inhibit the tumorigenic potential of human brain tumour-initiating cells. ***Nature*** 444, 761-765 (2006).

57. Archambault, V. & Glover, D. M. Polo-like kinases: conservation and divergence in their functions and regulation. ***Nat Rev Mol Cell Biol*** 10, 265-275 (2009).

58. van de Weerdt, B. C. & Medema, R. H. Polo-like kinases: a team in control of the division. ***Cell Cycle*** 5, 853-864 (2006).

59. van Vugt, M. A. & Medema, R. H. Getting in and out of mitosis with Polo-like kinase-1. ***Oncogene*** 24, 2844-2859 (2005).

60. Hamanaka, R., Smith, M. R., O'Connor, P. M., Maloid, S., Mihalic, K., Spivak, J. L., Longo, D. L. & Ferris, D. K. Polo-like kinase is a cell cycle-regulated kinase activated during mitosis. ***J Biol Chem*** 270, 21086-21091 (1995).

61. Martin, B. T. & Strebhardt, K. Polo-like kinase 1: target and regulator of transcriptional control. ***Cell Cycle*** 5, 2881-2885 (2006).

62. Uchiumi, T., Longo, D. L. & Ferris, D. K. Cell cycle regulation of the human polo-like kinase (PLK) promoter. ***J Biol Chem*** 272, 9166-9174 (1997).

63. Seki, A., Coppinger, J. A., Jang, C. Y., Yates, J. R. & Fang, G. Bora and the kinase Aurora a cooperatively activate the kinase Plk1 and control mitotic entry. ***Science*** 320, 1655-1658 (2008).

64. Gunawardena, R. W., Siddiqui, H., Solomon, D. A., Mayhew, C. N., Held, J., Angus, S. P. & Knudsen, E. S. Hierarchical requirement of SWI/SNF in retinoblastoma tumor suppressor-mediated repression of Plk1. ***J Biol Chem*** 279, 29278-29285 (2004).

65. Zhu, H., Chang, B. D., Uchiumi, T. & Roninson, I. B. Identification of promoter elements responsible for transcriptional inhibition of polo-like kinase 1 and topoisomerase IIalpha genes by p21(WAF1/CIP1/SDI1). ***Cell Cycle*** 1, 59-66 (2002).

66. Brehm, A., Miska, E. A., McCance, D. J., Reid, J. L., Bannister, A. J. & Kouzarides, T. Retinoblastoma protein recruits histone deacetylase to repress transcription. ***Nature*** 391, 597-601 (1998).

67. Dyson, N. The regulation of E2F by pRB-family proteins. ***Genes Dev*** 12, 2245-2262 (1998).

68. Fu, Z., Malureanu, L., Huang, J., Wang, W., Li, H., van Deursen, J. M., Tindall, D. J. & Chen, J. Plk1-dependent phosphorylation of FoxM1 regulates a transcriptional programme required for mitotic progression. ***Nat Cell Biol*** 10, 1076-1082 (2008).

69. Ji, J. H. & Jang, Y. J. Functional independency between catalytic activity and subcellular targeting of polo-like kinase-1: phenotypes of ectopic overexpression of various mutants. ***Cell Cycle*** 7, 1597-1603 (2008).

70. Petronczki, M., Glotzer, M., Kraut, N. & Peters, J. M. Polo-like kinase 1 triggers the initiation of cytokinesis in human cells by promoting recruitment of the RhoGEF Ect2 to the central spindle. ***Dev Cell*** 12, 713-725 (2007).

71. Reindl, W., Yuan, J., Kramer, A., Strebhardt, K. & Berg, T. Inhibition of polo-like kinase 1 by blocking polo-box domain-dependent protein-protein interactions. ***Chem Biol*** 15, 459-466 (2008).

72. Roshak, A. K., Capper, E. A., Imburgia, C., Fornwald, J., Scott, G. & Marshall, L. A. The human polo-like kinase, PLK, regulates cdc2/cyclin B through phosphorylation and activation of the cdc25C phosphatase. ***Cell Signal*** 12, 405-411 (2000).

73. Toyoshima-Morimoto, F., Taniguchi, E. & Nishida, E. Plk1 promotes nuclear translocation of human Cdc25C during prophase. ***EMBO Rep*** 3, 341-348 (2002).

74. Tsvetkov, L. & Stern, D. F. Phosphorylation of Plk1 at S137 and T210 is inhibited in response to DNA damage. ***Cell Cycle*** 4, 166-171 (2005).

75. Ando, K., Ozaki, T., Yamamoto, H., Furuya, K., Hosoda, M., Hayashi, S., Fukuzawa, M. & Nakagawara, A. Polo-like kinase 1 (Plk1) inhibits p53 function by physical interaction and phosphorylation. ***J Biol Chem*** 279, 25549-25561 (2004).

76. Lee, M., Daniels, M. J. & Venkitaraman, A. R. Phosphorylation of BRCA2 by the Polo-like kinase Plk1 is regulated by DNA damage and mitotic progression. ***Oncogene*** 23, 865-872 (2004).

77. Lane, H. A. & Nigg, E. A. Antibody microinjection reveals an essential role for human polo-like kinase 1 (Plk1) in the functional maturation of mitotic centrosomes. ***J Cell Biol*** 135, 1701-1713 (1996).

78. Casenghi, M., Meraldi, P., Weinhart, U., Duncan, P. I., Korner, R. & Nigg, E. A. Polo-like kinase 1 regulates Nlp, a centrosome protein involved in microtubule nucleation. ***Dev Cell*** 5, 113-125 (2003).

79. Feng, Y., Hodge, D. R., Palmieri, G., Chase, D. L., Longo, D. L. & Ferris, D. K. Association of polo-like kinase with alpha-, beta- and gamma-tubulins in a stable complex. ***Biochem J*** 339 (Pt 2), 435-442 (1999).

80. Yarm, F. R. Plk phosphorylation regulates the microtubule-stabilizing protein TCTP. ***Mol Cell Biol*** 22, 6209-6221 (2002).

81. Nasmyth, K., Peters, J. M. & Uhlmann, F. Splitting the chromosome: cutting the ties that bind sister chromatids. ***Science*** 288, 1379-1385 (2000).

82. Hanisch, A., Wehner, A., Nigg, E. A. & Sillje, H. H. Different Plk1 functions show distinct dependencies on Polo-Box domain-mediated targeting. ***Mol Biol Cell*** 17, 448-459 (2006).

83. Ahonen, L. J., Kallio, M. J., Daum, J. R., Bolton, M., Manke, I. A., Yaffe, M. B., Stukenberg, P. T. & Gorbsky, G. J. Polo-like kinase 1 creates the tension-sensing 3F3/2 phosphoepitope and modulates the association of spindle-checkpoint proteins at kinetochores. ***Curr Biol*** 15, 1078-1089 (2005).

84. Neef, R., Preisinger, C., Sutcliffe, J., Kopajtich, R., Nigg, E. A., Mayer, T. U. & Barr, F. A. Phosphorylation of mitotic kinesin-like protein 2 by polo-like kinase 1 is required for cytokinesis. ***J Cell Biol*** 162, 863-875 (2003).

85. Zhou, T., Aumais, J. P., Liu, X., Yu-Lee, L. Y. & Erikson, R. L. A role for Plk1 phosphorylation of NudC in cytokinesis. ***Dev Cell*** 5, 127-138 (2003).

86. Dietzmann, K., Kirches, E., von, B., Jachau, K. & Mawrin, C. Increased human polo-like kinase-1 expression in gliomas. ***J Neurooncol*** 53, 1-11 (2001).

87. Gray, P. J., Jr., Bearss, D. J., Han, H., Nagle, R., Tsao, M. S., Dean, N. & Von Hoff, D. D. Identification of human polo-like kinase 1 as a potential therapeutic target in pancreatic cancer. ***Mol Cancer Ther*** 3, 641-646 (2004).

88. Jalili, A., Moser, A., Pashenkov, M., Wagner, C., Pathria, G., Borgdorff, V., Gschaider, M., Stingl, G., Ramaswamy, S. & Wagner, S. N. Polo-like kinase 1 is a potential therapeutic target in human melanoma. ***J Invest Dermatol*** 131, 1886-1895 (2011).

89. Jang, Y. J., Kim, Y. S. & Kim, W. H. Oncogenic effect of Polo-like kinase 1 expression in human gastric carcinomas. ***Int J Oncol*** 29, 589-594 (2006).

90. Lee, C., Fotovati, A., Triscott, J., Chen, J., Venugopal, C., Singhal, A., Dunham, C., Kerr, J. M., Verreault, M., Yip, S., Wakimoto, H., Jones, C., Jayanthan, A., Narendran, A., Singh, S. K. & Dunn, S. E. Polo-Like Kinase 1 (PLK1) Inhibition Kills Glioblastoma Multiforme Brain Tumour Cells in Part Through Loss of SOX2 and Delays Tumour Progression in Mice. ***Stem Cells*** (2012).

91. Renner, A. G., Dos Santos, C., Recher, C., Bailly, C., Creancier, L., Kruczynski, A., Payrastre, B. & Manenti, S. Polo-like kinase 1 is overexpressed in acute myeloid leukemia and its inhibition preferentially targets the proliferation of leukemic cells. ***Blood*** 114, 659-662 (2009).

92. Cheng, M. W., Wang, B. C., Weng, Z. Q. & Zhu, X. W. Clinicopathological significance of Polo-like kinase 1 (PLK1) expression in human malignant glioma. ***Acta Histochem*** 114, 503-509 (2012).

93. Knecht, R., Elez, R., Oechler, M., Solbach, C., von Ilberg, C. & Strebhardt, K. Prognostic significance of polo-like kinase (PLK) expression in squamous cell carcinomas of the head and neck. ***Cancer Res*** 59, 2794-2797 (1999).

94. Weichert, W., Schmidt, M., Gekeler, V., Denkert, C., Stephan, C., Jung, K., Loening, S., Dietel, M. & Kristiansen, G. Polo-like kinase 1 is overexpressed in prostate cancer and linked to higher tumor grades. ***Prostate*** 60, 240-245 (2004).

95. Holtrich, U., Wolf, G., Brauninger, A., Karn, T., Bohme, B., Rubsamen-Waigmann, H. & Strebhardt, K. Induction and down-regulation of PLK, a human serine/threonine kinase expressed in proliferating cells and tumors. ***Proc Natl Acad Sci U S A*** 91, 1736-1740 (1994).

96. Smith, M. R., Wilson, M. L., Hamanaka, R., Chase, D., Kung, H., Longo, D. L. & Ferris, D. K. Malignant transformation of mammalian cells initiated by constitutive expression of the polo-like kinase. ***Biochem Biophys Res Commun*** 234, 397-405 (1997).

97. Simizu, S. & Osada, H. Mutations in the Plk gene lead to instability of Plk protein in human tumour cell lines. ***Nat Cell Biol*** 2, 852-854 (2000).

98. Buchner, J. Hsp90 & Co. - a holding for folding. ***Trends Biochem Sci*** 24, 136-141 (1999).

99. Chong, Y. K., Toh, T. B., Zaiden, N., Poonepalli, A., Leong, S. H., Ong, C. E., Yu, Y., Tan, P. B., See, S. J., Ng, W. H., Ng, I., Hande, M. P., Kon, O. L., Ang, B. T. & Tang, C. Cryopreservation of neurospheres derived from human glioblastoma multiforme. ***Stem Cells*** 27, 29-39 (2009).

100. Gritti, A., Parati, E. A., Cova, L., Frolichsthal, P., Galli, R., Wanke, E., Faravelli, L., Morassutti, D. J., Roisen, F., Nickel, D. D. & Vescovi, A. L. Multipotential stem cells from the adult mouse brain proliferate and self-renew in response to basic fibroblast growth factor. ***J Neurosci*** 16, 1091-1100 (1996).

101. Madhavan, S., Zenklusen, J. C., Kotliarov, Y., Sahni, H., Fine, H. A. & Buetow, K. Rembrandt: helping personalized medicine become a reality through integrative translational research. ***Mol Cancer Res*** 7, 157-167 (2009).

102. Gravendeel, L. A., Kouwenhoven, M. C., Gevaert, O., de Rooi, J. J., Stubbs, A. P., Duijm, J. E., Daemen, A., Bleeker, F. E., Bralten, L. B., Kloosterhof, N. K., De Moor, B., Eilers, P. H., van der Spek, P. J., Kros, J. M., Sillevis Smitt, P. A., van den Bent, M. J. & French, P. J. Intrinsic gene expression profiles of gliomas are a better predictor of survival than histology. ***Cancer Res*** 69, 9065-9072 (2009).

103. Gentleman, R., Carey, V. J., Huber, W. & Hahne, F. genefilter: methods for filtering genes from microarray experiments. R package version 1.36.0. Genefilter [accessed on 03/March/2012]. (http://bioconductor.org/packages/release/bioc/html/genefilter.html).

104. GSEA [accessed on 09/March/2012]. http://www.broadinstitute.org/gsea/index.jsp.

105. MsigDB [accessed on 09/March/2012]. http://www.broadinstitute.org/gsea/msigdb/index.jsp.

106. Lottaz, C., Beier, D., Meyer, K., Kumar, P., Hermann, A., Schwarz, J., Junker, M., Oefner, P. J., Bogdahn, U., Wischhusen, J., Spang, R., Storch, A. & Beier, C. P. Transcriptional profiles of CD133+ and CD133- glioblastoma-derived cancer stem cell lines suggest different cells of origin. ***Cancer Res*** 70, 2030-2040 (2010).

107. Gunther, H. S., Schmidt, N. O., Phillips, H. S., Kemming, D., Kharbanda, S., Soriano, R., Modrusan, Z., Meissner, H., Westphal, M. & Lamszus, K. Glioblastoma-derived stem cell-enriched cultures form distinct subgroups according to molecular and phenotypic criteria. ***Oncogene*** 27, 2897-2909 (2008).

108. Pollard, S. M., Yoshikawa, K., Clarke, I. D., Danovi, D., Stricker, S., Russell, R., Bayani, J., Head, R., Lee, M., Bernstein, M., Squire, J. A., Smith, A. & Dirks, P. Glioma stem cell lines

expanded in adherent culture have tumor-specific phenotypes and are suitable for chemical and genetic screens. ***Cell Stem Cell*** 4, 568-580 (2009).

109. Beier, C. P., Kumar, P., Meyer, K., Leukel, P., Bruttel, V., Aschenbrenner, I., Riemenschneider, M. J., Fragoulis, A., Rummele, P., Lamszus, K., Schulz, J. B., Weis, J., Bogdahn, U., Wischhusen, J., Hau, P., Spang, R. & Beier, D. The cancer stem cell subtype determines immune infiltration of glioblastoma. ***Stem Cells Dev*** (2012).

110. Anido, J., Saez-Borderias, A., Gonzalez-Junca, A., Rodon, L., Folch, G., Carmona, M. A., Prieto-Sanchez, R. M., Barba, I., Martinez-Saez, E., Prudkin, L., Cuartas, I., Raventos, C., Martinez-Ricarte, F., Poca, M. A., Garcia-Dorado, D., Lahn, M. M., Yingling, J. M., Rodon, J., Sahuquillo, J., Baselga, J. & Seoane, J. TGF-beta Receptor Inhibitors Target the CD44(high)/Id1(high) Glioma-Initiating Cell Population in Human Glioblastoma. ***Cancer Cell*** 18, 655-668 (2010).

111. Penuelas, S., Anido, J., Prieto-Sanchez, R. M., Folch, G., Barba, I., Cuartas, I., Garcia-Dorado, D., Poca, M. A., Sahuquillo, J., Baselga, J. & Seoane, J. TGF-beta increases glioma-initiating cell self-renewal through the induction of LIF in human glioblastoma. ***Cancer Cell*** 15, 315-327 (2009).

112. Yingling, J. M., Blanchard, K. L. & Sawyer, J. S. Development of TGF-beta signalling inhibitors for cancer therapy. ***Nat Rev Drug Discov*** 3, 1011-1022 (2004).

113. Diamandis, P., Wildenhain, J., Clarke, I. D., Sacher, A. G., Graham, J., Bellows, D. S., Ling, E. K., Ward, R. J., Jamieson, L. G., Tyers, M. & Dirks, P. B. Chemical genetics reveals a complex functional ground state of neural stem cells. ***Nat Chem Biol*** 3, 268-273 (2007).

114. Eyler, C. E., Foo, W. C., LaFiura, K. M., McLendon, R. E., Hjelmeland, A. B. & Rich, J. N. Brain cancer stem cells display preferential sensitivity to Akt inhibition. ***Stem Cells*** 26, 3027-3036 (2008).

115. Korur, S., Huber, R. M., Sivasankaran, B., Petrich, M., Morin, P., Jr., Hemmings, B. A., Merlo, A. & Lino, M. M. GSK3beta regulates differentiation and growth arrest in glioblastoma. ***PLoS One*** 4, e7443 (2009).

116. Wolf, G., Hildenbrand, R., Schwar, C., Grobholz, R., Kaufmann, M., Stutte, H. J., Strebhardt, K. & Bleyl, U. Polo-like kinase: a novel marker of proliferation: correlation with estrogen-receptor expression in human breast cancer. ***Pathol Res Pract*** 196, 753-759 (2000).

117. Takai, N., Miyazaki, T., Fujisawa, K., Nasu, K., Hamanaka, R. & Miyakawa, I. Expression of polo-like kinase in ovarian cancer is associated with histological grade and clinical stage. ***Cancer Lett*** 164, 41-49 (2001).

118. Ahmad, N. Polo-like kinase (Plk) 1: a novel target for the treatment of prostate cancer. ***FASEB J*** 18, 5-7 (2004).

119. Kneisel, L., Strebhardt, K., Bernd, A., Wolter, M., Binder, A. & Kaufmann, R. Expression of polo-like kinase (PLK1) in thin melanomas: a novel marker of metastatic disease. ***J Cutan Pathol*** 29, 354-358 (2002).

120. Sumara, I., Vorlaufer, E., Stukenberg, P. T., Kelm, O., Redemann, N., Nigg, E. A. & Peters, J. M. The dissociation of cohesin from chromosomes in prophase is regulated by Polo-like kinase. ***Mol Cell*** 9, 515-525 (2002).

121. Toyoshima-Morimoto, F., Taniguchi, E., Shinya, N., Iwamatsu, A. & Nishida, E. Polo-like kinase 1 phosphorylates cyclin B1 and targets it to the nucleus during prophase. ***Nature*** 410, 215-220 (2001).

122. Lee, K. S., Yuan, Y. L., Kuriyama, R. & Erikson, R. L. Plk is an M-phase-specific protein kinase and interacts with a kinesin-like protein, CHO1/MKLP-1. ***Mol Cell Biol*** 15, 7143-7151 (1995).

123. Steegmaier, M., Hoffmann, M., Baum, A., Lenart, P., Petronczki, M., Krssak, M., Gurtler, U., Garin-Chesa, P., Lieb, S., Quant, J., Grauert, M., Adolf, G. R., Kraut, N., Peters, J. M. & Rettig, W. J. BI 2536, a potent and selective inhibitor of polo-like kinase 1, inhibits tumor growth in vivo. ***Curr Biol*** 17, 316-322 (2007).

124. Hayne, C., Tzivion, G. & Luo, Z. Raf-1/MEK/MAPK pathway is necessary for the G2/M transition induced by nocodazole. ***J Biol Chem*** 275, 31876-31882 (2000).

125. Siddique, M. M., Balram, C., Fiszer-Maliszewska, L., Aggarwal, A., Tan, A., Tan, P., Soo, K. C. & Sabapathy, K. Evidence for selective expression of the p53 codon 72 polymorphs: implications in cancer development. ***Cancer Epidemiol Biomarkers Prev*** 14, 2245-2252 (2005).

126. Masica, D. L. & Karchin, R. Correlation of somatic mutation and expression identifies genes important in human glioblastoma progression and survival. ***Cancer Res*** 71, 4550-4561 (2011).

127. Singec, I., Knoth, R., Meyer, R. P., Maciaczyk, J., Volk, B., Nikkhah, G., Frotscher, M. & Snyder, E. Y. Defining the actual sensitivity and specificity of the neurosphere assay in stem cell biology. ***Nat Methods*** 3, 801-806 (2006).

128. Clement, V., Sanchez, P., de Tribolet, N., Radovanovic, I. & Ruiz i Altaba, A. HEDGEHOG-GLI1 signaling regulates human glioma growth, cancer stem cell self-renewal, and tumorigenicity. ***Curr Biol*** 17, 165-172 (2007).

129. Calabrese, C., Poppleton, H., Kocak, M., Hogg, T. L., Fuller, C., Hamner, B., Oh, E. Y., Gaber, M. W., Finklestein, D., Allen, M., Frank, A., Bayazitov, I. T., Zakharenko, S. S., Gajjar, A., Davidoff, A. & Gilbertson, R. J. A perivascular niche for brain tumor stem cells. ***Cancer Cell***, 69-82 (2007).

130. Quintana, E., Shackleton, M., Sabel, M. S., Fullen, D. R., Johnson, T. M. & Morrison, S. J. Efficient tumour formation by single human melanoma cells. ***Nature*** 456, 593-598 (2008).

131. Boiko, A. D., Razorenova, O. V., van de Rijn, M., Swetter, S. M., Johnson, D. L., Ly, D. P., Butler, P. D., Yang, G. P., Joshua, B., Kaplan, M. J., Longaker, M. T. & Weissman, I. L. Human melanoma-initiating cells express neural crest nerve growth factor receptor CD271. ***Nature*** 466, 133-137 (2010).

132. Rich, J. N. & Eyler, C. E. Cancer stem cells in brain tumor biology. ***Cold Spring Harb Symp Quant Biol*** 73, 411-420 (2008).

133. Hemmati, H. D., Nakano, I., Lazareff, J. A., Masterman-Smith, M., Geschwind, D. H., Bronner-Fraser, M. & Kornblum, H. I. Cancerous stem cells can arise from pediatric brain tumors. ***Proc Natl Acad Sci U S A*** 100, 15178-15183 (2003).

134. Fuerer, C. & Nusse, R. Lentiviral vectors to probe and manipulate the Wnt signaling pathway. ***PLoS One*** 5, e9370 (2010).

135. Chua, C., Zaiden, N., Chong, K. H., See, S. J., Wong, M. C., Ang, B. T. & Tang, C. Characterization of a side population of astrocytoma cells in response to temozolomide. ***J Neurosurg*** 109, 856-866 (2008).

136. Gilmartin, A. G., Bleam, M. R., Richter, M. C., Erskine, S. G., Kruger, R. G., Madden, L., Hassler, D. F., Smith, G. K., Gontarek, R. R., Courtney, M. P., Sutton, D., Diamond, M. A., Jackson, J. R. & Laquerre, S. G. Distinct concentration-dependent effects of the polo-like kinase 1-specific inhibitor GSK461364A, including differential effect on apoptosis. ***Cancer Res*** 69, 6969-6977 (2009).

137. Gumireddy, K., Reddy, M. V., Cosenza, S. C., Boominathan, R., Baker, S. J., Papathi, N., Jiang, J., Holland, J. & Reddy, E. P. ON01910, a non-ATP-competitive small molecule inhibitor of Plk1, is a potent anticancer agent. ***Cancer Cell*** 7, 275-286 (2005).

138. Rudolph, D., Steegmaier, M., Hoffmann, M., Grauert, M., Baum, A., Quant, J., Haslinger, C., Garin-Chesa, P. & Adolf, G. R. BI 6727, a Polo-like kinase inhibitor with improved pharmacokinetic profile and broad antitumor activity. ***Clin Cancer Res*** 15, 3094-3102 (2009).

139. Cai, J., Wu, Y., Mirua, T., Pierce, J. L., Lucero, M. T., Albertine, K. H., Spangrude, G. J. & Rao, M. S. Properties of a fetal multipotent neural stem cell (NEP cell). ***Dev Biol*** 251, 221-240 (2002).

140. Hermansen, S. K., Christensen, K. G., Jensen, S. S. & Kristensen, B. W. Inconsistent immunohistochemical expression patterns of four different CD133 antibody clones in glioblastoma. ***J Histochem Cytochem*** 59, 391-407 (2011).

141. Li, A., Walling, J., Ahn, S., Kotliarov, Y., Su, Q., Quezado, M., Oberholtzer, J. C., Park, J., Zenklusen, J. C. & Fine, H. A. Unsupervised analysis of transcriptomic profiles reveals six glioma subtypes. ***Cancer Res*** 69, 2091-2099 (2009).

142. Phillips, H. S., Kharbanda, S., Chen, R., Forrest, W. F., Soriano, R. H., Wu, T. D., Misra, A., Nigro, J. M., Colman, H., Soroceanu, L., Williams, P. M., Modrusan, Z., Feuerstein, B. G. & Aldape, K. Molecular subclasses of high-grade glioma predict prognosis, delineate a pattern of disease progression, and resemble stages in neurogenesis. ***Cancer Cell*** 9, 157-173 (2006).

143. Subramanian, A., Tamayo, P., Mootha, V. K., Mukherjee, S., Ebert, B. L., Gillette, M. A., Paulovich, A., Pomeroy, S. L., Golub, T. R., Lander, E. S. & Mesirov, J. P. Gene set enrichment analysis: a knowledge-based approach for interpreting genome-wide expression profiles. ***Proc Natl Acad Sci U S A*** 102, 15545-15550 (2005).

144. Wang, J., Wang, H., Li, Z., Wu, Q., Lathia, J. D., McLendon, R. E., Hjelmeland, A. B. & Rich, J. N. c-Myc is required for maintenance of glioma cancer stem cells. ***PLoS ONE*** 3, e3769 (2008).

145. Reynolds, B. A., Tetzlaff, W. & Weiss, S. A multipotent EGF-responsive striatal embryonic progenitor cell produces neurons and astrocytes. ***J Neurosci*** 12, 4565-4574 (1992).

146. Ackerman, A. B. Neoplasms with follicular differentiation, Ardor Scrsibendi Publishers, New York. (2001).

147. Gleixner, K. V., Ferenc, V., Peter, B., Gruze, A., Meyer, R. A., Hadzijusufovic, E., Cerny-Reiterer, S., Mayerhofer, M., Pickl, W. F., Sillaber, C. & Valent, P. Polo-like kinase 1 (Plk1) as a novel drug target in chronic myeloid leukemia: overriding imatinib resistance with the Plk1 inhibitor BI 2536. ***Cancer Res*** 70, 1513-1523 (2010).

148. Grinshtein, N., Datti, A., Fujitani, M., Uehling, D., Prakesch, M., Isaac, M., Irwin, M. S., Wrana, J. L., Al-Awar, R. & Kaplan, D. R. Small molecule kinase inhibitor screen identifies polo-like kinase 1 as a target for neuroblastoma tumor-initiating cells. ***Cancer Res*** 71, 1385-1395 (2011).

149. Hofheinz, R. D., Al-Batran, S. E., Hochhaus, A., Jager, E., Reichardt, V. L., Fritsch, H., Trommeshauser, D. & Munzert, G. An open-label, phase I study of the polo-like kinase-1 inhibitor, BI 2536, in patients with advanced solid tumors. ***Clin Cancer Res*** 16, 4666-4674 (2010).

150. Mross, K., Frost, A., Steinbild, S., Hedbom, S., Rentschler, J., Kaiser, R., Rouyrre, N., Trommeshauser, D., Hoesl, C. E. & Munzert, G. Phase I dose escalation and pharmacokinetic study of BI 2536, a novel Polo-like kinase 1 inhibitor, in patients with advanced solid tumors. ***J Clin Oncol*** 26, 5511-5517 (2008).

151. Olmos, D., Barker, D., Sharma, R., Brunetto, A. T., Yap, T. A., Taegtmeyer, A. B., Barriuso, J., Medani, H., Degenhardt, Y. Y., Allred, A. J., Smith, D. A., Murray, S. C., Lampkin, T. A., Dar, M. M., Wilson, R., de Bono, J. S. & Blagden, S. P. Phase I study of GSK461364, a specific and competitive Polo-like kinase 1 inhibitor, in patients with advanced solid malignancies. ***Clin Cancer Res*** 17, 3420-3430 (2011).

152. Schoffski, P., Awada, A., Dumez, H., Gil, T., Bartholomeus, S., Wolter, P., Taton, M., Fritsch, H., Glomb, P. & Munzert, G. A phase I, dose-escalation study of the novel Polo-like kinase inhibitor volasertib (BI 6727) in patients with advanced solid tumours. ***Eur J Cancer*** 48, 179-186 (2012).

153. Liu, R., Wang, X., Chen, G. Y., Dalerba, P., Gurney, A., Hoey, T., Sherlock, G., Lewicki, J., Shedden, K. & Clarke, M. F. The prognostic role of a gene signature from tumorigenic breast-cancer cells. ***New Engl J Med*** 356, 217-226 (2007).

154. Lamb, J., Crawford, E. D., Peck, D., Modell, J. W., Blat, I. C., Wrobel, M. J., Lerner, J., Brunet, J. P., Subramanian, A., Ross, K. N., Reich, M., Hieronymus, H., Wei, G., Armstrong, S. A., Haggarty, S. J., Clemons, P. A., Wei, R., Carr, S. A., Lander, E. S. & Golub, T. R. The Connectivity Map: using gene-expression signatures to connect small molecules, genes, and disease. ***Science*** 313, 1929-1935 (2006).

155. Yeo, C. W., Ng, F. S., Chai, C., Tan, J. M., Koh, G. R., Chong, Y. K., Koh, L. W., Foong, C. S., Sandanaraj, E., Holbrook, J. D., Ang, B. T., Takahashi, R., Tang, C. & Lim, K. L. Parkin pathway activation mitigates glioma cell proliferation and predicts patient survival. ***Cancer Res*** 72, 2543-2553 (2012).

156. Li, A., Walling, J., Kotliarov, Y., Center, A., Steed, M. E., Ahn, S. J., Rosenblum, M., Mikkelsen, T., Zenklusen, J. C. & Fine, H. A. Genomic changes and gene expression profiles reveal that established glioma cell lines are poorly representative of primary human gliomas. ***Mol Cancer Res*** 6, 21-30 (2008).

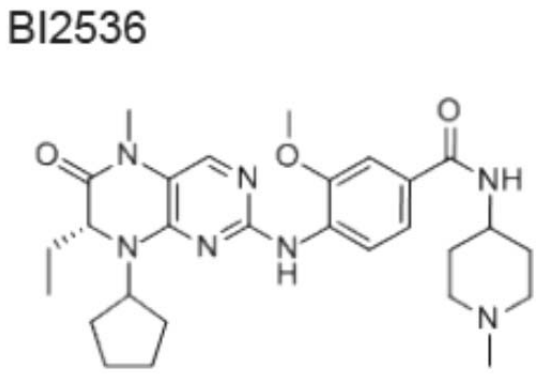

Figure-S1: Chemical structure of BI2536.

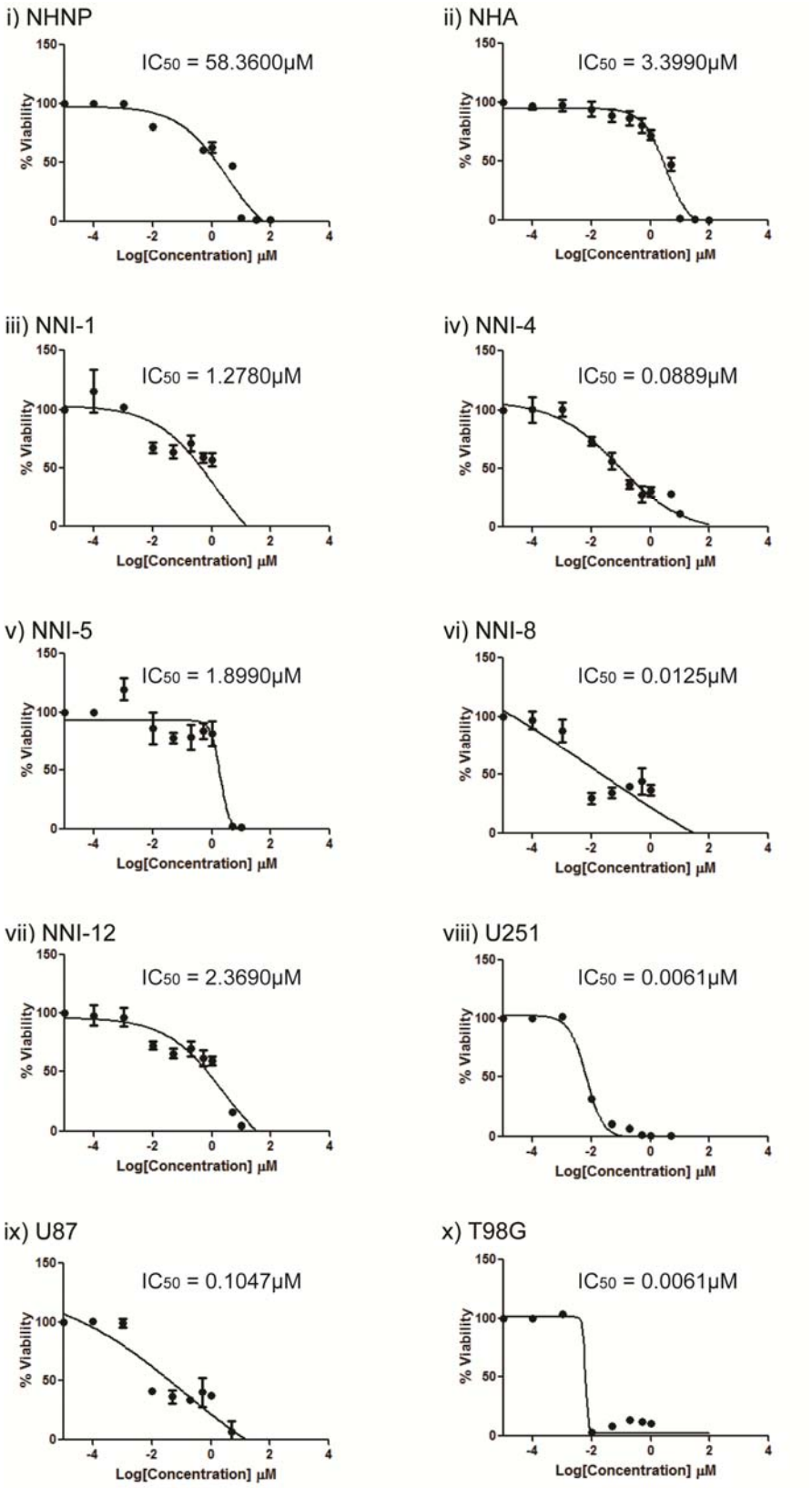

Figure-S2: BI2536 IC_{50} kill curve in GPCs and ATCC glioma cell lines.

Supplementary Table-1. BI2536 kinase selectivity profile

Kinase	IC50 (μM)	Kinase	IC50 (μM)	Kinase	IC50 (μM)
Plk1*	0.013	Erk2	>20	Nik*	>20
Plk2*	0.019	Fgfr1	>20	Nlk	>20
Plk3*	0.016	Fgfr2	>20	p38a	>20
Plk4*	>20	Fgfr3	>20	p38b	>20
Abl	>20	Fgfr4	>20	p38d	>20
Akt1	>20	Flt1	>20	p70s6	>20
Akt2	>20	Flt3	>20	Pak2	>20
Akt3	>20	Flt4	>20	Pak3	>20
Alk*	3.700	Fms	>20	Pak5	>20
Alk4	>20	Gsk3a	>20	Pask	>20
Ask	>20	Gsk3b	>20	Pdgfra	>20
AurA	>20	Hipk2	>20	Pdgfrb	>20
AurB	>20	Ikka	>20	Pdk1	>20
Brk	>20	Ikkb	>20	Pim1	>20
Brsk	>20	Ikke*	>20	Pim2	>20
Camk1	>20	InsR	>20	Pkaa	>20
Camk2a*	3.750	Irak1	>20	Pkca	>20
Camk4	>20	Irr	>20	Pkcb	>20
Cdc7	>20	Jak2	>20	Pkca	>20
Cdk1/cycB	>20	Jak3	>20	Pkcb1	>20
Cdk2/cycE	>20	Jnk1	>20	Pkcb2	>20
Cdk3/cycE	>20	Jnk2	>20	Pkc eta	>20
Cdk4/cycD1*	7.830	Kit	>20	Pkc t	>20
Cdk5/p35	>20	Limk1	>20	Pkc z	>20
Cdk6/cycD3	>20	Lkb1	>20	Pkg1b	>20
Cdk7/cycH/MAT	>20	Lok	>20	Raf	>20
Cdk8*	>20	Lrrk2*	>20	Ripk2	>20
Chk1	>20	Mark1	>20	Rock1	>20
Ck2	>20	Mek1	>20	Rock2	>20
Csk	>20	Met	>20	Ron	>20
Dapk1	>20	Mink1	>20	Ros	>20
Ddr2	>20	Mk2	>20	Rse	>20
Dmpk	>20	Mk3	>20	Sgk	>20
Drak1	>20	Mk5	>20	Sgk3	>20
Dyrk2	>20	Mkk6	>20	Sik	>20
Eef2k	>20	Mlk1	>20	Src	>20
EphA3	>20	Mlk2*	>20	Srpk1	>20
EphA5	>20	Mnk2	>20	Tak1	>20
EphA7	>20	Mst1	>20	Tie2	>20
EphB1	>20	Mst2	>20	TrkB	>20
EphB2	>20	mTor	>20	Ulk1*	>20
EphB3	>20	Musk	>20	VEGFR2	>20
EphB4	>20	Nek6	>20	Wnk3	>20
ErbB4	>20	Nek7	>20	Zap70	>20
Erk1	>20	Nek11	>20		

Supplementary Table-2. Genes associated *PLK1* expression

Genes	Entrez	Description	Rembrandt				Gravendeel			
			Mean HighPLK 1	Mean LowPLK 1	Log Fold difference	*p*-value	Mean HighPLK 1	Mean LowPLK 1	Fold difference	*p*-value
CHAF1A	10036	chromatin assembly factor 1, subunit A (p150) [Source:HGNC Symbol;Acc:1910]	8.0338	6.7268	1.3070	4.66E-27	8.1335	7.2393	0.8941	1.92E-17
SMC4	10051	structural maintenance of chromosomes 4 [Source:HGNC Symbol;Acc:14013]	10.9876	9.2451	1.7425	1.71E-61	11.4750	9.7853	1.6897	7.19E-42
KIF20A	10112	kinesin family member 20A [Source:HGNC Symbol;Acc:9787]	8.9651	5.7365	3.2286	1.70E-63	8.7840	6.3825	2.4016	1.30E-61
CDK2	1017	cyclin-dependent kinase 2 [Source:HGNC Symbol;Acc:1771]	10.2607	9.0639	1.1968	1.35E-52	9.0890	7.9091	1.1798	8.10E-27
CDK4	1019	cyclin-dependent kinase 4 [Source:HGNC Symbol;Acc:1773]	12.1169	11.0676	1.0493	8.72E-17	12.1518	11.3260	0.8258	7.61E-10
DDX39A	10212	DEAD (Asp-Glu-Ala-Asp) box polypeptide 39A [Source:HGNC Symbol;Acc:17821]	11.5090	10.5799	0.9291	1.50E-41	11.8086	11.0664	0.7422	8.14E-19
CDKN3	1033	cyclin-dependent kinase inhibitor 3 [Source:HGNC Symbol;Acc:1791]	9.4705	7.8117	1.6588	1.36E-56	9.7579	7.5741	2.1838	1.11E-45
NDC80	10403	NDC80 homolog, kinetochore complex component (S. cerevisiae) [Source:HGNC	8.8037	6.0337	2.7699	2.23E-52	9.5024	6.9389	2.5635	7.61E-57

		Symbol;Acc:16909]								
MAD2L2	10459	MAD2 mitotic arrest deficient-like 2 (yeast) [Source:HGNC Symbol;Acc:6764]	10.4184	9.6223	0.7960	2.49E-31	10.3377	9.8208	0.5170	2.01E-09
TACC3	10460	transforming, acidic coiled-coil containing protein 3 [Source:HGNC Symbol;Acc:11524]	8.6514	5.4576	3.1938	1.13E-71	8.6616	6.7097	1.9519	1.73E-43
CENPA	1058	centromere protein A [Source:HGNC Symbol;Acc:1851]	8.7886	6.7708	2.0178	2.17E-68	9.0543	6.5865	2.4678	2.34E-56
SMC2	10592	structural maintenance of chromosomes 2 [Source:HGNC Symbol;Acc:14011]	9.3616	8.5402	0.8214	2.09E-31	9.4129	8.4242	0.9887	5.40E-25
CENPE	1062	centromere protein E, 312kDa [Source:HGNC Symbol;Acc:1856]	8.2865	5.6933	2.5932	1.11E-76	8.4972	6.3121	2.1851	5.62E-45
CENPF	1063	centromere protein F, 350/400kDa (mitosin) [Source:HGNC Symbol;Acc:1857]	9.3378	7.2442	2.0936	2.75E-71	10.5029	7.8150	2.6879	1.56E-57
RAD51AP1	10635	RAD51 associated protein 1 [Source:HGNC Symbol;Acc:16956]	9.0233	7.2594	1.7639	1.89E-59	9.6456	7.6685	1.9771	6.46E-39
PLK4	10733	polo-like kinase 4 [Source:HGNC Symbol;Acc:11397]	5.3015	3.5711	1.7304	5.95E-25	7.4838	6.0600	1.4238	1.25E-27

DBF4	10926	DBF4 homolog (S. cerevisiae) [Source:HGNC Symbol;Acc:17364]	9.4506	7.9167	1.5338	2.66E-58	9.9944	8.8320	1.1625	2.18E-30
KIF2C	11004	kinesin family member 2C [Source:HGNC Symbol;Acc:6393]	9.6167	8.2752	1.3415	8.33E-70	9.4811	7.3855	2.0955	3.84E-49
UBE2C	11065	ubiquitin-conjugating enzyme E2C [Source:HGNC Symbol;Acc:15937]	10.5868	8.8950	1.6917	1.09E-73	9.8943	7.7198	2.1744	3.89E-48
CHEK1	1111	CHK1 checkpoint homolog (S. pombe) [Source:HGNC Symbol;Acc:1925]	8.6634	6.9958	1.6676	4.74E-65	8.6288	6.6159	2.0130	1.56E-53
ZWINT	11130	ZW10 interactor [Source:HGNC Symbol;Acc:13195]	10.3856	9.2152	1.1704	1.49E-49	10.5091	8.9004	1.6087	4.34E-37
WDHD1	11169	WD repeat and HMG-box DNA binding protein 1 [Source:HGNC Symbol;Acc:23170]	7.0907	5.4477	1.6430	4.16E-45	7.0289	6.0118	1.0172	6.38E-22
FAM54A	113115	family with sequence similarity 54, member A [Source:HGNC Symbol;Acc:21115]	7.9523	6.9721	0.9802	1.16E-36	7.8543	6.4716	1.3826	1.03E-32
CDCA5	113130	cell division cycle associated 5 [Source:HGNC Symbol;Acc:14626]	7.9553	5.7082	2.2472	5.08E-51	8.5648	7.0744	1.4904	3.72E-36
OIP5	11339	Opa interacting protein 5 [Source:HGNC Symbol;Acc:20300]	8.4456	6.9265	1.5190	8.79E-54	8.3612	6.5476	1.8136	4.61E-38

RMI2	116028	RMI2, RecQ mediated genome instability 2, homolog (S. cerevisiae) [Source:HGNC Symbol;Acc:28349]	9.3693	8.6630	0.7063	1.46E-22	8.3547	6.7954	1.5593	7.11E-37
CKS2	1164	CDC28 protein kinase regulatory subunit 2 [Source:HGNC Symbol;Acc:2000]	10.7549	8.9108	1.8441	6.33E-55	11.6929	9.8737	1.8193	8.17E-37
E2F7	144455	E2F transcription factor 7 [Source:HGNC Symbol;Acc:23820]	8.8554	6.9121	1.9432	3.18E-50	8.2748	6.1298	2.1450	7.88E-40
SPC24	147841	SPC24, NDC80 kinetochore complex component, homolog (S. cerevisiae) [Source:HGNC Symbol;Acc:26913]	7.8770	5.6009	2.2761	1.62E-58	8.1292	6.3024	1.8268	5.25E-54
CTPS	1503	CTP synthase [Source:HGNC Symbol;Acc:2519]	9.5899	8.7194	0.8705	3.74E-40	9.4427	8.4001	1.0426	8.07E-26
CKAP2L	150468	cytoskeleton associated protein 2-like [Source:HGNC Symbol;Acc:26877]	8.6408	6.6119	2.0289	8.05E-56	7.9289	5.8705	2.0584	9.44E-53
SGOL2	151246	shugoshin-like 2 (S. pombe) [Source:HGNC Symbol;Acc:30812]	8.1701	7.0805	1.0896	1.46E-22	8.9351	7.6153	1.3198	3.03E-22
CDCA2	157313	cell division cycle associated 2 [Source:HGNC Symbol;Acc:14623]	8.1627	5.6542	2.5085	4.17E-58	8.0912	6.2555	1.8357	1.74E-46

ESCO2	157570	establishment of cohesion 1 homolog 2 (S. cerevisiae) [Source:HGNC Symbol;Acc:27230]	6.4373	3.3950	3.0423	3.21E-54	6.8225	5.9136	0.9089	4.44E-18
DNMT1	1786	DNA (cytosine-5-)-methyltransferase 1 [Source:HGNC Symbol;Acc:2976]	10.7011	9.9093	0.7918	1.39E-47	11.0198	10.3755	0.6443	5.36E-18
E2F1	1869	E2F transcription factor 1 [Source:HGNC Symbol;Acc:3113]	7.8353	6.9487	0.8866	4.54E-17	7.6906	6.6499	1.0407	3.71E-18
ECT2	1894	epithelial cell transforming sequence 2 oncogene [Source:HGNC Symbol;Acc:3155]	10.0423	8.3374	1.7049	6.40E-71	10.0407	8.3038	1.7369	3.22E-43
ZNF367	195828	zinc finger protein 367 [Source:HGNC Symbol;Acc:18320]	9.7429	8.3375	1.4055	6.30E-42	9.4195	7.9040	1.5155	3.13E-27
TUBB	203068	tubulin, beta class I [Source:HGNC Symbol;Acc:20778]	13.9398	13.2572	0.6826	1.36E-44	13.6300	12.9629	0.6671	1.83E-15
EZH2	2146	enhancer of zeste homolog 2 (Drosophila) [Source:HGNC Symbol;Acc:3527]	9.8426	8.1810	1.6616	1.08E-48	9.7992	8.3761	1.4230	1.26E-30
FANCD2	2177	Fanconi anemia, complementation group D2 [Source:HGNC Symbol;Acc:3585]	8.2252	6.4856	1.7396	2.04E-46	8.4972	6.9794	1.5178	5.33E-33
C11orf82	220042	chromosome 11 open reading frame 82 [Source:HGNC Symbol;Acc:26351]	7.9940	6.2639	1.7301	8.74E-46	8.2339	6.4856	1.7483	3.41E-39

SKA3	221150	spindle and kinetochore associated complex subunit 3 [Source:HGNC Symbol;Acc:20262]	8.4439	7.5435	0.9004	1.97E-37	8.1452	6.9060	1.2392	6.11E-34
FEN1	2237	flap structure-specific endonuclease 1 [Source:HGNC Symbol;Acc:3650]	9.9153	9.1389	0.7765	1.45E-33	10.2159	9.2437	0.9722	2.48E-23
TPX2	22974	TPX2, microtubule-associated, homolog (Xenopus laevis) [Source:HGNC Symbol;Acc:1249]	10.3370	7.9426	2.3944	2.33E-74	9.8806	7.6392	2.2414	1.79E-50
FOXM1	2305	forkhead box M1 [Source:HGNC Symbol;Acc:3818]	9.1005	5.5275	3.5729	1.96E-74	8.8000	6.3617	2.4383	2.66E-51
TMEM194A	23306	transmembrane protein 194A [Source:HGNC Symbol;Acc:29001]	9.6573	8.7635	0.8938	1.32E-34	7.4632	6.5466	0.9167	2.26E-18
NCAPH	23397	non-SMC condensin I complex, subunit H [Source:HGNC Symbol;Acc:1112]	7.9510	4.8045	3.1465	6.64E-90	7.2859	5.7983	1.4876	1.41E-29
ORC6	23594	origin recognition complex, subunit 6 [Source:HGNC Symbol;Acc:17151]	9.7295	9.0126	0.7169	3.82E-31	10.3432	8.8481	1.4951	4.50E-36
POLA2	23649	polymerase (DNA directed), alpha 2 (70kD subunit) [Source:HGNC Symbol;Acc:30073]	8.4734	7.5124	0.9609	4.19E-30	8.4773	7.7554	0.7219	2.79E-19
KIF4A	24137	kinesin family member 4A [Source:HGNC Symbol;Acc:13339]	9.1331	6.8204	2.3127	2.44E-54	9.2867	7.0380	2.2487	9.04E-57

CENPI	2491	centromere protein I [Source:HGNC Symbol;Acc:3968]	6.4015	5.2264	1.1751	2.93E-20	7.4870	6.2415	1.2455	2.78E-27
ASPM	259266	asp (abnormal spindle) homolog, microcephaly associated (Drosophila) [Source:HGNC Symbol;Acc:19048]	9.7937	5.7367	4.0569	2.39E-69	10.0228	6.9801	3.0427	7.75E-62
PTTG3P	NA	pituitary tumor-transforming 3, pseudogene [Source:HGNC Symbol;Acc:13422]	7.6188	5.4477	2.1711	1.21E-48	7.3575	6.1274	1.2301	9.86E-27
FBXO5	26271	F-box protein 5 [Source:HGNC Symbol;Acc:13584]	8.8553	6.9321	1.9232	2.51E-44	9.3090	8.0031	1.3059	1.09E-26
NKIRAS 2	28511	NFKB inhibitor interacting Ras-like 2 [Source:HGNC Symbol;Acc:17898]	9.4603	9.0071	0.4532	2.01E-19	9.3901	8.8732	0.5169	3.68E-12
ATAD2	29028	ATPase family, AAA domain containing 2 [Source:HGNC Symbol;Acc:30123]	8.4357	7.4092	1.0265	7.87E-39	9.6193	8.5442	1.0752	2.47E-20
UBE2T	29089	ubiquitin-conjugating enzyme E2T (putative) [Source:HGNC Symbol;Acc:25009]	9.2444	7.5460	1.6984	2.32E-41	9.5929	7.7382	1.8547	1.67E-37
RACGAP 1	29127	Rac GTPase activating protein 1 [Source:HGNC Symbol;Acc:9804]	10.9846	9.8163	1.1683	2.77E-54	11.1031	9.9679	1.1352	3.93E-28
UHRF1	29128	ubiquitin-like with PHD and ring finger domains 1 [Source:HGNC	11.1791	9.4706	1.7085	3.93E-34	10.7426	9.8598	0.8827	4.51E-09

		Symbol;Acc:12556]								
H2AFX	3014	H2A histone family, member X [Source:HGNC Symbol;Acc:4739]	11.8683	11.0698	0.7985	1.50E-34	11.1708	10.6416	0.5293	1.03E-08
H2AFZ	3015	H2A histone family, member Z [Source:HGNC Symbol;Acc:4741]	12.9892	12.2821	0.7071	8.21E-58	13.4269	12.6859	0.7410	4.28E-30
HMGB2	3148	high mobility group box 2 [Source:HGNC Symbol;Acc:5000]	12.4713	11.1380	1.3333	1.31E-57	12.8764	11.8088	1.0676	1.44E-24
HMMR	3161	hyaluronan-mediated motility receptor (RHAMM) [Source:HGNC Symbol;Acc:5012]	8.6904	6.4156	2.2748	5.80E-52	9.1852	6.6637	2.5216	5.50E-47
HNRNPAB	3182	heterogeneous nuclear ribonucleoprotein A/B [Source:HGNC Symbol;Acc:5034]	12.1976	11.3527	0.8449	8.95E-44	12.5020	11.8531	0.6489	5.38E-20
BIRC5	332	baculoviral IAP repeat containing 5 [Source:HGNC Symbol;Acc:593]	9.4652	6.1781	3.2871	8.35E-77	9.6955	6.7468	2.9487	5.52E-62
ILF2	3608	interleukin enhancer binding factor 2, 45kDa [Source:HGNC Symbol;Acc:6037]	11.7139	11.1266	0.5874	4.30E-28	11.8184	11.3695	0.4489	5.31E-11
ILF3	3609	interleukin enhancer binding factor 3, 90kDa [Source:HGNC	10.8788	9.9501	0.9287	2.78E-43	9.2167	8.7693	0.4473	2.33E-06

		Symbol;Acc:6038]								
C5orf34	375444	chromosome 5 open reading frame 34 [Source:HGNC Symbol;Acc:24738]	8.2333	7.1888	1.0446	1.42E-38	8.2807	7.2686	1.0121	3.87E-27
KIF11	3832	kinesin family member 11 [Source:HGNC Symbol;Acc:6388]	8.9035	7.2203	1.6832	2.06E-54	9.1539	7.3362	1.8176	2.63E-37
CENPW	387103	centromere protein W [Source:HGNC Symbol;Acc:21488]	8.6031	7.2550	1.3481	2.12E-51	9.4123	7.9588	1.4535	2.39E-36
LMNB1	4001	lamin B1 [Source:HGNC Symbol;Acc:6637]	9.8493	7.9812	1.8681	3.77E-53	9.1698	7.7341	1.4357	1.24E-20
MAD2L1	4085	MAD2 mitotic arrest deficient-like 1 (yeast) [Source:HGNC Symbol;Acc:6763]	10.5933	8.8714	1.7219	4.86E-67	10.5842	8.9133	1.6709	2.74E-38
MCM2	4171	minichromosome maintenance complex component 2 [Source:HGNC Symbol;Acc:6944]	10.5545	9.0631	1.4914	1.31E-63	10.0160	8.2441	1.7719	6.43E-46
MCM3	4172	minichromosome maintenance complex component 3 [Source:HGNC Symbol;Acc:6945]	10.7303	9.7834	0.9469	3.24E-50	10.1694	9.3696	0.7998	2.53E-21
MCM4	4173	minichromosome maintenance complex component 4 [Source:HGNC Symbol;Acc:6947]	8.8025	7.1173	1.6852	5.21E-45	7.8372	6.6382	1.1990	1.39E-26

MCM5	4174	minichromosome maintenance complex component 5 [Source:HGNC Symbol;Acc:6948]	9.7075	8.4588	1.2488	5.23E-26	9.6294	8.8383	0.7911	7.06E-15
MKI67	4288	antigen identified by monoclonal antibody Ki-67 [Source:HGNC Symbol;Acc:7107]	8.6159	6.8940	1.7219	7.47E-56	8.4161	6.3936	2.0225	5.95E-43
MYBL1	4603	v-myb myeloblastosis viral oncogene homolog (avian)-like 1 [Source:HGNC Symbol;Acc:7547]	9.0439	8.1040	0.9399	5.86E-25	9.2956	8.2243	1.0713	1.96E-16
MYBL2	4605	v-myb myeloblastosis viral oncogene homolog (avian)-like 2 [Source:HGNC Symbol;Acc:7548]	8.1246	5.7072	2.4174	2.00E-62	7.3421	5.6987	1.6434	6.14E-25
NEK2	4751	NIMA (never in mitosis gene a)-related kinase 2 [Source:HGNC Symbol;Acc:7745]	8.8379	6.1252	2.7127	7.13E-64	7.0361	5.7707	1.2654	2.46E-26
ORC1	4998	origin recognition complex, subunit 1 [Source:HGNC Symbol;Acc:8487]	6.2915	4.5656	1.7259	2.08E-35	6.4233	5.7365	0.6868	3.30E-12
NUSAP1	51203	nucleolar and spindle associated protein 1 [Source:HGNC Symbol;Acc:18538]	11.1491	8.9112	2.2379	7.87E-73	11.2450	8.6978	2.5472	3.43E-56
GTSE1	51512	G-2 and S-phase expressed 1 [Source:HGNC	7.3226	5.5635	1.7591	1.19E-36	8.1173	6.2181	1.8992	1.23E-32

		Symbol;Acc:13698]								
DTL	51514	denticleless homolog (Drosophila) [Source:HGNC Symbol;Acc:30288]	9.5406	7.2216	2.3190	1.34E-59	9.7598	7.1350	2.6247	4.34E-55
GINS2	51659	GINS complex subunit 2 (Psf2 homolog) [Source:HGNC Symbol;Acc:24575]	9.0754	6.7370	2.3384	1.33E-53	9.1096	7.3019	1.8076	8.30E-43
PLK1	5347	polo-like kinase 1 [Source:HGNC Symbol;Acc:9077]	8.1295	6.7781	1.3514	8.47E-46	7.3309	6.1888	1.1421	4.20E-21
MIS18A	54069	MIS18 kinetochore protein homolog A (S. pombe) [Source:HGNC Symbol;Acc:1286]	9.1813	8.4135	0.7678	8.33E-27	9.1874	8.4653	0.7221	1.46E-14
FAM64A	54478	family with sequence similarity 64, member A [Source:HGNC Symbol;Acc:25483]	9.7818	7.8121	1.9697	3.60E-65	9.2255	6.9665	2.2590	1.48E-45
ERCC6L	54821	excision repair cross-complementing rodent repair deficiency, complementation group 6-like [Source:HGNC Symbol;Acc:20794]	6.6315	4.7157	1.9159	1.08E-42	6.7891	5.7972	0.9919	2.21E-19
NCAPG2	54892	non-SMC condensin II complex, subunit G2 [Source:HGNC Symbol;Acc:21904]	9.4861	8.1006	1.3855	3.91E-64	9.4305	8.1523	1.2782	5.39E-37

CCDC99	54908	coiled-coil domain containing 99 [Source:HGNC Symbol;Acc:26010]	9.1873	8.5654	0.6218	1.32E-26	9.5048	8.8346	0.6702	3.84E-19
C12orf48	55010	chromosome 12 open reading frame 48 [Source:HGNC Symbol;Acc:26074]	6.4690	3.9608	2.5082	2.29E-47	6.7017	5.8005	0.9012	3.10E-18
CDCA4	55038	cell division cycle associated 4 [Source:HGNC Symbol;Acc:14625]	9.1136	8.3956	0.7180	2.13E-37	8.8439	7.9973	0.8467	3.22E-23
ZWILCH	55055	Zwilch, kinetochore associated, homolog (Drosophila) [Source:HGNC Symbol;Acc:25468]	8.2003	7.0644	1.1359	1.29E-23	8.8429	7.5070	1.3359	2.30E-30
CDCA8	55143	cell division cycle associated 8 [Source:HGNC Symbol;Acc:14629]	8.4091	5.3266	3.0824	2.20E-93	7.9332	5.9715	1.9618	1.61E-42
CEP55	55165	centrosomal protein 55kDa [Source:HGNC Symbol;Acc:1161]	8.5129	5.7006	2.8123	7.92E-58	8.1190	6.1331	1.9859	6.19E-46
FANCI	55215	Fanconi anemia, complementation group I [Source:HGNC Symbol;Acc:25568]	9.5296	7.8888	1.6408	1.67E-60	9.4004	7.5609	1.8395	2.56E-42
NEIL3	55247	nei endonuclease VIII-like 3 (E. coli) [Source:HGNC Symbol;Acc:24573]	7.9734	6.6751	1.2983	1.51E-47	7.1672	5.8962	1.2711	1.73E-27

HJURP	55355	Holliday junction recognition protein [Source:HGNC Symbol;Acc:25444]	8.8850	6.0179	2.8672	2.43E-71	8.4500	6.0975	2.3525	1.31E-58
MCM10	55388	minichromosome maintenance complex component 10 [Source:HGNC Symbol;Acc:18043]	7.4689	5.0035	2.4655	2.21E-45	7.2290	5.8255	1.4035	4.87E-24
DEPDC1	55635	DEP domain containing 1 [Source:HGNC Symbol;Acc:22949]	7.2267	4.6602	2.5666	1.48E-55	7.8686	5.8915	1.9771	1.55E-43
ASF1B	55723	ASF1 anti-silencing function 1 homolog B (S. cerevisiae) [Source:HGNC Symbol;Acc:20996]	9.4123	8.1839	1.2284	2.23E-54	8.3880	6.8184	1.5696	7.68E-43
DEPDC1B	55789	DEP domain containing 1B [Source:HGNC Symbol;Acc:24902]	7.8767	5.4267	2.4500	4.54E-59	7.8894	5.9075	1.9819	3.15E-40
CENPN	55839	centromere protein N [Source:HGNC Symbol;Acc:30873]	7.7543	5.4521	2.3022	8.58E-52	8.7617	6.9215	1.8402	2.08E-42
PBK	55872	PDZ binding kinase [Source:HGNC Symbol;Acc:18282]	10.1144	7.3776	2.7368	2.54E-67	10.7520	7.6417	3.1103	2.19E-55
KIF15	56992	kinesin family member 15 [Source:HGNC Symbol;Acc:17273]	8.9357	7.5387	1.3970	1.73E-51	8.9620	7.2289	1.7331	1.17E-40
PTBP1	5725	polypyrimidine tract binding protein 1 [Source:HGNC Symbol;Acc:9583]	9.8496	8.8699	0.9797	1.12E-27	8.7026	8.2041	0.4985	0.0003398

SPC25	57405	SPC25, NDC80 kinetochore complex component, homolog (S. cerevisiae) [Source:HGNC Symbol;Acc:24031]	8.0893	6.4851	1.6041	3.91E-39	7.9712	6.4748	1.4965	3.25E-25
KIAA1524	57650	KIAA1524 [Source:HGNC Symbol;Acc:29302]	7.0620	6.4342	0.6278	3.04E-18	7.8545	7.0773	0.7772	6.70E-16
RFC2	5982	replication factor C (activator 1) 2, 40kDa [Source:HGNC Symbol;Acc:9970]	9.6545	8.7627	0.8917	1.38E-45	9.9808	9.0754	0.9054	2.08E-23
RFC3	5983	replication factor C (activator 1) 3, 38kDa [Source:HGNC Symbol;Acc:9971]	8.3840	7.4615	0.9225	2.93E-34	8.6236	7.7364	0.8873	1.66E-15
RFC4	5984	replication factor C (activator 1) 4, 37kDa [Source:HGNC Symbol;Acc:9972]	10.3626	9.3857	0.9770	1.01E-45	10.8849	9.9707	0.9142	3.82E-30
RRM2	6241	ribonucleotide reductase M2 [Source:HGNC Symbol;Acc:10452]	10.6266	7.6172	3.0093	9.62E-64	10.2850	7.3752	2.9098	1.14E-60
CENPK	64105	centromere protein K [Source:HGNC Symbol;Acc:29479]	9.2188	6.8485	2.3703	1.22E-55	9.2613	6.8406	2.4207	1.02E-50
NCAPG	64151	non-SMC condensin I complex, subunit G [Source:HGNC Symbol;Acc:24304]	8.4423	5.3213	3.1210	7.71E-68	9.2362	6.8365	2.3997	4.77E-51
NT5DC2	64943	5'-nucleotidase domain containing 2 [Source:HGNC	10.3437	8.8774	1.4663	6.38E-43	9.6906	8.8684	0.8222	1.20E-13

		Symbol;Acc:25717]								
CENPH	64946	centromere protein H [Source:HGNC Symbol;Acc:17268]	8.4024	7.1272	1.2751	7.05E-39	8.2458	7.1752	1.0706	1.08E-21
SNRPA	6626	small nuclear ribonucleoprotein polypeptide A [Source:HGNC Symbol;Acc:11151]	10.4298	9.9855	0.4443	9.46E-21	10.4099	10.1184	0.2915	4.11E-05
BRCA2	675	breast cancer 2, early onset [Source:HGNC Symbol;Acc:1101]	6.8008	4.8048	1.9960	6.85E-39	6.9319	5.8815	1.0504	3.87E-24
AURKA	6790	aurora kinase A [Source:HGNC Symbol;Acc:11393]	8.8679	7.0080	1.8599	1.88E-70	9.0387	7.2292	1.8095	1.43E-40
TCF19	6941	transcription factor 19 [Source:HGNC Symbol;Acc:11629]	8.9557	8.0280	0.9277	1.77E-37	8.1761	6.8675	1.3085	8.01E-28
BUB1	699	budding uninhibited by benzimidazoles 1 homolog (yeast) [Source:HGNC Symbol;Acc:1148]	7.1234	4.2885	2.8349	1.46E-62	7.2005	5.7469	1.4535	7.10E-28
BUB1B	701	budding uninhibited by benzimidazoles 1 homolog beta (yeast) [Source:HGNC Symbol;Acc:1149]	9.5191	7.4934	2.0257	1.12E-73	9.4701	7.1502	2.3200	2.18E-51
TK1	7083	thymidine kinase 1, soluble [Source:HGNC Symbol;Acc:11830]	8.7870	6.7932	1.9938	5.51E-54	7.5752	5.9099	1.6653	3.63E-38

TOP2A	7153	topoisomerase (DNA) II alpha 170kDa [Source:HGNC Symbol;Acc:11989]	9.7974	6.3258	3.4717	7.35E-48	10.2423	7.1752	3.0671	3.95E-47
TTK	7272	TTK protein kinase [Source:HGNC Symbol;Acc:12401]	8.7681	6.5246	2.2435	1.60E-66	8.8309	6.5530	2.2779	2.05E-53
TUBG1	7283	tubulin, gamma 1 [Source:HGNC Symbol;Acc:12417]	9.9889	9.1657	0.8232	4.15E-38	10.1427	9.3966	0.7462	2.17E-23
TYMS	7298	thymidylate synthetase [Source:HGNC Symbol;Acc:12441]	11.8748	9.6850	2.1898	1.68E-71	11.9910	9.5496	2.4414	2.76E-55
WHSC1	7468	Wolf-Hirschhorn syndrome candidate 1 [Source:HGNC Symbol;Acc:12766]	9.2374	7.8143	1.4230	1.04E-35	8.4800	7.6085	0.8715	5.72E-18
CENPM	79019	centromere protein M [Source:HGNC Symbol;Acc:18352]	6.5355	4.1767	2.3588	1.56E-46	7.8727	6.1098	1.7629	5.86E-32
CENPO	79172	centromere protein O [Source:HGNC Symbol;Acc:28152]	8.7264	8.0795	0.6470	1.09E-22	8.5880	7.5993	0.9887	4.28E-25
MLF1IP	79682	MLF1 interacting protein [Source:HGNC Symbol;Acc:21348]	10.2172	8.3036	1.9136	1.77E-69	10.5278	8.0311	2.4967	1.15E-55
E2F8	79733	E2F transcription factor 8 [Source:HGNC Symbol;Acc:24727]	7.5291	5.5919	1.9372	6.28E-41	7.3022	5.8106	1.4915	8.96E-32
SHCBP1	79801	SHC SH2-domain binding protein 1 [Source:HGNC Symbol;Acc:29547]	8.9083	7.1508	1.7576	4.66E-70	8.9815	7.1443	1.8372	4.35E-42

BORA	79866	bora, aurora kinase A activator [Source:HGNC Symbol;Acc:24724]	8.2419	7.5809	0.6609	4.57E-33	8.2057	7.3351	0.8707	5.06E-24
DSN1	79980	DSN1, MIND kinetochore complex component, homolog (S. cerevisiae) [Source:HGNC Symbol;Acc:16165]	8.5072	7.5973	0.9099	2.12E-45	8.4604	7.7434	0.7170	7.31E-17
FAM83D	81610	family with sequence similarity 83, member D [Source:HGNC Symbol;Acc:16122]	9.0276	8.0925	0.9350	1.88E-37	8.4979	6.6797	1.8181	2.89E-32
CDT1	81620	chromatin licensing and DNA replication factor 1 [Source:HGNC Symbol;Acc:24576]	7.3169	5.8423	1.4745	6.28E-29	6.4428	5.8364	0.6064	1.03E-09
KIF18A	81930	kinesin family member 18A [Source:HGNC Symbol;Acc:29441]	7.7208	5.6393	2.0816	2.38E-52	7.7269	6.0248	1.7021	1.53E-46
CDCA3	83461	cell division cycle associated 3 [Source:HGNC Symbol;Acc:14624]	8.4089	5.9979	2.4110	3.35E-65	9.3245	7.4663	1.8582	4.02E-48
MXD3	83463	MAX dimerization protein 3 [Source:HGNC Symbol;Acc:14008]	7.2034	6.2193	0.9841	2.43E-23	7.4752	6.0901	1.3852	2.84E-22
NUF2	83540	NUF2, NDC80 kinetochore complex component, homolog (S. cerevisiae) [Source:HGNC Symbol;Acc:14621]	8.9759	6.4191	2.5568	5.73E-69	9.3201	6.8125	2.5076	1.05E-54

CDCA7	83879	cell division cycle associated 7 [Source:HGNC Symbol;Acc:14628]	10.3534	8.9111	1.4423	1.22E-45	10.1583	8.5487	1.6096	1.60E-32
BRIP1	83990	BRCA1 interacting protein C-terminal helicase 1 [Source:HGNC Symbol;Acc:20473]	7.1677	5.4038	1.7640	8.69E-36	6.7973	5.7502	1.0471	2.27E-17
LMNB2	84823	lamin B2 [Source:HGNC Symbol;Acc:6638]	9.3400	8.1133	1.2267	2.16E-45	8.2155	7.3309	0.8846	1.82E-15
GGH	8836	gamma-glutamyl hydrolase (conjugase, folylpolygammaglutamyl hydrolase) [Source:HGNC Symbol;Acc:4248]	10.4859	9.4511	1.0348	5.86E-46	10.7143	9.3686	1.3457	5.12E-34
CCNA2	890	cyclin A2 [Source:HGNC Symbol;Acc:1578]	9.3812	7.8430	1.5381	6.41E-73	8.0304	6.0754	1.9550	8.53E-45
CCNB1	891	cyclin B1 [Source:HGNC Symbol;Acc:1579]	8.4965	6.4571	2.0394	1.34E-68	10.1327	7.8995	2.2332	1.12E-52
TIMELESS	8914	timeless homolog (Drosophila) [Source:HGNC Symbol;Acc:11813]	9.3945	8.1190	1.2755	1.01E-63	9.1474	7.7565	1.3908	3.46E-38
CCNF	899	cyclin F [Source:HGNC Symbol;Acc:1591]	5.9143	3.9436	1.9707	4.11E-30	7.5624	6.6209	0.9415	1.11E-20
C15orf42	90381	chromosome 15 open reading frame 42 [Source:HGNC Symbol;Acc:28704]	6.2177	4.1142	2.1035	9.67E-32	6.4914	5.8746	0.6167	7.21E-12
PRC1	9055	protein regulator of cytokinesis 1 [Source:HGNC Symbol;Acc:9341]	10.4396	8.2427	2.1969	5.39E-78	10.6130	8.3971	2.2160	2.66E-55

CCNB2	9133	cyclin B2 [Source:HGNC Symbol;Acc:1580]	9.8702	7.0807	2.7895	6.72E-79	10.0130	7.1047	2.9083	8.85E-63
CENPL	91687	centromere protein L [Source:HGNC Symbol;Acc:17879]	8.4603	7.5986	0.8617	1.29E-34	8.9941	7.8015	1.1926	4.30E-32
PTTG1	9232	pituitary tumor-transforming 1 [Source:HGNC Symbol;Acc:9690]	11.2857	9.9657	1.3200	6.09E-63	11.5863	9.3091	2.2772	8.98E-55
TRIP13	9319	thyroid hormone receptor interactor 13 [Source:HGNC Symbol;Acc:12307]	8.9281	7.6339	1.2943	1.53E-67	8.8892	7.1916	1.6976	3.21E-44
HAUS8	93323	HAUS augmin-like complex, subunit 8 [Source:HGNC Symbol;Acc:30532]	6.9398	5.0545	1.8853	5.53E-34	7.1935	6.1396	1.0538	2.84E-20
KIF23	9493	kinesin family member 23 [Source:HGNC Symbol;Acc:6392]	7.7676	4.8863	2.8812	3.62E-57	7.7023	5.8130	1.8894	4.68E-42
ESPL1	9700	extra spindle pole bodies homolog 1 (S. cerevisiae) [Source:HGNC Symbol;Acc:16856]	8.6914	6.7135	1.9779	2.58E-63	8.2019	6.4806	1.7213	1.73E-44
KNTC1	9735	kinetochore associated 1 [Source:HGNC Symbol;Acc:17255]	8.9291	7.5968	1.3323	1.39E-41	8.9247	7.8847	1.0400	1.02E-29
KIAA0101	9768	KIAA0101 [Source:HGNC Symbol;Acc:28961]	10.9522	8.8394	2.1128	1.10E-71	11.3150	8.4052	2.9098	5.18E-60
DLGAP5	9787	discs, large (Drosophila) homolog-associated protein 5 [Source:HGNC Symbol;Acc:16864]	8.7537	6.4683	2.2854	4.98E-61	8.7590	6.2096	2.5494	5.40E-55

ARHGAP 11A	9824	Rho GTPase activating protein 11A [Source:HGNC Symbol;Acc:15783]	6.1781	4.5535	1.6246	3.44E-31	6.4541	5.7623	0.6918	1.48E-13
CDK1	983	cyclin-dependent kinase 1 [Source:HGNC Symbol;Acc:1722]	10.3362	7.5994	2.7368	1.57E-63	11.3017	8.5033	2.7983	6.61E-53
MELK	9833	maternal embryonic leucine zipper kinase [Source:HGNC Symbol;Acc:16870]	9.6807	6.9320	2.7487	7.90E-58	9.9502	7.3984	2.5518	2.31E-51
GINS1	9837	GINS complex subunit 1 (Psf1 homolog) [Source:HGNC Symbol;Acc:28980]	10.0007	8.3507	1.6500	9.39E-67	10.1735	8.5328	1.6407	2.73E-39
CDC6	990	cell division cycle 6 homolog (S. cerevisiae) [Source:HGNC Symbol;Acc:1744]	7.7926	6.6014	1.1912	3.24E-43	7.2167	5.8355	1.3812	4.23E-31
CDC20	991	cell division cycle 20 homolog (S. cerevisiae) [Source:HGNC Symbol;Acc:1723]	8.9181	6.1547	2.7634	1.02E-65	8.8269	6.2887	2.5382	8.78E-60
KIF14	9928	kinesin family member 14 [Source:HGNC Symbol;Acc:19181]	8.6156	6.1656	2.4500	5.57E-55	9.0334	6.5892	2.4441	2.19E-58
CDC25C	995	cell division cycle 25 homolog C (S. pombe) [Source:HGNC Symbol;Acc:1727]	7.3041	5.5986	1.7055	5.38E-40	7.3626	5.8443	1.5182	9.66E-36
NEBL	10529	nebulette [Source:HGNC Symbol;Acc:16932]	7.7592	9.4798	-1.7207	2.64E-41	7.7998	9.4949	-1.6951	1.01E-23
CBX7	23492	chromobox homolog 7 [Source:HGNC	9.3023	10.5047	-1.2024	1.96E-36	9.1335	10.0464	-0.9128	3.14E-24

		Symbol;Acc:1557]								
C5orf53	NA	NA	10.2513	11.3361	-1.0848	3.77E-42	11.1165	11.8510	-0.7344	5.59E-15
ELOVL7	79993	ELOVL fatty acid elongase 7 [Source:HGNC Symbol;Acc:26292]	7.6916	8.9771	-1.2855	2.08E-23	8.2908	9.2058	-0.9149	4.11E-08

Supplementary Table 3. Summary of Gene Set Enrichment Analysis (GSEA) results with FDR < 0.25. List of top-ranking stem cell-related genesets positively enriched with high *PLK1* group of glioma patients.

Genesets	Description	Size	Normalized enrichment Score	FDR q-val
DAZARD_RESPONSE_TO_UV_NHEK_DN	Genes down-regulated in NHEK cells (normal keratinocytes) by UV-B irradiation.	15	1.15586	1
RIGGI_EWING_SARCOMA_PROGENITOR_DN	Genes down-regulated in mesenchymal stem cells (MSC) engineered to express EWS-FLI1 fusion protein.	15	1.1429	1
BENPORATH_CYCLING_GENES	Embryonic stem cell signature related poorly differntiated glioblastoma and basal like subtypes	88	1.130648	0.9675661
GRAHAM_CML_DIVIDING_VS_NORMAL_QUIESCENT_UP	Transcriptome related to CML stem cells and active chemokine signaling	65	1.06929	1
BENPORATH_PROLIFERATION	Identical embryonic stem cell profiles similar to poorly differentiated histological subtypes	44	1.06517	0.87619877
ZHAN_MULTIPLE_MYELOMA_PR_UP	Prolifearative signaling in the patient subgroups received stem cell transplants and high-dose therapy	33	1.0561	0.7729226
GAL_LEUKEMIC_STEM_CELL_DN	Down-regulated in leukemic stem cells (LSC), defined as CD34+CD38- cells from AML (acute myeloid leukemia patients) compared to the CD34+CD38+ cells.	35	1.0178	0.7698555
GRAHAM_CML_QUIESCENT_VS_NORMAL_QUIESCENT_UP	Genes up-regulated in quiescent (G0) CD34+ cells isolated from peripheral blood of CML (chronic myeloid leukemia) patients compared to the quiescent cells from normal donors.	24	0.9156618	0.9054327

WONG_EMBRYONIC_STEM_CELL_CORE	Genes The 'core ESC-like gene module': genes coordinately up-regulated in a compendium of mouse embryonic stem cells (ESC) which are shared with the human ESC-like module	56	0.8943225	0.84800136
GRAHAM_NORMAL_QUIESCENT_VS_NORMAL_DIVIDING_DN	Genes down-regulated in quiescent vs dividing CD34+ [GeneID=8842] cells isolated from peripheral blood of normal donors.	44	0.872945	0.82181394
BENPORATH_ES_1	Set 'ES exp1': genes overexpressed in human embryonic stem cells according to 5 or more out of 20 profiling studies.	40	0.8567	0.7744122
MUELLER_PLURINET	Genes constituting the PluriNet protein-protein network shared by the pluripotent cells (embryonic stem cells, embryonical carcinomas and induced pluripotent cells).	29	0.8417691	0.7328983
BENPORATH_NANOG_TARGETS	Set 'Nanog targets': genes upregulated and identified by ChIP on chip as Nanog transcription factor targets in human embryonic stem cells.	24	0.6847	0.8637875
BENPORATH_MYC_MAX_TARGETS	Set 'Myc targets2': targets of c-Myc and Max identified by ChIP on chip in a Burkitt's lymphoma cell line; overlap set.	20	0.6211	0.86531216

Supplementary Table-4. List of primers used in quantitative real-time RT-PCR and TP53 mutational analysis

Gene Target	Primer sequence	Product size (bp)
NEK2	Forward: 5'- CGA GAG CGA GCT CTC AAA GCA A -3' Reverse: 5'- CCC CAC TGA AAT GAA CTT TCT TCT -3'	220
TOP2A	Forward: 5'- GTG GTC GAA ATG GCT ATG GAG C -3' Reverse: 5'- ATC TTT GGT GGA TCC AGC AAT ATC -3'	278
PRC1	Forward: 5'- AAG TCT GCT CCA GCT CCA CGA T-3' Reverse: 5'- GGG CAG CAT TTT CTG GAG CTT G -3'	217
ECT2	Forward: 5'- GTT GCT GTG AGT CTA GGT ACT C -3' Reverse: 5'- GTG CAT CTT TCA TCT CCA AGC GG -3'	242
FOXM1	Forward: 5'- CCT TTG CGA GCA GAA ACG GG –3' Reverse: 5'- CTT AAC CTG TCG CTG CTC CAG –3'	181
HPRT	Forward: 5'- CAC TGG CAA AAC AAT GCA GAC T-3' Reverse: 5'- GTC TGG CTT ATA TCC AAC ACT TCG T-3'	118
P53 mutation analysis	Forward: 5'- TCA GAC ACT GGC ATG GTG TT -3' Reverse: 5'- AAG CCT AAG GGT GAA GAG GA -3'	880

Appendix A

List of publications during candidature – Charlene Foong

Primary Author:

1. Foong, C.S., Sandanaraj, E., Brooks, H.B., Campbell, R.M., Ang, B.T., Chong, Y.K., & Tang, C. Glioma-propagating cells as an in vitro screening platform: PLK1 as a case study. ***J Biomol Screen*** 9, 1136-1150. IF 2.049.
2. Foong, C. S., Ng, F. S., Phong, M., Toh, T. B., Chong, Y. K., Tucker-Kellogg, G., Campbell, R. M., Ang, B. T. & Tang, C. Cryopreservation of cancer-initiating cells derived from glioblastoma. ***Front Biosci (Schol Ed)*** 3, 698-708 (2011). IF 3.520.

Supporting Author:

3. Yeo, C. W., Ng, F. S., Chai, C., Tan, J. M., Koh, G. R., Chong, Y. K., Koh, L. W., Foong, C. S., Sandanaraj, E., Holbrook, J. D., Ang, B. T., Takahashi, R., Tang, C. & Lim, K. L. Parkin pathway activation mitigates glioma cell proliferation and predicts patient survival. ***Cancer Res*** 72, 2543-2553 (2012). IF 7.856.